

Correlation Between Refractive Indices and Other Fuel-Related
Physical/Chemical Properties of Pyrolysis Liquids
Derived From Coal, Oil Shale, and Tar Sand

M. Rashid Khan

U.S. Department of Energy
Morgantown Energy Technology Center
Morgantown, WV 26507-0880

ABSTRACT

In the literature, characterization techniques based upon the liquid's refractive index are used with petroleum distillates to predict fuel-related properties; however, essentially nothing has been reported on the application of this technique to pyrolysis liquids. Measurements of the refractive indices of the pyrolysis liquids derived from various feedstocks (coal, oil shale, and tar sand) were made and appear to correlate well with the liquids' physical and chemical properties. The refractive indices of the pyrolysis liquids show good correlations with liquid density (correlation coefficient of 0.98), carbon and proton aromaticities (correlation coefficients of 0.88 and 0.91, respectively), and liquid carbon residue (i.e., correlation coefficient of 0.88 with the Conradson carbon residue). The above and other correlations were developed using data from at least 7 to as many as 35 discrete samples. These correlations have been used to develop empirical models. These findings demonstrate the potential of using the liquid's refractive index as a rapid technique to characterize the fuel-related properties of fossil fuel liquids generated by pyrolysis (before they are hydrogenated).

INTRODUCTION AND OBJECTIVES

The Morgantown Energy Technology Center (METC) results demonstrated that relatively high-quality liquid fuels (low sulfur, high H/C) can be produced by low-temperature devolatilization of coal (1,2). Physical and chemical properties characterization of these liquids has been the focus of several studies during the last few years (1-5).

Correlations based on the data obtained from relatively simple characterization techniques for predicting fuel-related physical and chemical properties of pyrolysis liquids would facilitate the utilization of these liquids in various processing schemes. Properties such as molecular weight and aromaticity of liquids influence their utilization behavior/properties (e.g., viscosity, smoke point). Measurements of molecular weight or aromaticity can be difficult, time consuming, and expensive; can require skilled operators; and are often beyond the resources of most small laboratories.

The correlations between properties of petroleum liquids and their refractive indices are available in the literature (6-8). Sturm et al. (8a), fractionated the pyrolysis liquid generated in a rapid-rate reactor (Coal Oil Energy Development, COED) into various distillate cuts. It was not stated at what condition hydrogenation was effected. The COED liquids were hydrogenated (8b) to remove the heteroatom contents (e.g., sulfur, nitrogen) and to improve their fuel value.

White et al. (6) compared the refractive indices of coal liquefaction products with their chemical properties (e.g., molecular weight). These researchers also reported an excellent review of previous work in this area (6).

In previous studies, it was demonstrated by Khan (9) that the pyrolysis liquids generated from weathered fossil fuel samples (including coal and oil shale) had higher liquid refractive indices than those obtained from unweathered samples.

The objective of this paper is to illustrate the relationship between the refractive indices of pyrolysis liquids and their fuel-related physical (density, Conradson carbon residue) and chemical properties (aromaticity, molecular weight, hydrocarbon type, etc.).

EXPERIMENTAL SECTION

A fixed-bed reactor (slow heating-rate organic devolatilization reactor, SHRODR) was used to generate pyrolysis liquids at 500°C. More details on this reactor system as well as the experimental procedures used and the reproducibility of data are available (1,2,5). A range of feedstocks (primarily coal, but also oil shale, and tar sand) were devolatilized in this reactor. Coal samples were supplied by the Penn State/DOE coal data bank (10). The origin of shale samples (eastern and western) and the Pittsburgh No. 8 coal has been discussed elsewhere (9). Tar sand samples were procured from the Western Research Institute (WRI).

Sample preservation and avoidance of air oxidation of samples were key considerations to this investigation as reported in previous studies (9,11-14). Availability of fresh (well preserved, not weathered) samples was the criterion used for sample selection. Some coal samples utilized by Given et al. (15) for an investigation on direct liquefaction were selected in this study for comparison. Primarily bituminous coals were used in this study as these are known to yield the highest liquid product during pyrolysis (1,3). All sample preparation and handling were performed in an inert atmosphere.

The refractive index of liquid samples were measured at 20°C by Huffmann Laboratories, Inc., applying ASTM D-1218 methods. The refractive index of 1-bromonaphthalene was measured as a standard before the refractive index of each pyrolysis liquid. The refractive index measurement of 1-bromonaphthalene was within ± 0.0005 units of the reference value (reported by Hoffmann). Conradson carbon residue was determined at Saybolt Lab (Pasadena, Texas) using ASTM D-189. The density measurements were (reproducible within ± 0.0001), also performed at Saybolt at 15.5°C by ASTM D-70.

The aromaticity of the liquids was measured at the University of North Dakota Energy and Minerals Research Center (UNDEMRC) by proton NMR, using the Clutter et al. (16) procedure with a Varian XL200 NMR Spectrometer. ^1H NMR was used for determination of aromaticities. Molecular weights were calculated based on the NMR data applying the equation used by Clutter et al. (16).

Neutral fractions of pyrolysis liquids were generated chromatographically on activated alumina. A 20-inch x 3/8-inch column was loaded with 25 g of activated alumina (Biorad). A sample of 0.2 g was charged to the column and the neutral fraction was eluted with 50 mL of benzene. The benzene was removed from the sample by rotary evaporation. To ensure that the lower-boiling point components of the sample were not lost during benzene removal, the benzene was not completely removed from the sample. The concentration of the residual benzene was then determined by combined gas chromatography/mass spectrometry (GC/MS) and the final weights of the neutral fractions were adjusted to account for the residual benzene. The polar material was not eluted from the column, but was determined by difference.

The neutral fractions were analyzed using WRI's GC/MS hydrocarbon group type analysis. A Hewlett-Packard Model 5985B GC/MS system was used. The GC column was a 50-meter quartz capillary, coated with methylsilicone, and operated in programmed-temperature modes, which optimized the resolution of components. The method determines the composition of the hydrocarbon group by using selected ions that are

representative of each hydrocarbon group type and relies on the gas chromatographic separation to minimize interferences from fragment ions of other hydrocarbon groups. The results from the analyses are reported as weight percentages of the neutral fractions. The results are provided as weight percentages of the total sample that was charged to the column. The results for the neutral fractions reflect the adjusted weights of the neutral fractions after accounting for the residual benzene. Detailed analysis and distribution of the components identified in various fractions will be presented in a future communication. The distillate cut between 300° and 600°F is of interest because its properties is expected based on literature studies to match the target properties of the high-density fuels (17,18). Liquids were combusted in a thermogravimetric analysis system (TGA) at 100°C/min in air (flowrate of 120 cc/min). In addition TGA distillation of the liquids was performed (heating rate, 5°C/min, He flowrate 50 cc/min). Statistical Analyses System (SAS) Package developed by SAS Institute was used for data analyses. The linear regression analysis available in this package was applied to develop empirical models (19,20).

RESULTS

A detailed study on the influence of feedstock type on pyrolysis liquid product yield and composition will be presented separately. In addition, comprehensive characterization data for the liquids are the subject of a separate report. Table 1 presents a summary of equations used to predict the properties of pyrolysis liquids.

The hydrogen-to-carbon ratio (H/C) of the pyrolysis liquids is an important fundamental property of liquid fuels that influences various physical (e.g., viscosity, density) and chemical (e.g., molecular weight, aromaticity, etc.) properties. The relationship (negative) between the liquid H/C ratios and the refractive indices of the liquid is presented in Figure 1A (correlation coefficient of 0.90). The following regression model was used for predicting the liquid H/C ratios:

$$[H/C] = 6.876 - 3.50 n. \quad 1)$$

The refractive indices (n) of the liquids correlated with the corresponding weight percent (of tar) hydrogen (H) contents (correlation coefficient = -0.83; Figure 1B). A model defined by equation (2),

$$H = 57.264 - 30.5 n, \quad 2)$$

was used to predict the hydrogen contents.

Figure 2 shows the correlation between the carbon aromaticities (C_{aro}) and the refractive indices (n) for the pyrolysis liquids derived from various fossil fuels. The correlation coefficient between the variables was 0.91. The carbon aromaticity (C_{aro}) could be predicted by equation (3) using a linear regression fit:

$$C_{\text{aro}} = 3.657 n - 5.228. \quad 3)$$

The carbon aromaticity of the same data set could be predicted somewhat better with a two-variable model that includes the liquid H/C atomic ratio:

$$C_{\text{aro}} = 2.887 n - 0.227 (H/C) - 3.71. \quad 4)$$

Figure 3 compares the proton aromaticity with the refractive indices of the liquids (correlation coefficient of 0.88). The actual aromaticity data can be predicted based on a single-variable model, defined by

$$H_{\text{aro}} = 2.102 n - 3.103. \quad 5)$$

TABLE 1

Summary of Predictive Equations for Pyrolysis Liquids

Model	R ^{2*}	F	P
1. (H) = 57.264 - 30.50 n (H/C) = 6.876 - 3.50 n	0.70 0.55	65.3 35.4	0.0001 0.0001
n = refractive index H/C = hydrogen-to-carbon ratio of liquids (atomic)			
2. C _{aro} = 3.657 n - 5.228 C _{aro} = 2.887 n - 0.222 (H/C) - 3.71	0.82 0.86	131.9 82.5	0.0001 0.0001
C _{aro} = carbon aromaticity			
3. H _{aro} = 2.102 n - 3.103 H _{aro} = 1.739 n - 0.105 (H/C) - 2.39 H _{aro} = n ^{-0.56168} x (H/C) ^{-4.484}	0.77 0.79 0.97**	96.8 50.5 531.5	0.0001 0.0001 0.0001
H _{aro} = proton aromaticity			
4. MW = 4383.2 - 2655 n MW = 1.332 T ₅₀ - 1573.28d + 1589.1 MW = 1.348 T _m - 1249.24d + 1234.6	0.70 0.82 0.94	65.3 9.03 23.0	0.0001 0.033 0.015
MW = molecular weight T ₅₀ = temperature of mid-distillation point (TGA) T _m = temperature of mid-distillation point (ASTM D-86)			
5. d = 1.977 n - 2.08	0.97	155.2	0.0001
d = density, gm/cc			
6. C _{con} = 37.75 n - 55.29	0.77	16.5	0.0097
C _{con} = Conradson carbon residue			

* R² measures how much variation in the dependent variable can be accounted for by the model (i.e., independent variable).

** R² is redefined for the no-intercept case by SAS (20). Note that this is a non-linear equation.

The F-ratio is the ratio produced by dividing the mean square for the model by the mean square of error. It tests how well the model as a whole (after adjusting for the mean) accounts for the behavior of the dependent variable (20).

P defines the "observed level of significance." In statistical terms, the level of significance, α , of a test is defined as the probability of rejecting the null hypothesis (i.e., no linear relationship between the dependent and independent variables) given the null hypothesis is true. P gives us the largest value of α that would lead to the acceptance of the null hypothesis.

The predicted model, based on a two-variable model, can be defined by the equation

$$H_{\text{aro}} = 1.739 n - 0.105 (H/C) - 2.39. \quad (6)$$

Proton aromaticity could also be predicted based on the following nonlinear model (see also Table 2).

$$H_{\text{aro}} = n^{-.56168} \times (H/C)^{-4.484}.$$

The molecular weights (MW) of the pyrolysis liquids (determined using NMR data) could be predicted from the refractive indices. For example, a single-variable model based on the refractive indices of the liquid could be used for this prediction. This model is given by the equation

$$MW = 4383.2 - 2655 n \quad (7)$$

A two-variable model based on the liquid density (d) and the mid-distillation point (T_m) could also be used for predicting the MW of the pyrolysis liquids (Figure 4):

$$MW = 1.348 T_m - 1249.24d + 1234.6. \quad (8)$$

The distillation data were obtained using the ASTM D-86 procedure. A new model, based on the same two-variable model (similar to Equation 8) but the distillation data are obtained from TGA evaporation, can be defined by the equation

$$MW = 1.332 T_{50} - 1573.28d + 1589.1. \quad (9)$$

In the above equation, T_{50} stands for the mid-distillation temperature as determined by a TGA. The correlation coefficient between the refractive index and the density (Figure 5) of the liquids was 0.98. A linear regression fit provided the following model:

$$d = 1.977 n - 2.08. \quad (10)$$

The correlation coefficient between the refractive indices of various distillation cuts and the corresponding density for the COED syncrudes (reported by Strum et al.¹⁰) was 0.99, calculated in this study.

The correlation coefficient between the Conradson carbon (C_{con}) residue of the mild pyrolysis liquids derived in this study and the refractive indices of the liquids was 0.88 (Figure 6). A single-variable model was defined by the equation

$$C_{\text{con}} = 37.75 n - 55.29 \quad (11)$$

A liquid combustion parameter (second maximum peak of combustion) measured in a thermogravimetric analyses system (TGA) could be positively correlated somewhat with the refractive indices of the liquids (data not shown).

The significance of this TGA peak is not known. It may be worthwhile to attempt correlations of liquid combustion properties with their refractive indices, keeping previous relationships observed in this study in mind.

Additional correlations between the refractive indices and the pyrolysis liquid characterization data are presented in Figures 7 and 8. Figure 7 shows a relationship between the refractive indices of the whole liquid and the tricyclic saturated compound (so-called "high density fuels") in the 300° to 600°F cut of the neutral fraction of the pyrolysis liquids as determined by a GC/MS technique (the correlation coefficient of the data set was 0.8). The liquid distilled between 300° to 600°F was

of particular interest because this boiling range approximates the range of JP-8, a high-density aviation fuel (17,18,21). The total naphthalenes content in Cut 2 (boiling between 300° and 600°F) of the pyrolysis liquids present in the neutral fraction could be directly correlated with the refractive indices of the whole liquids (Figure 8, correlation coefficient 0.98).

Conradson carbon residue (C_{con}) could be correlated with the hydrogen content (correlation coefficient of -0.92). C_{con} also showed correlations with the carbon and proton aromaticities (correlation coefficients of 0.91 and 0.84, respectively). Thus, the observed correlation between the refractive index and C_{con} is not surprising. The observed relation may reflect the well known fact that aromatic compounds are more susceptible to coke formation during severe heat treatment. Figure 9 compares the cetane index of the hydrogenated (8b) COED liquids distilled at various temperature ranges [data from Strum et al. (8a)] with the corresponding refractive index. A summary of correlations developed in this study are presented in Table 1.

DISCUSSION

The results of this study demonstrate that the refractive index, used in petroleum literature to correlate fuel properties, is a relevant property to evaluate pyrolysis liquids derived from coal, oil shale, and tar sand. It is demonstrated that the liquids' H/C, density, hydrogen content, molecular weight, and aromaticity correlate with refractive indices of the pyrolysis liquids.

The relationship between the refractive index (n) and density (d) and other properties (e.g., Conradson carbon residue) of the liquids is consistent with our physical understanding of the structural properties of hydrocarbons. Paraffins have the highest hydrogen content and tend to have "fluffy" chain structures with low densities. For pure compounds, the lower the density, the lower the refractive indices. On the other hand, relatively compact cyclic (dense) aromatics are deficient in hydrogen. Cycloparaffins, which are both cyclic and hydrogen saturated, represent the best compromise between density and hydrogen content (21).

The refractive indices of pyrolysis liquids correlate with the liquid H/C ratio (correlation coefficient 0.90) or the hydrogen contents of the liquid (correlation coefficient 0.86). In this study, models have been developed to predict the H/C ratio or hydrogen contents of the liquids based on their refractive indices.

It is not surprising that refractive index correlates well with the liquid aromaticity. An increase in hydrogen content of fuels often lead to a decrease in aromaticity. For example, benzene with H/C = 1 has $f_a = 1$, while C_6H_{12} (cyclohexane) with H/C = 2 has $f_a = 0$. Here, f_a is the proton or carbon aromaticity. The correlation coefficients between refractive index and proton, or refractive index and carbon aromaticity were 0.88 and 0.91, respectively. One- and two-variable models were applied to predict the carbon and proton aromaticities of the pyrolysis liquids, based on their refractive indices.

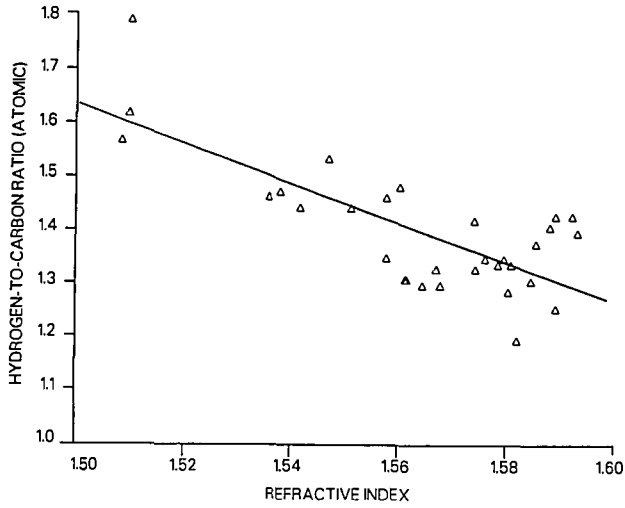
Molecular weights are fundamental properties of liquids. For various classes of pure compounds, refractive indices tend to change rapidly at low molecular weight but less rapidly at higher molecular weight. It appeared that refractive indices of the pure liquids correlated with the negative one-half power of molecular weight (data not shown). In this study, molecular weight could be predicted based on a single (e.g., refractive index, n) or a two-variable model [including density (d) and temperatures of 50 percent evaporation as determined in a TGA (T_{50}) or by an ASTM technique (ASTM D-86, T_m)].

SUMMARY AND CONCLUSIONS

It is demonstrated that the refractive indices of pyrolysis liquids derived from coal, oil shale, and tar sand serve as a useful property to evaluate the fuel-related physical/chemical properties of these fuels. The refractive indices of the liquids correlate well with the liquid hydrogen content (weight percent) and the H/C ratio, aromaticity (carbon and proton), molecular weight, density, and Conradson carbon residue. A number of empirical equations have been developed based on these correlations.

REFERENCES

1. Khan, M. R. Fuel Science and Technology International, 1987, 5(2), 105-231.
2. Khan, M. R. Proceedings. International Conference on Coal Science, 1987. Netherlands, International Energy Agency, IEA.
3. Khan, M. R. "Characterization and Mechanisms of Mild Gasification Processes: Low-Temperature Devolatilization Studies," Proceedings, Fifth Annual Gasification Contractors' Meeting, June 25-27, Morgantown, WV 26505 (1985).
4. Khan, M. R.; Kurata, T. M. July 1985. The Feasibility of Mild Gasification of Coal: Research Needs. DOE/METC-85/4019. NTIS/DE85013625. 73 pp.
5. Khan, M. R. March 1986. "Production of a High-Quality Liquid Fuel From Coal by Mild Pyrolysis of Coal-Lime Mixtures," DOE/METC-86/4060 (DE86006603).
6. White, C.; Perry, M. B.; Schmidt, C. E.; Douglas, L. J. Energy and Fuels, 1987, 1, 99-105.
7. Riazi, M. R.; Daubert, T. E. Ind. Eng. Chem. Process Des. Dev. 1980, 19, 289-294.
- 8a. Sturm, G. P., Jr.; Woodward, P. W.; Vogh, S. A.; Holmes, S. A.; Dooley, J. E. BERG/RI-75/12, November 1975.
- 8b. Personal Communication with S. Holms, 1988.
9. Khan, M. R. Energy and Fuels, 1987, 1(4), 366-376.
10. Penn State/DOE Coal Data Bank, Office of Coal Research, Penn State University, University Park, Pennsylvania 16802.
11. Khan, M. R. 193rd ACS Petroleum Division Chemistry Preprint 1987, Denver, Colorado, April 1987.
12. Khan, M. R. Proceedings, 19th Oil Shale Symposium, Col. School of Mines, Golden, Colorado, 1986, 139-148.
13. Khan, M. R.; Jenkins, R.G. Fuel, 1985, 64 (2), 189-192.
14. Khan, M. R.; Jenkins, R.G. Fuel, 1985, 64 (11), 1,618-1,622.
15. Given, P. H., et al. Fuel, 1982, 61 (10), 971.
16. Clutter, D. R., et al. Anal. Chem., 1972, 44, 1,395.
17. Korosi, A.; Rubin, J.N. "Hydroprocessing of Light Pyrolysis Fuel Oil for Kerosene Type Jet Fuel," Wright-Patterson Air Force Base, Ohio 45433, February 1980, Technical Report AFWAL TR-83-2048.
18. "High-Density Candidate Hydrocarbon Fuels from Refinery By-Product Streams," Universal Energy Systems, Dayton, Ohio 45432, September 1985, Technical Report (Interim). Contract No. F33615-83-C-2360/585842-83-C-0383, Project No. 745, Task 001, 002.
19. Box, G. E. P. Statistics for Experiments. Wiley and Sons, New York, 1978.
20. SAS User's Guide: Basics, Version 5 Edition, SAS Institute, Box 8000, Cary, North Carolina 27511-8000.
21. Personal Communication with F. Guffy (1987).



888-783-1A BP4

FIGURE 1A. Correlation between the liquid hydrogen-to-carbon ratio and the refractive indices of the liquid.

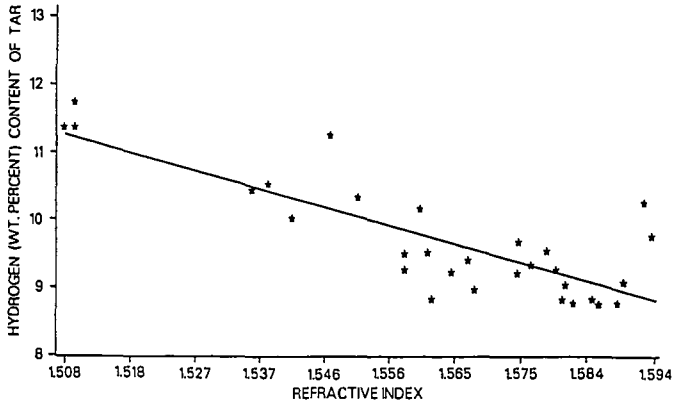


FIGURE 1B. Correlation between the liquid hydrogen content (dry basis) and the refractive indices of the liquid.

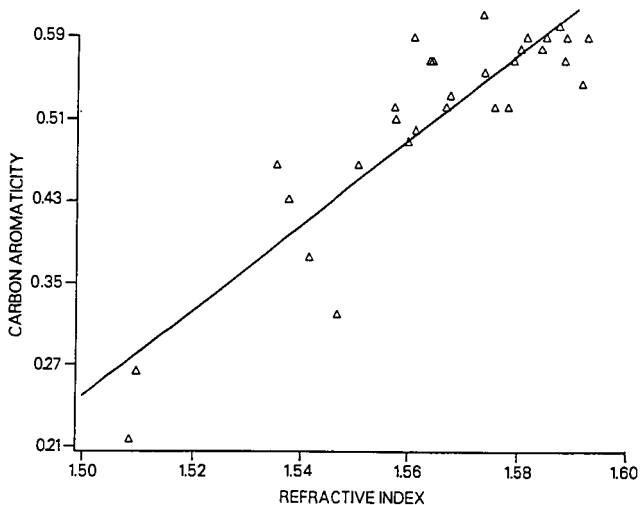


FIGURE 2. Correlation between the carbon aromaticity and the refractive indices (correlation coefficient 0.91). C88-783-2A BP4

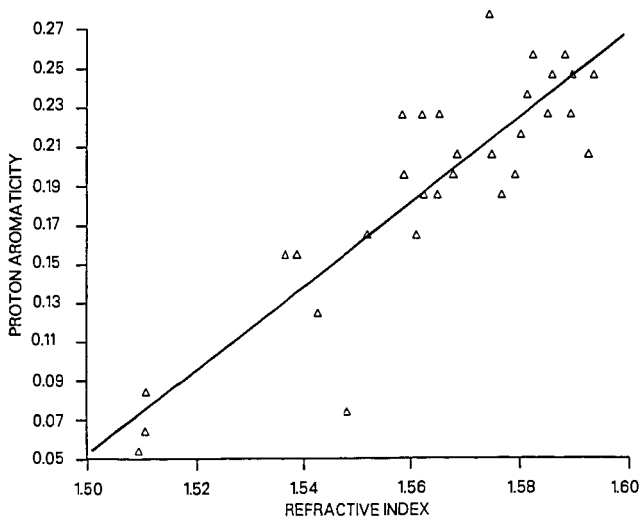
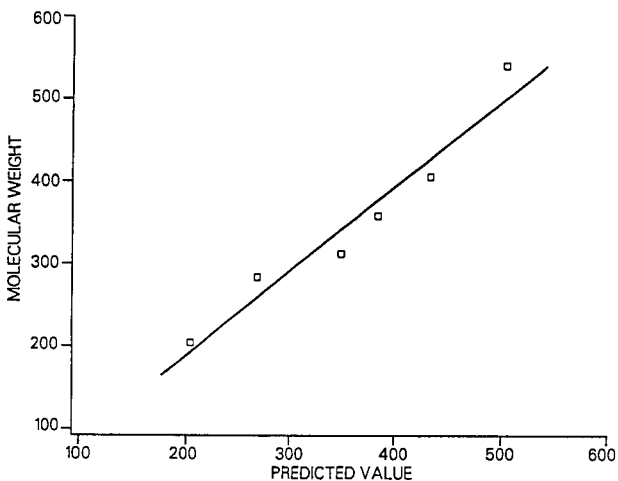
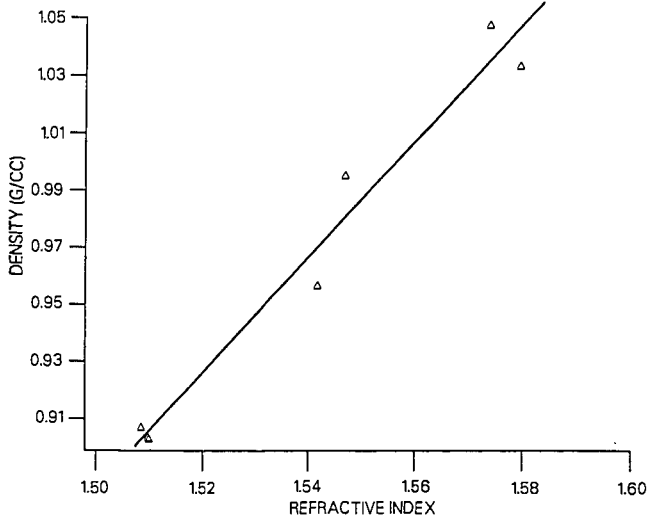


FIGURE 3. Correlation between proton aromaticity and refractive indices (correlation coefficient 0.88). 188-783-3A BP4



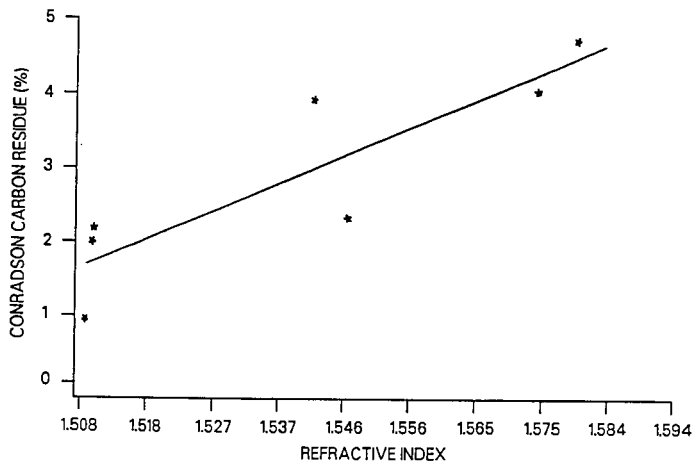
BB-783-4B BP4

FIGURE 4. Predicted and measured molecular weight based on a two-variable model (including density and mid-distillation point (T_{50})). ($R^2 = 0.93$); distillation data obtained by a TGA unit.



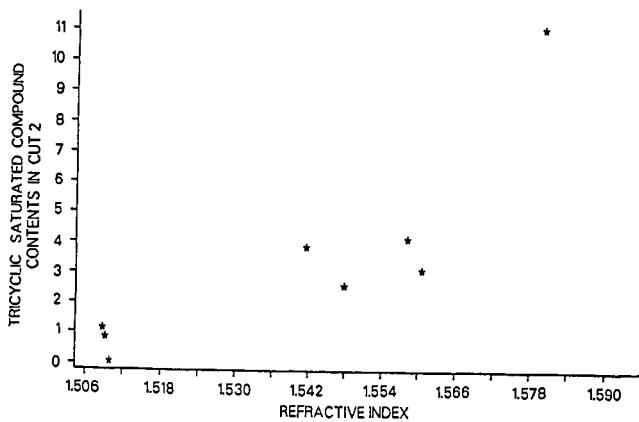
BB-783-5A BP4

FIGURE 5. The relationship between the density and the refractive indices of the pyrolysis liquids (correlation coefficient 0.98).



188-783-6A BP4

FIGURE 6. The relationship between the refractive indices and the Conradson carbon residue (correlation coefficient 0.88).



027-1010-10 BP10

FIGURE 7. Correlation between refractive indices and triaromatic content of the liquids (in Cut 2; i.e., 300° to 600°F fraction of the neutral position of pyrolysis liquids) (correlation coefficient of 0.8).

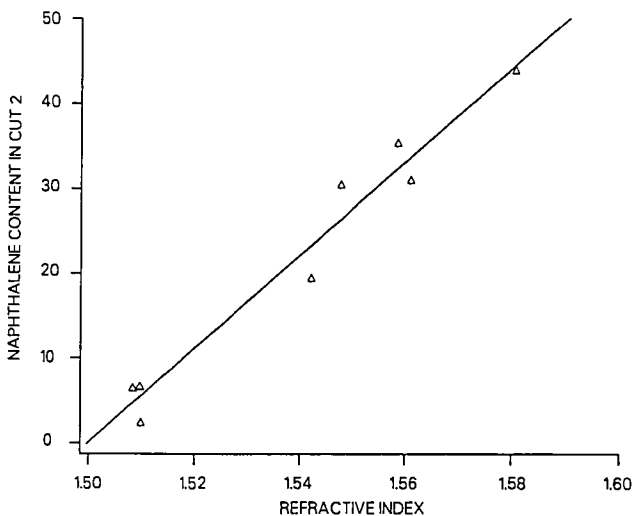


FIGURE 8. Relationship between the total naphthalene contents of the pyrolysis liquids with the refractive indices of the liquids.

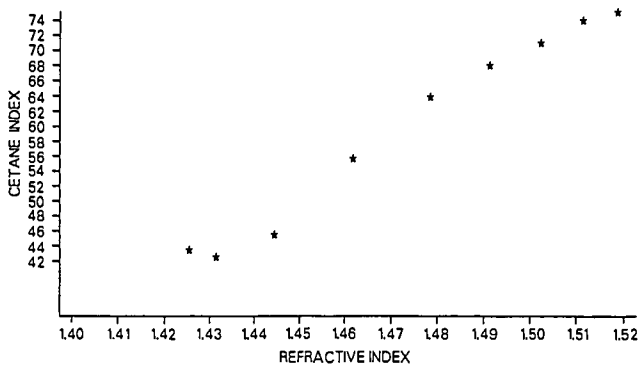


FIGURE 9. Relationship between the Cetane index with the refractive indices for the COED (hydrogenated) syncrude.

Prediction of the Composition of Coal Tars from the Pyrolysis Mass Spectra of the Parent Coals Using Canonical Correlation Techniques

Tanmoy Chakravarty, Henk L.C. Meuzelaar, Patrick R. Jones

Biomaterials Profiling Center, University of Utah,
Salt Lake City, UT 84102

M. Rashid Khan

Morgantown Energy Technology Center, Morgantown, W. Virginia

INTRODUCTION

In this study, we show that the mass spectrometric composition of coal tars can be predicted from the pyrolysis mass spectra of their parent coals. Curie-point low voltage electron ionization mass spectrometry (CuPy-EIMS) was performed on nineteen coals and on their respective pyrolysis liquids prepared by means of a fixed bed reactor method described elsewhere (1). Using factor and discriminant analysis techniques, the spectra can be classified and underlying structural variables responsible for the above classification identified. Furthermore, compositional similarities and dissimilarities between the solid samples and their liquids can be brought out using canonical correlation methods (2). Table I lists the samples, their PSOC numbers, geological origin and the rank information. Of the nineteen coal samples, two are of subbituminous rank, three of high volatile B and C bituminous rank and the remainder of high volatile A bituminous rank. Twelve coals are from the Eastern/Appalachian coal province, six are from the interior province and one is a Western coal from the Northern Great Plains province.

EXPERIMENTAL

Details of sample preparation and CuPy-EIMS analysis procedures have been described elsewhere (3). Experimental conditions were as follows: Curie-point temperature 610°C; heating rate approx. 100 K/s; total heating time 10s; electron energy 12eV; mass range scanned 20-260 amu; scanning rate 1000 amu s⁻¹; total scan time approximately 10s. Each sample was analyzed in triplicate and the spectra recorded and stored by computer (IBM 9000).

Data Processing

Mass variables with m/z values higher than 90 were selected for multivariate analysis. The reason for this is that the low mass range variables are not suitable for correlating the coals with their tars because of the loss of low molecular weight volatile products in the fixed bed reactor. The remaining data sets consisting of 171 variables were preprocessed, normalized and factor and discriminant analysis performed (4,5). Four discriminant functions were found to be significant, accounting for 55% of the variance in the coal data and 53% variance in the tar data, respectively.

Using four discriminant functions from both the coal and the tar data sets, canonical correlation analysis was done. Two canonical variates were obtained with correlation coefficients >0.9. The two canonical variates for the coal data set accounted for 35% of the total variance; whereas 30% of the total variance was accounted for by the two canonical variates for the tar data set.

Using a "jackknifing" procedure the topology of the canonical variate space was checked. The scores of the "unknown" sample were projected in the canonical variate space and the pyrolysis mass spectra of these unknown samples were then

predicted by calculating a distance weighted average from the spectra of the two nearest neighbors.

Methods and Procedures

A brief description of the methodology and mathematical rationalization is given below. Factor analysis (6) is an efficient way of reducing a data set (the data is generally preprocessed to form a correlation matrix). The first factor describes the maximum correlated variance in the data set, the second (orthogonal to the first) the maximum of the residual correlated variance, etc.:

$$F_j = a_{1j}z_1 + a_{2j}z_2 + \dots + a_{mj}z_m \quad 1)$$

where F_j is factor j , with loading a_{ij} , which describe the contribution of the variable z_i to the factor.

The scores, i.e., the contributions of the spectra to the factors, are obtained by substituting the intensities of the mass variables in the spectra for z_i . The relationship between the data matrix D (size $s \times m$ where s is the number of spectra and m is the number of mass variables) and the calculated factor matrix is:

$$D = S \times F \quad 2)$$

where S is the score matrix (size $s \times n$, n = number of factors) and F (size $n \times m$) contains the factors. The scores in the principal component analysis are calculated in the following way:

$$S = D \times (E \times \wedge^{-1/2}) \quad 3)$$

where S contains the standardized scores (mean is zero, standard deviation is 1), and D the standardized data matrix. E is the orthonormal eigenvector for matrix $Z = 1/s D^T D$, with the eigenvalues given in \wedge .

The standardized data matrix, D , can be reconstructed from the scores using this relation:

$$\begin{aligned} D &= S \times (E \times \wedge^{-1/2})^{-1} \\ &= S \times (E^{-1} \times \wedge^{1/2}) \\ &= S \times (E^T \times \wedge^{1/2}) \\ &= \text{standardized scores} * \text{factor loadings} \end{aligned} \quad 4)$$

The score of an unknown sample, defined in terms of a standardized data matrix, can be projected using Equation 3. Similarly, the projected unknown score, based on a training data set, can be used to predict a standardized data matrix (in this case of the unknown sample) using Equation 4. The factor loadings, before being used in Equation 4, have to be transformed to the canonical variate space by using the canonical variate matrix.

RESULTS AND DISCUSSION

The results will be discussed under two separate subheadings; canonical correlation results and prediction results.

Canonical Correlation Results

Canonical variate scores (CVI vs. CVII) for the two data sets are plotted in Figure 1. The result shows that the data is primarily two-dimensional. The clustering of the samples suggests that the Interior hvb coals (samples #15, 16 and

17, Table I) are more alike in composition than the Eastern hvb coals. The subbit C Upper Block Indiana coal (sample #7) is different from the subbit A coal of the Northern Great Plains (sample #18). The Lower Kittanning coal from West Virginia (hvAb, sample #9) and the Lower Banner Virginia coal (also hvAb, sample #6) do not fall close to the cluster with other hvAb coals. Although the Lower Banner coal has been found to be different from other hvAb coals petrographically, similar data is unavailable for the Lower Kittanning coal.

The clustering pattern of the corresponding tar data set is almost the same as that for the coal data; the scores of the coal and the tar are very close in this two-dimensional canonical variate space. The closer the score of the tar sample to that of the coal, the more alike their spectral patterns are. The average relative deviation between the coal and tar scores is 10% in the direction of CVI and 25% in the direction of CVII (this is related to the uncertainty in the predicted composition). Based on this canonical score plot, it is possible to predict the composition of the coal tars starting from the Py-MS patterns of the coals with the help of Equation 4.

As mentioned before, the prediction is based on the location of the projected score of the unknown sample in the canonical variate space of the coal data set. Two samples were selected for jackknifing tests - one from each marked cluster representing coals of different rank and origin (samples #16 and 2, respectively). Figures 2 and 3 show the score plots for the first two canonical variates with the score of the particular unknown sample projected. The topology of the CVI/CVII space is preserved in both cases (Figures 2 and 3); the projected score of the particular sample falls almost in the same location as if it were a part of the data set.

Prediction Results

Because the projected score of the jackknifed sample lies in the same space as the original data set, we have used a simple technique to predict the mass spectra of the selected samples. For example, the spectrum of sample #16 is derived from the distance weighted averaging of those of samples 15 and 17 (Figure 2). Similarly, the spectrum of sample #2 is derived by weighted averaging of those of samples 4 and 14 (Figure 3).

Since some coal and tar components are not strongly represented in this space the distance weighted averaging method makes the assumption that clustering behavior observed in canonical correlation space is representative of overall clustering tendencies. This assumption can and should be verified by inspection of clustering behavior in multidimensional factor space.

Figure 4a, b, c shows the spectra of the IL #6 coal, that of the corresponding tar, and the predicted tar. Most of the components present in the coal spectrum, Figure 4a, are also seen in the tar spectrum, Figure 4b. For example, the mass peaks at m/z 94, 108, 122 ("phenols"), 110, 124, 138 ("dihydroxybenzenes"); 142, 156, 170, 184, 198 ("naphthalenes"); 168, 182, 196, 210, 224 ("acenaphthenes") and 178, 192, 206 ("phenanthrenes/anthracenes") are all found in both the coal and the tar spectra. The differences between these two spectra should also be noted here. The higher molecular weight masses all have stronger signals in the tar spectrum, and the patterns of the components such as naphthalenes (m/z 142, 156, 170, 184), acenaphthenes (m/z 168, 182, 196) and anthracenes (m/z 178, 192, 206) are different in the tar spectrum. The naphthalene series reaches its maximum at m/z 156 in the coal spectrum, and at m/z 170 in the tar spectrum; similar shifts in the relative intensity patterns are observed for other components mentioned above. The predicted spectrum, Figure 4c, shows that it preserves the spectral subpatterns of the individual components. Also note that the ratio of the peak heights between

and within separate components in the original tar spectrum (Figure 4b) and the predicted spectrum (Figure 4c) is alike.

Figure 5a, b, c shows the spectra of a typical Eastern hvAb coal from Pennsylvania, of the corresponding tar, and of the predicted tar. In this case the spectral subpatterns of the important components are markedly different between the coal and the tar. Nevertheless, when comparing Figures 5b and 5c the predicted and measured tar patterns show a very high degree of similarity and are distinctly different from the corresponding patterns in Figure 4.

CONCLUSIONS

The data presented here demonstrate that pyrolysis mass spectrometry in combination with canonical correlation analysis enables modeling and prediction of complex coal conversion processes such as the fixed bed liquefaction method. To the best of our knowledge this represents the first time that the chemical composition of coal-derived liquids has been predicted directly from feed coal characterization data. Moreover, the method is completely general and can be applied to all coal characterization data (whether obtained by conventional or by advanced spectroscopic techniques) and coal conversion processes in which the end products have been carefully characterized.

A shortcoming of the present study is the lack of a sufficiently large number of feed coal/coal tar pairs to allow adequate modeling and prediction of coal conversion behavior for more than two coal clusters. Also, a somewhat simplistic method was used to calculate predicted tar spectra based on a distance weighted average of the two nearest neighbors in a two-dimensional canonical correlation space.

REFERENCES

1. Khan, M.R., Proc. of Int. Symp. on Coal Science, Coal Science and Technology Series, J.A. Moulijn (ed.), Elsevier, 1987, p. 647.
2. Metcalf, G.S., Windig, W., Hill, G.R., Meuzelaar, H.L.C., Int. J. Coal Geology, 1987, 7, 245-268.
3. Chakravarty, T., Meuzelaar, H.L.C., Report to U.S. Dept. of Energy, July 1987, Contract #DEAP21-87MCO5073.
4. Windig, W., Meuzelaar, H.L.C., Anal. Chem., 1984, 56, 2297-2303.
5. Chakravarty, T., Windig, W., Taghizadeh, K., Meuzelaar, H.L.C., Shadle, L.J., Energy & Fuels, 1988 (in press).
6. Malinowski, E.R., Factor Analysis in Chemistry, Academic Press, New York, 1980.

ACKNOWLEDGEMENTS

The authors wish to acknowledge Ms. Barbara Hoesterey for her assistance in sample preparation and analyses. Helpful discussions with Dr. Willem Windig is also appreciated. This work was supported by the Department of Energy (Contract #DEAP21-87MCO5073). This work was sponsored in part by the Advanced Combustion Engineering Research Center. Funds for this Center are received from the National Science Foundation, the State of Utah, 21 industrial participants, and the U.S. Department of Energy. Additional funding was also provided by the Consortium for Fossil Fuel Liquefaction Science.

TABLE I
GEOGRAPHICAL ORIGIN AND RANK INFORMATION OF NINETEEN COAL SAMPLES

SERIAL #	PSOC #	GEOLOGICAL INFORMATION	RANK INFORMATION
1	-	Eastern/Appalachian, OH #6	hvAb
2	1481	ibid, Upper Clarion	hvAb
3	-	ibid, Wellmore #8	hvAb
4	375	ibid, Hazard #9	hvAb
5	267	ibid, Clintwood	hvAb
6	1472	ibid, Lower Banner	hvAb
7	-	ibid, Arkwright	hvAb
8	1469	ibid, Mary Lee	hvAb
9	123	ibid, Lower Kittanning	hvAb
10	1471	ibid, Pee Wee	hvAb
11	306	ibid, OH #12	hvAb
12	296	ibid, OH #5	hvAb
13	1475	ibid, Elkhorn #3	hvAb
14	275	ibid, OH #6A	hvAb
15	1492	Interior/Eastern, IL#5	hvBb
16	-	ibid, IL#6	hvCb
17	1323	ibid, IL#6	hvCb
18	181	ibid, Upper Block	sub. A
19	1520	N. Great Plains/Fort Union, Wyodak	sub. C

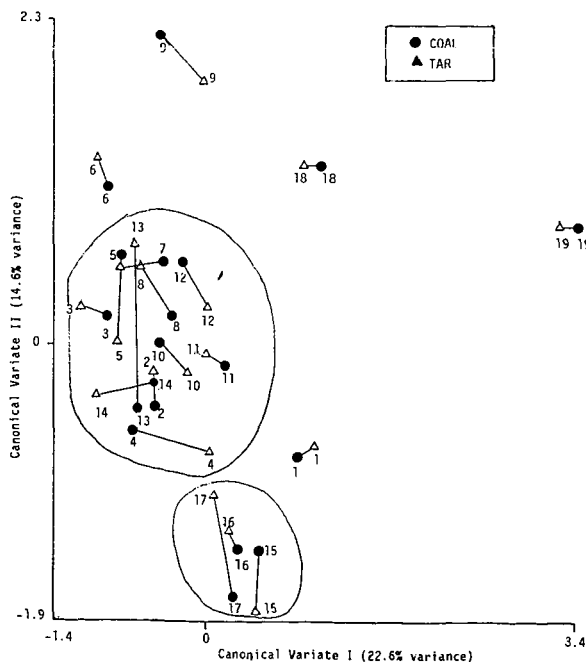


Figure 1. Score plot in the CVI/CVII space for both the coal and the tar samples. Note that only the means of the three scores for each category are plotted.

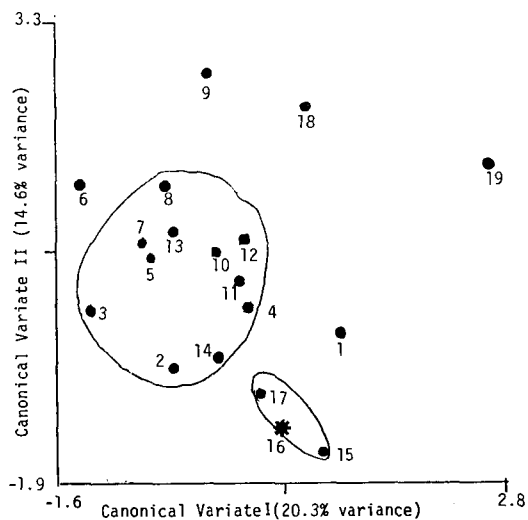


Figure 2. Effect of removing sample #16 from the coal data set on the score plot in the CVI/CVII space. Note the projected score of sample #16 (marked by *).

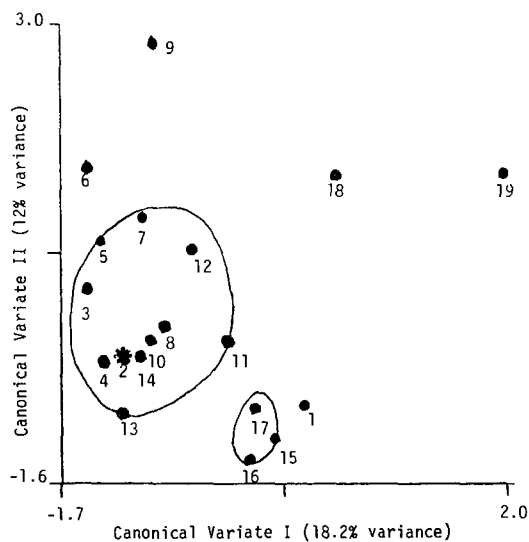


Figure 3. Effect of removing sample #2 from the coal data set on the score plot in the CVI/CVII space. Note the projected score of sample #2 (marked by *).

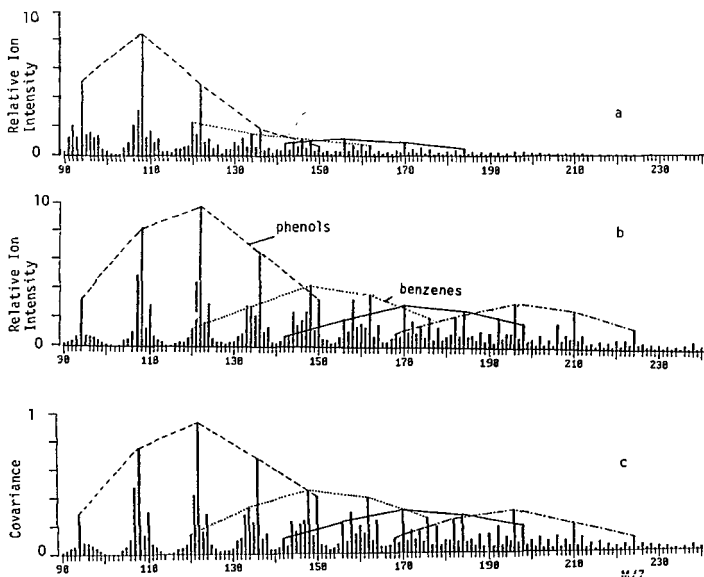


Figure 4. Pyrolysis mass spectrum of: (a) Illinois #6 hvCb coal; (b) direct probe mass spectrum of the corresponding tar, and (c) mathematically predicted spectrum.

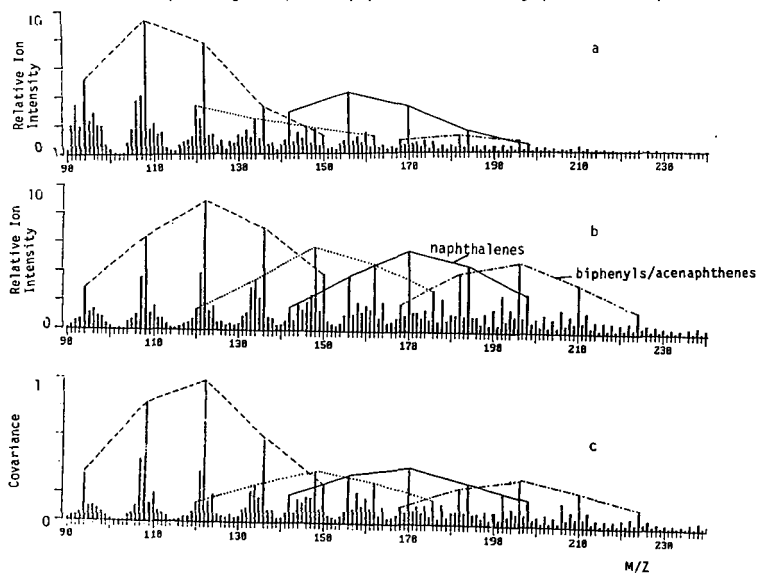


Figure 5. Pyrolysis mass spectrum of: (a) Upper Clarion hvAb coal; (b) direct probe mass spectrum of the corresponding tar, and (c) mathematically predicted spectrum.

PYROLYSIS OF COMPOUNDS CONTAINING POLYCYCLIC AROMATIC MOIETIES

MINOO JAVANMARDIAN, PATRICK J. SMITH, AND PHILLIP E. SAVAGE

DEPARTMENT OF CHEMICAL ENGINEERING
UNIVERSITY OF MICHIGAN
ANN ARBOR, MI 48109

INTRODUCTION

Coal is thought to exist in a complex, cross-linked, macromolecular framework in which polycyclic moieties are covalently linked together by aliphatic and heteroatomic bridges (1-3). The condensed aromatic groups can also bear peripheral, non-bridging moieties, including long aliphatic chains (4).

The pyrolysis of numerous compounds mimicking these structural features has provided considerable insight to the thermal reactions of coal. Previous pyrolyses were typically of compounds containing a single aromatic ring, which was intended to mimic the more massive condensed aromatic moieties in coal. It is possible, however, that single-ring compounds might not display the same reaction pathways and kinetics as otherwise identical compounds containing polycyclic aromatic moieties.

One difference between a single aromatic ring and the condensed aromatic moieties in coal is their sizes. This difference suggests that the model-compound-derived free radicals could be considerably more mobile than their coal-derived counterparts. To probe the influence of radical mobility on pyrolysis pathways Poutsma and coworkers (5-7) pyrolyzed coal model compounds immobilized on silica surfaces. They found that surface immobilization can lead to an enhancement of unimolecular pathways relative to bimolecular ones.

In an attempt to gain additional insight into the fundamentals of coal pyrolysis, and particularly the effects of condensed aromatics, we recently initiated experiments with compounds containing polycyclic aromatic moieties, which better represent the aromatic clusters in coal than do single-ring compounds. In this paper, we report on the pyrolysis of two compounds; 2-(3-phenylpropyl)-naphthalene (PPN), and 1-dodecylpyrene (DDP).

EXPERIMENTAL

PPN and DDP were pyrolyzed at isothermal temperatures between 350 and 425°C for batch holding times between 10 and 180 min.

Materials.

All chemicals were obtained commercially; 1-Dodecylpyrene (DDP) from Molecular Probes and 2-(3-phenylpropyl)-naphthalene (PPN) from API Standard Reference Materials, and used as received. The nominal purity of each compound was > 99%, and this was confirmed by GC analysis. PPN pyrolyses were accomplished in 1.5 x 100 mm Kimax glass capillary tubes, and DDP pyrolyses were in nominal 3/8" tubing bomb microreactors. The latter reactors were fashioned from a single Swagelok stainless steel port connector and two caps. The glass reactors were not routinely used with DDP because it is a fluffy solid and was difficult to load into the small diameter tubes. However, one experiment was done in a glass reactor to verify the absence of catalysis by the stainless steel surfaces in the tubing bomb microreactor.

Procedure.

The tubing bomb microreactors were typically loaded with about 10 - 30 mg of DDP and then about 10 mg of biphenyl was added to serve as an internal standard in the chromatographic analyses. All quantities were carefully (± 0.1 mg) weighed. The glass capillary tubes used for PPN pyrolyses were typically charged with 10 μ l of a previously prepared stock solution containing the model compound and the internal standard. The reactors were then sealed and immersed in a preheated, fluidized sand bath. After the desired reaction time had elapsed, the reactors were removed from the sand bath, rapidly cooled to room temperature to quench the reaction, and then opened. Reaction products were extracted in spectrophotometric grade acetone and analyzed by GC and GC-MS. Molar yields were calculated as the number of moles of product divided by the number of moles of reactant initially charged to the reactor.

RESULTS

The experimental results are presented primarily as the temporal variations of the products' molar yields. Tables I and II provide representative results for PPN and DDP, respectively, at each of the temperatures investigated. Based on the reproducibility of the results we estimate the uncertainty in product molar yields for PPN and DDP to be roughly $\pm 10\%$ and $\pm 25\%$, respectively.

PPN Pyrolysis.

PPN pyrolysis at 350°C yielded toluene, styrene, 2-methylnaphthalene, and 2-vinylnaphthalene as the major products, and at 60 min traces of ethylbenzene and 2-ethylnaphthalene were also detected. GC-MS analysis of the reaction products permitted tentative identification of two additional minor products as 2-isopropyl-naphthalene and 1,3-diphenylpropane. The pseudo-first-order rate constant for PPN disappearance was 0.007 min^{-1} .

Figure 1, which displays the temporal variation of the major products from PPN pyrolysis at 375°C, shows that the yields of toluene and 2-methylnaphthalene increased steadily throughout the 60 min reaction. The yields of styrene and 2-vinylnaphthalene decreased with holding time. The yields of ethylbenzene and 2-ethylnaphthalene were zero at short times, but they reached 6.2% and 8.5%, respectively at 60 minutes. The pseudo-first-order rate constant for PPN conversion at 375°C was 0.028 min^{-1} .

PPN pyrolysis at 400°C proceeded rapidly and was essentially complete at 60 min. Toluene and 2-methylnaphthalene were the major products, but the yields of ethylbenzene and 2-ethylnaphthalene were also substantial. The product alignment at 60 min was toluene (52%), 2-methylnaphthalene (48%), 2-ethylnaphthalene (19%), ethylbenzene (19%), styrene (0.8%), and 2-vinylnaphthalene ($< 0.1\%$). The pseudo-first-order rate constant was 0.076 min^{-1} .

Figure 2 presents the variation of the major products' molar yields with PPN conversion. Toluene and 2-vinylnaphthalene were present in nearly equal yields at low conversions. The yield of toluene increased to roughly 50% at complete conversion, whereas the yield of 2-vinylnaphthalene went through a maximum value (3.6%) and then decreased to 0. The yield of 2-ethylnaphthalene was very low at conversions $< 30\%$, but it increased rapidly at very high conversions. The yield of 2-methylnaphthalene increased steadily with conversion to an ultimate value of nearly 50%. The yield of styrene, like that of 2-vinylnaphthalene, exhibited a maximum value and then decreased to zero. Finally, the yield of ethylbenzene was very low for conversions less than 50%, but it increased to 19% when conversion was nearly complete.

The disappearance of PPN correlated well with first-order kinetics, and the Arrhenius parameters for the pseudo-first-order rate constant were $[\log_{10} A (\text{sec}^{-1}), E^* (\text{kcal/mol})] = [10.0, 39.8]$.

DDP Pyrolysis.

DDP pyrolyses led to pyrene, methylpyrene, dodecane, nonane, and undecene as the major products at short reaction times. Minor products included series of n-alkanes ($C_8 - C_{12}$), α -olefins ($C_8 - C_{12}$), and alkylpyrenes. GC-MS analysis revealed the presence of a compound tentatively identified as pyrenylpropene. No other pyrenylalkenes were present in yields sufficiently high to be quantified. In addition to the molecular products noted above, an acetone-insoluble char formed as a result of DDP pyrolysis.

The yields of each of the major products from DDP pyrolysis at 375°C increased with batch holding time. The ultimate yields of pyrene, dodecane, nonane, methylpyrene, and undecene were 52%, 28%, 7.0%, 6.7%, and 1.4%, respectively, at 180 min. The yields of several n-alkanes and ethylpyrene increased more rapidly than did the yield of undecene, and these products were more abundant than undecene at the more severe conditions.

The major products from DDP pyrolysis at 400°C and at short times were pyrene, dodecane, methylpyrene, nonane, and undecene. At longer batch holding times the yields of some n-alkanes increased and surpassed the undecene yield, which reached a maximum value of 1.9% at 60 min. The yields of pyrene, dodecane, nonane, and methylpyrene increased with time and achieved ultimate values of 49%, 32%, 9.4%, and 8.3%, respectively at 180 min.

DDP pyrolysis at 425°C was rapid and essentially complete at 45 min. The major products at short reaction times were the same as those observed at the lower temperatures, and Figure 3 displays the temporal variation of their yields. The yields of pyrene, dodecane, nonane, and methylpyrene were relatively time invariant after 60 minutes, and their ultimate values were approximately 49%, 25%, 10%, and 10%, respectively. Undecene, on the other hand, exhibited a maximum yield of 3.1% at 15 min and then its yield decreased to undetectable levels at 120 min.

Figure 4 displays the distribution of alkanes and olefins produced from DDP pyrolysis at 425°C and 17 min. The alkane distribution exhibits a peak at nonane (C₉) and a higher one at dodecane (C₁₂). The olefinic products were relatively evenly distributed with the exception of the high undecene yield. Note that with the exception of C₁₁, alkanes were present in yields higher than the corresponding olefins.

DISCUSSION

PPN Pyrolysis.

Figure 2 shows that the product pairs toluene plus 2-vinylnaphthalene and 2-methylnaphthalene plus styrene were present in nearly equal yields at low conversions. This is consistent with the formation of each product pair in a common reaction step. Furthermore, the non-zero initial slopes apparent in the molar yield vs. time curves (i.e., Figure 1) for each of these four products indicates that these are primary reaction products. On the other hand, the initial slopes associated with 2-ethylnaphthalene and ethylbenzene are zero, thus these are secondary products. That the yields of 2-vinylnaphthalene and styrene go through a maximum and then decrease to zero is consistent with their participating in secondary reactions. Toluene and 2-methylnaphthalene were apparently stable at the temperatures studied.

These observations combine to suggest the reaction pathway shown in Figure 5 for PPN pyrolysis. The nearly equal yields of 2-methylnaphthalene and toluene (e.g., both were nearly 50% at essentially complete PPN conversion) indicate that the stoichiometric coefficients ν_1 and ν_2 are both approximately equal to 0.5.

The primary pyrolysis pathway deduced for PPN is essentially the same as that reported for 1,3-diphenylpropane (8-10), the single-ring analogue of PPN. This suggests that, in this instance, substituting a naphthyl for a phenyl moiety does not detectably alter the operative reaction pathways or the reaction mechanism. Note however that this is not true of the reaction rates. The pseudo-first-order rate constants for PPN reported here were 4-10 times as high as pseudo-first-order rate constants determined from data presented by Poutsma and Dyer (8) for the liquid-phase pyrolysis of diphenylpropane. [Note: diphenylpropane pyrolysis was reported to be 3/2 order (8,9) thus the calculated pseudo-first-order rate constants are the product of the intrinsic rate constant and the square root of the concentration. We used the highest reaction rates reported (e.g., for liquid-phase pyrolyses) to calculate pseudo-first-order rate constants for diphenylpropane.]

DDP Pyrolysis.

Some aspects of DDP pyrolysis are consistent with previous results from the thermal cracking of dodecylbenzene (11,12) and other long-chain n-alkylbenzenes (13,14). Dodecylbenzene pyrolysis (11, 12) was via a free-radical mechanism, and the two pairs of major products, toluene plus undecene and styrene plus decane, arose from β -scission of a γ and an α -dodecylbenzene radical, respectively. The minor products comprised complete series of n-alkanes, α -olefins, alkylbenzenes, and phenylalkenes. Only traces of benzene were detected.

Elements of similar free-radical reactions appear to be operative in DDP pyrolysis. Methylpyrene and undecene were present in relatively high yields at mild reaction conditions, and these are the expected ultimate products from β -scission of a γ -DDP radical. Similarly the product pair nonane plus pyrenylpropene could have been formed via β -scission of a β -DDP radical. Finally, as observed in dodecylbenzene pyrolysis, series of alkanes and olefins and some alkylaromatics were produced as minor products from DDP pyrolysis.

Although some aspects of DDP pyrolysis parallel those of its single-ring analogue, there are several interesting differences. The appearance of pyrene and dodecane as the major products from DDP pyrolysis indicates that rupture of the aryl-alkyl C-C bond was facile. This is not expected on the basis of the free-radical reaction mechanism proposed (12) for dodecylbenzene because this C-C bond is the strongest in the

alkyl chain and hence most resistant to cleavage. Furthermore, the alkane distribution for DDP pyrolysis showed a peak at n-nonane, but no such preferential formation of nonane was observed in the pyrolysis of n-alkylbenzenes (11-14).

Finally, pyrene and dodecane together contain more hydrogen than the reactant, DDP. Thus formation of these as major products requires the simultaneous formation of hydrogen-deficient products in relatively high yields. GC analyses revealed no such products, thus we conclude that the experimentally observed, acetone-insoluble char was the source of this hydrogen.

SUMMARY AND CONCLUSIONS

The pyrolytic pathway for PPN was identical to that of its single-ring analogue, 1,3-diphenylpropane. The apparent first-order kinetics of PPN disappearance were 4-10 times more rapid however. On the other hand, both the pathways and kinetics of DDP pyrolysis differed from those of its single-ring analogue, dodecylbenzene. The major products of DDP pyrolysis, pyrene and dodecane, indicate that bond cleavage occurred predominantly at the ring, whereas the primary pathways in dodecylbenzene pyrolysis involved cleavage of the covalent bonds between the α and β carbons and the β and γ carbons to produce toluene plus undecene and styrene plus decane, respectively. The results of this study demonstrate that the thermal reaction pathways and kinetics of compounds containing condensed aromatic moieties can differ from those of their single-ring analogues.

ACKNOWLEDGEMENT

This work was supported in part by a grant from the University of Michigan Office of Energy Research.

LITERATURE CITED

1. Gorbaty, M. L., Ouchi, K., Eds. Coal Structure, ACS Adv. Chem. Ser. No. 192 1981.
2. Gorbaty, M. L., Larsen, J. W., Wender, I., Eds. Coal Science, Academic Press, NY 1982.
3. Meyers, R. A., Ed. Coal Structure, Academic Press, NY 1982.
4. Nelson, P. F., *Fuel* 1987, 66, 1264.
5. Buchanan, A. C., Dunstan, T. D. J., Douglas, E. C., Poutsma, M. L. *J. Am. Chem. Soc.* 1986, 108, 7703.
6. Poutsma, M. L., Douglas, E. C., Leach, J. E. *J. Am. Chem. Soc.* 1984, 106, 1136.
7. Buchanan, A. C., Biggs, C. A. *ACS Div. Fuel Chem. Prepr.* 1987, 32, 175.
8. Poutsma, M. L., Dyer, C. W. *J. Org. Chem.* 1982, 47, 4903.
9. Gilbert, K. E., Gajewski, J. J. *J. Org. Chem.* 1982, 47, 4899.
10. Sweeting, J. W., Wilshire, J. F. K. *Aust. J. Chem.* 1962, 15, 89.
11. Blouri, B., Hamdan, F., Herault, D., *Ind. Eng. Chem. Process Des. Dev.* 1985, 24, 30.
12. Savage, P. E., Klein, M. T., *Ind. Eng. Chem. Research* 1987, 26, 374.
13. Mushrush, G. W., Hazlett, R. N., *Ind. Eng. Chem. Fundam.* 1984, 23, 288.
14. Savage, P. E., Klein, M. T., *Ind. Eng. Chem. Research* 1987, 26, 488.

TABLE I: Yields (%) of Major Products from PPN Pyrolysis

TIME (min) →	350°C			375°C			400°C		
	10	31	61	11	30	60	20	30	60
Toluene	2.0	5.7	10.	7.8	20.	35.	39.	44.	52.
Ethylbenzene	-	-	0.6	-	1.5	6.2	6.9	11.	19.
Styrene	1.9	3.5	3.8	10.	6.0	4.1	7.1	4.5	0.8
2-Methylnaphthalene	2.2	6.2	11.	8.2	21.	35.	39.	43.	48.
2-Ethyl-naphthalene	-	-	1.0	-	2.4	8.5	9.7	14.	19.
2-Vinylnaphthalene	1.8	2.1	2.1	3.5	2.9	1.5	2.8	1.2	-
PPN	88.	78.	64.	77.	44.	20.	15.	8.4	1.1

TABLE II: Yields (%) of Major Products from DDP Pyrolysis

TIME (min) →	375°C			400°C			425°C		
	60	120	180	30	90	180	11	60	120
Hexene	-	-	-	-	-	-	-	1.3	1.5
Hexane	-	-	-	-	1.5	2.6	-	4.1	8.5
Heptene	-	-	-	-	-	-	-	1.1	1.5
Heptane	-	-	1.1	-	1.3	2.2	-	3.2	5.6
Octene	-	-	-	-	-	-	-	0.9	0.8
Octane	0.4	1.2	1.7	0.5	2.0	3.2	-	4.0	5.9
Nonene	-	-	-	-	-	-	-	0.7	0.6
Nonane	1.4	4.9	7.0	2.8	7.7	9.4	2.6	10.	13.
Decene	-	-	-	-	-	-	-	0.6	0.6
Decane	0.7	1.6	2.3	1.5	3.6	4.5	2.0	5.5	6.9
Undecene	0.8	1.2	1.4	1.8	1.2	-	2.5	1.1	-
Undecane	0.5	2.0	3.5	0.8	4.9	6.5	-	6.4	7.7
Dodecene	-	-	0.6	-	0.6	-	-	0.9	-
Dodecane	4.5	19.	28.	9.6	28.	32.	6.9	25.	28.
Pyrene	8.6	46.	52.	17.	40.	49.	12.	48.	50.
Methylpyrene	2.0	6.3	6.7	3.6	5.5	8.3	4.4	10.	10.
Ethylpyrene	0.7	2.2	2.1	1.6	1.9	1.8	2.4	2.5	1.7
Pyrenylpropene	-	-	-	2.2	-	-	1.9	-	-
DDP	69.	68.	36.	46.	4.8	-	51.	-	-

Note: - indicates product yields too low to be determined quantitatively

FIGURE 1: TEMPORAL VARIATION OF PRODUCT YIELDS FROM PPN PYROLYSIS AT 375C

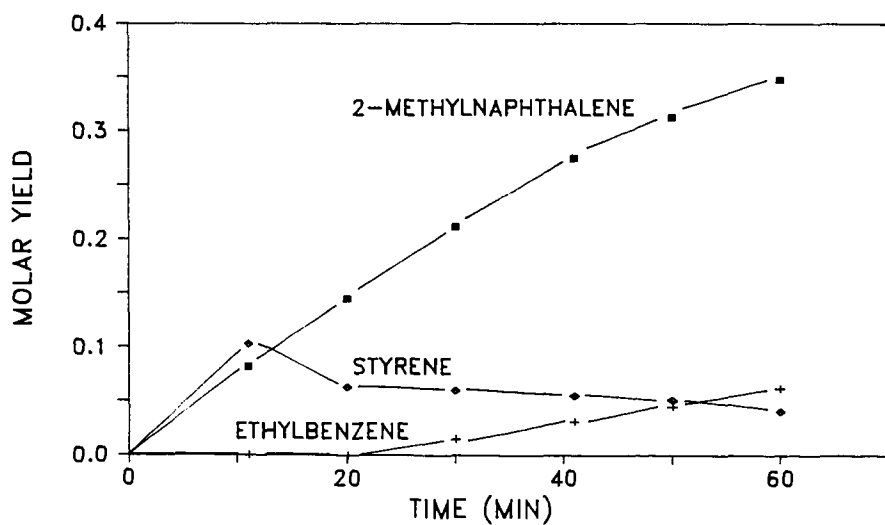
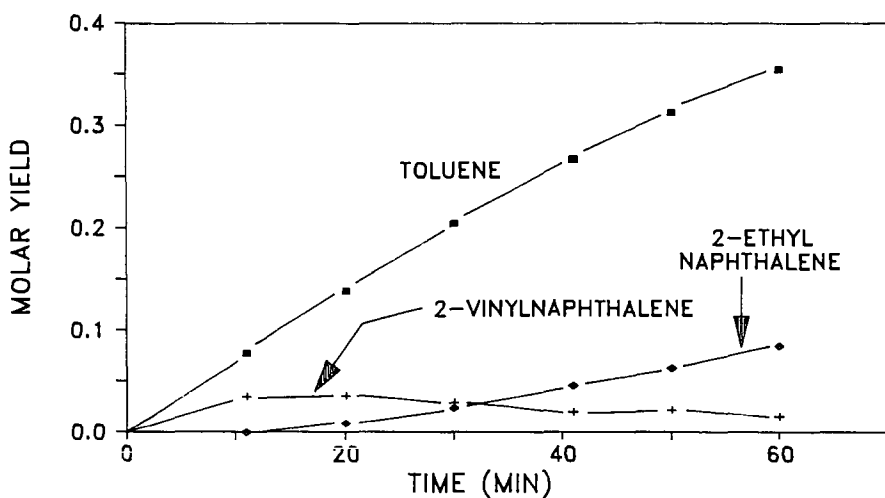


FIGURE 2: VARIATION OF PRODUCT YIELDS WITH PPN CONVERSION

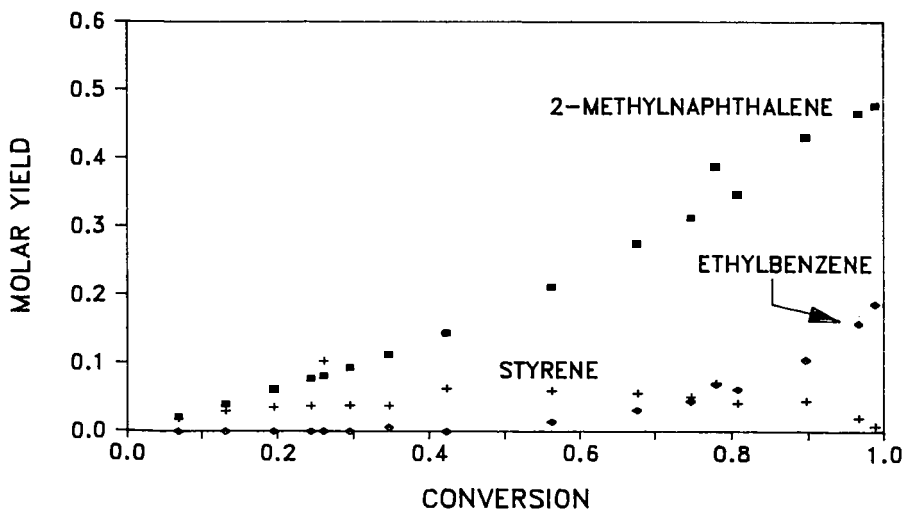
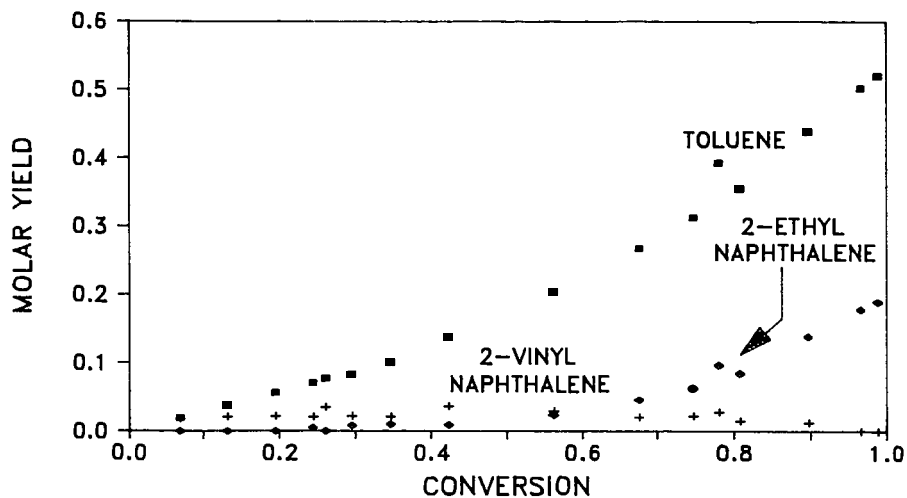


FIGURE 3: TEMPORAL VARIATION OF PRODUCT YIELDS FROM DDP PYROLYSIS AT 425C

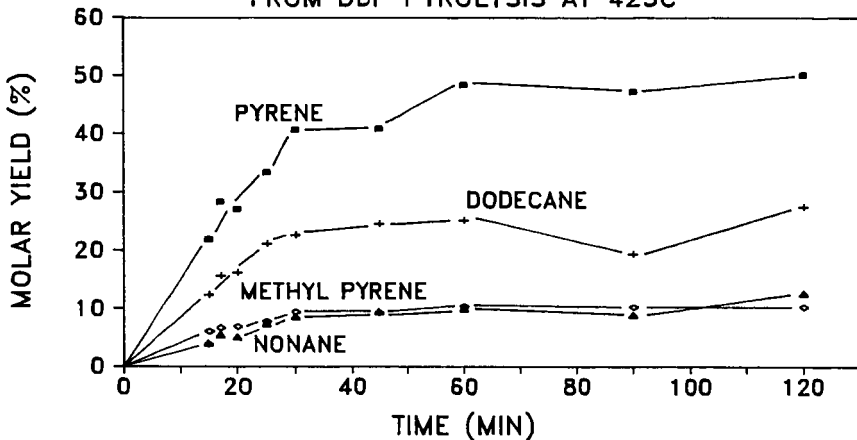


FIGURE 4: VARIATION OF OLEFIN AND ALKANE YIELDS FROM DDP PYROLYSIS (425C, 17 MIN)

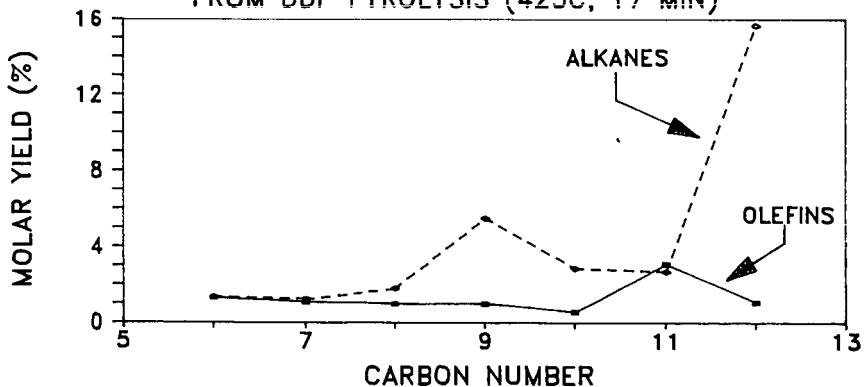
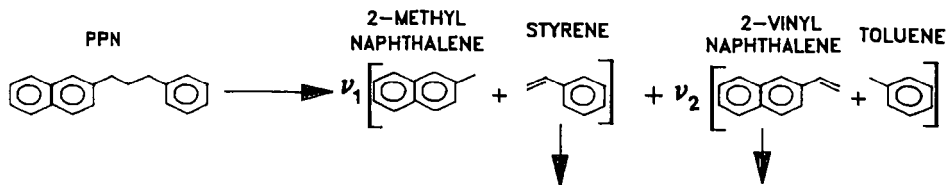


FIGURE 5: PPN PYROLYSIS PATHWAY



PYROLYSIS OF A BINARY HYDROCARBON MIXTURE: REACTION MODELING

PHILLIP E. SAVAGE

DEPARTMENT OF CHEMICAL ENGINEERING
UNIVERSITY OF MICHIGAN
ANN ARBOR, MI 48109

INTRODUCTION

Numerous pyrolyses of coal model compounds (e.g., refs 1-5) have provided substantial insight into the thermal reactions of the moieties they mimicked. The results of experiments with single compounds, however, provide no information about the interactions that can occur between the distinct chemical components in complex reactants such as coal. Because an active center (e.g., free radical) derived from one chemical moiety can react with a second, different moiety, reaction pathways that are important for the pyrolysis of a single model compound might not be equally important for the model-compound-like moiety in a coal macromolecule. Conversely, pathways unobserved in single-component pyrolyses might be operative in coal pyrolysis.

Previous reports of the pyrolysis of binary mixtures of high-molecular-weight compounds, though few (6), demonstrated that reactions between active centers derived from the two different compounds or between an active center from one compound and the second compound itself can affect the reaction rates, product selectivities, and reaction pathways. Zhou and Crynes (7), for example, pyrolyzed isomeric ethylphenols in dodecane and found that ethylphenol inhibited the rate of dodecane cracking and that dodecane accelerated the rate of ethylphenol conversion. They postulated that the interactions between the ethylphenol-derived and dodecane-derived radicals were considerable and were responsible for the differences between the pure compound and copyrolysis results. Allen and Gavalas (8) reported that the rate of decomposition of methylene and ether bridges in coal model compounds was enhanced when the compounds were pyrolyzed in 1,2-dihydronaphthalene (dialin). They suggested that an aromatic displacement reaction with atomic hydrogen (formed from dialin decomposition) was responsible for the accelerated bridge decomposition.

To gain additional insight into the pyrolysis of binary mixtures of high-molecular-weight compounds, a reaction model has been developed to simulate the copyrolysis of tetradecylbenzene (TDB) and dodecylcyclohexane (DDC). These compounds mimic alkylaromatic and alkylnaphthenic moieties in coal and asphaltenes.

REACTION MODEL

The essential features of the free-radical pyrolysis of both long-chain alkylbenzenes and alkylcyclohexanes can be modeled as three parallel chains coupled via chain transfer steps (9-11). These three chains arise because there are only three types of aliphatic carbons in TDB and in DDC that exhibit unique reactivities. In TDB, hydrogen abstraction at the α carbon leads to a resonance-stabilized, secondary benzylic radical whereas abstraction at all other positions produces a less stable secondary alkyl radical. Thus the α carbon possesses unique kinetics in the hydrogen abstraction step. Unique among the non- α radicals in TDB, the γ radical leads to a resonance-stabilized, primary benzyl radical upon β -scission, whereas β -scission of all other TDB radicals produces a primary alkyl radical. Thus β -scission of the γ radical is the fastest decomposition step. All non- α and non- γ positions in TDB share roughly equal reactivities for hydrogen abstraction and β -scission and therefore collectively constitute the third category.

Similar to the influence of the aromatic ring and the resultant preferential formation of benzylic radicals in TDB, the naphthenic ring in DDC affords preferential formation of tertiary radicals in hydrogen abstraction steps and secondary radicals in β -scission steps. Hydrogen abstraction at the ring carbon bearing the aliphatic chain, which produces a tertiary DDC radical, is the fastest abstraction step because abstraction

at all other positions yields less stable secondary radicals. β -scission of the β -DDC radical, which produces a secondary cyclohexyl radical is the unique decomposition step because all other β -scission steps lead to primary alkyl radicals. All non- β and non-tertiary positions in DDC share roughly equal reactivities for both hydrogen abstraction and β -scission.

The previously discerned (9-11) elementary reaction steps for neat pyrolysis of TDB and DDC, summarized in Figure 1, include a single initiation step and termination by all possible radical recombinations. R denotes a reactant molecule, and the superscripts A and B refer to TDB and DDC, respectively. Following standard notation, μ radicals are those that participate in unimolecular propagation steps, and β radicals propagate chain reactions via bimolecular steps. Table I provides the chemical identities of the species in Figure 1.

Pyrolysis proceeds via the three parallel chain reactions in the center column of Figure 1 to produce β_1 H plus Q_1 , β_2 H plus Q_2 , and β_3 H plus Q_3 as the major products. Chain transfer, depicted in the two peripheral columns, can occur via both μ and β radicals. The interaction steps take the form of a free radical derived from one compound abstracting hydrogen from the second compound and additional termination steps involving the recombination of radicals derived from the two different substrates. Note that the copyrolysis mechanism of Figure 1 depicts only the primary reactions.

KINETICS DEVELOPMENT

Reaction rate expressions were derived for TDB and DDC on the basis of the mechanism in Figure 1 by invoking the pseudo-steady-state and long-chain approximations (12,13). These approximations allow formulation of the algebraic β_i balance for compound A (TDB) as Equation 1,

$$r_{\beta_i}^A = 0 = k_{\mu_i}^A \mu_i^A - \sum_{j=1}^3 k_{ij}^{AA} \beta_j^A R^A - \sum_{j=1}^3 k_{ij}^{AB} \beta_j^A R^B \quad (1)$$

and this permits solution for μ_i^A as

$$\mu_i^A = y_i^A \beta_i^A \quad (2)$$

where

$$y_i^A = \frac{k_i^{AA} R^A + k_i^{AB} R^B}{k_{\mu_i}^A} \quad (3)$$

with $k_i^{AA} = \sum_{j=1}^3 k_{ij}^{AA}$ and $k_i^{AB} = \sum_{j=1}^3 k_{ij}^{AB}$.

Similarly, the β_i^B balance leads to

$$\mu_i^B = y_i^B \beta_i^B \quad (4)$$

where the expression for y_i^B can be obtained from Equation 3 by transposing the A and B superscripts.

The double subscript notation employed for the hydrogen abstraction rate constants identifies, respectively, the attacking radical and the resultant μ radical. The double superscript notation identifies, respectively, the substrate from which the attacking radical was derived and the substrate attacked. Primed and unprimed rate constants denote hydrogen abstraction from either of the substrates by μ and β radicals, respectively.

The long-chain, steady-state μ_i^A balance is given as Equation 5.

$$r_{\mu_i}^A = 0 = \sum_{j=1}^3 k_{ji}^{AA} \beta_j^A R^A - k_{\mu_i}^A \mu_i^A - \sum_{j=1, j \neq i}^3 k_{ij}^{AA} \mu_j^A R^A + \sum_{j=1, j \neq i}^3 k_{ji}^{AA} \mu_j^A R^A - \sum_{j=1}^3 k_{ij}^{AB} \mu_i^A R^B + \sum_{j=1}^3 k_{ji}^{BA} \mu_j^B R^A + \sum_{j=1}^3 k_{ji}^{BA} \beta_j^B R^A \quad (5)$$

The balance for μ_i^B is completely analogous and can be obtained by transposing the A and B superscripts in Equation 5.

Substituting Equations 2 and 4 for the concentrations of the μ_i^A and μ_i^B radicals, respectively, into Equation 5 leads, after considerable rearrangement, to Equation 6.

$$\sum_{j=1 \neq i}^3 Z_{ji}^{AA} \beta_j^A + \sum_{j=1}^3 Z_{ji}^{BA} \beta_j^B = \beta_i^A \left(\sum_{j=1 \neq i}^3 Z_{ij}^{AA} + \frac{R^B}{R^A} \left(\sum_{j=1}^3 Z_{ij}^{AB} \right) \right) \quad (6)$$

where

$$Z_{ij}^{AA} = k_{ij}^{AA} + y_i^A k_{ij}^{AA} \quad (7)$$

$$Z_{ij}^{BA} = k_{ij}^{BA} + y_i^B k_{ij}^{BA} \quad (8)$$

Expressions for Z_{ij}^{BB} and Z_{ij}^{AB} can be obtained from Equations 7 and 8, respectively, by transposing their superscripts.

Equation 6 and the analogous set of equations for substrate B provide five independent equations in the six unknowns β_i^A and β_i^B . Thus a balance on the total radical population must be written to solve for the individual radical concentrations and ultimately the reaction rate. The free radical concentration changes only as a result of initiation and termination steps, thus applying the pseudo-steady-state approximation to the net rate of radical production results in equating the rates of initiation and termination.

Since both theory and experimental evidence suggest that rate constants for radical recombinations are typically $10^{9.0 \pm 0.5}$ l/mol-s (14,15), all termination rate constants were taken to be equal except for the statistical factor (16) that renders the rate constant for combination of two identical radicals, ω_T , one-half that for two dissimilar species. This approximation combines with the initiation and termination steps depicted in Figure 1 to give Equation 9 as the steady-state radical balance.

$$\alpha_f^A R^A + \alpha_f^B R^B = \omega_T \left[\sum_{i=1}^3 (\mu_i^A + \mu_i^B + \beta_i^A + \beta_i^B) \right]^2 \quad (9)$$

Eliminating μ_i^A and μ_i^B from Equation 9 via Equations 2 and 4, respectively, gives Equation 10.

$$\left[\frac{\alpha_f^A R^A + \alpha_f^B R^B}{\omega_T} \right]^{1/2} = \sum_{i=1}^3 \left[\beta_i^A (1 + y_i^A) + \beta_i^B (1 + y_i^B) \right] \quad (10)$$

This equation, Equation 6, and analogous expressions for substrate B were solved numerically for the β radical concentrations with estimated rate constants as parameters. Table II summarizes the Arrhenius parameter estimates used in the reaction model. These values are representative of literature estimates (1,2,14,15,17-22) for similar types of reactions.

The reaction rates were then determined from the long-chain rate expressions below.

$$-r_A = R^A \sum_{i=1}^3 \left[\beta_i^A (k_i^{AA} - \frac{R^B}{R^A} k_i^{AB} y_i^A) + \beta_i^B (k_i^{BA} + k_i^{BA} y_i^B) \right] \quad (11)$$

$$-r_B = R^B \sum_{i=1}^3 \left[\beta_i^B (k_i^{BB} - \frac{R^A}{R^B} k_i^{BA} y_i^B) + \beta_i^A (k_i^{AB} + k_i^{AB} y_i^A) \right] \quad (12)$$

Relative rates for DDC and TDB pyrolysis were calculated as the ratio of the rate at a given value of [TDB]/[DDC] (or [DDC]/[TDB]) to the rate calculated for the pyrolysis of the pure compound.

RESULTS AND DISCUSSION

Figure 2 displays the relative rates calculated for DDC and TDB pyrolysis at 400°C as functions of the absolute concentration of substrate and the relative concentrations of the two components.

At a DDC concentration of 0.001M, the addition of small quantities of TDB accelerated DDC pyrolysis, and the relative rate reached a maximum value of 1.14. Further additions of TDB inhibited the rate, and it decreased to a minimum value of 1.06. Interestingly, upon continued addition, TDB again accelerated DDC pyrolysis. At $[DDC] = 0.01M$, TDB initially accelerated the rate, and a maximum value of 1.28 was attained. Additional quantities of TDB reduced the relative rate. A maximum relative rate was also observed at $[DDC] = 0.10M$. In this case the maximum value was 1.10 at a $[TDB]/[DDC]$ ratio of 0.0158. When $[DDC] = 1.00M$, however, TDB acted only as an inhibitor.

The results for simulated TDB pyrolysis in the presence of added DDC at 400°C show that DDC had little effect on the relative rate until high ($> 10^{-1}$) $[DDC]/[TDB]$ ratios were attained. At these high ratios, DDC accelerated TDB pyrolysis for $[TDB] = 0.001$ and $0.01M$. The addition of DDC had little ($< 0.3\%$) effect on TDB pyrolysis kinetics at the higher TDB concentrations.

These results clearly demonstrate that interactions occurring during the pyrolysis of a binary mixture of high-molecular-weight hydrocarbons can alter the apparent kinetics from those observed in pure component pyrolysis. They also show that inhibition and acceleration of reaction rates is a complex function of both the relative amounts of the two components as well as their absolute concentrations. For example, at a $[TDB]/[DDC]$ ratio of 0.05, TDB can either inhibit, accelerate, or have no effect on the relative rate of DDC disappearance depending on the DDC concentration.

ACKNOWLEDGEMENT

This work was supported in part by the University of Michigan Office of Energy Research.

LITERATURE CITED

1. Gilbert, K. E., Gajewski, F. J. *J. Org. Chem.*, **1982**, *47*, 4899.
2. Poutsma, M. L., Dyer, C. W. *J. Org. Chem.*, **1982**, *47*, 4903.
3. Panvelker, S. V., Shah, Y. T., Cronauer, D. C., *Ind. Eng. Chem. Fundam.*, **1982**, *21*, 236.
4. Benjamin, B. M., Raaen, V. F., Maupin, P. H., Brown, L. L., Collins, C. J., *Fuel*, **1978**, *57*, 269.
5. Cronauer, D. C., Jewell, D. M., Shah, Y. T., Modi, R. J., *Ind. Eng. Chem. Fundam.*, **1979**, *18*, 153.
6. Rebeck, C. in *Pyrolysis: Theory and Industrial Practice*, L. F. Albright, B. L. Crynes, W. H. Corcoran, Eds. Academic press **1983**.
7. Zhou, P., Crynes, B. L., *Ind. Eng. Chem. Process Des. Dev.*, **1986**, *25*, 898.
8. Allen, D. T., Gavalas, G. R. *Fuel*, **1984**, *63*, 586.
9. Savage, P. E., Klein, M. T., *Ind. Eng. Chem. Research* **1987**, *26*, 488.
10. Savage, P. E., Klein, M. T., *Ind. Eng. Chem. Research* submitted.
11. Savage, P. E., Klein, M. T., *Chem. Eng. Sci.* submitted.
12. Come, G., *J. Phys. Chem.*, **1977**, *81*, 2560.
13. Gavalas, G. R., *Chem. Eng. Sci.*, **1966**, *21*, 133.
14. Benson, S. W., *Thermochemical Kinetics*, John Wiley & Sons, New York **1976**.
15. Kochi, J. K., *Free Radicals*, John Wiley & Sons, New York **1973**.
16. Pryor, W. A., *Free Radicals*, McGraw-Hill **1966**.
17. Sundaram, K. W., Froment, G. F., *Ind. Eng. Chem. Fundam.*, **1978**, *17*, 174.
18. Kissin, Y. V., *Ind. Eng. Chem. Research*, **1987**, *26*, 1633.
19. Ranzi, E., Dente, M., Pierucci, S., Biardi, G., *Ind. Eng. Chem. Fundam.*, **1983**, *22*, 132.
20. Edelson, D., Allara, D. L., *Int. J. Chem. Kin.*, **1980**, *12*, 605.
21. Ebert, K. H., H. J. Ederer, and P. S. Schmidt, in *ACS Symposium Series No. 65*, V. W. Weekman and D. Luss, Eds. **1978**, 313.
22. Miller, R. E., Stein, S. E., *J. Phys. Chem.*, **1981**, *85*, 580.

TABLE I: IDENTITY OF SPECIES IN FIGURE 1 FOR TDB-DDC COPYROLYSIS

β_1^A	Benzyl Rad	μ_1^A	γ -TDB Rad	β_1^B	Cyclohexyl Rad	μ_1^B	β -DDC Rad
β_2^A	Dodecyl Rad	μ_2^A	α -TDB Rad	β_2^B	Undecyl Rad	μ_2^B	3°-DDC Rad
β_3^A	Non-TDB Rad	μ_3^A	Other TDB Rad	β_3^B	Non-DDC Rad	μ_3^B	Other DDC Rad
$\beta_1^A H$	Toluene	Q_1^A	Tridecene	$\beta_1^B H$	Cyclohexane	Q_1^B	Dodecene
$\beta_2^A H$	Dodecane	Q_2^A	Styrene	$\beta_2^B H$	Undecane	Q_2^B	Methylene Cyclohexane
$\beta_3^A H$	Minor Products	Q_3^A	Minor Products	$\beta_3^B H$	Minor Products	Q_3^B	Minor Products

TABLE II: RATE CONSTANT ESTIMATES FOR TDB-DDC COPYROLYSIS

Type of Reaction	log A (s^{-1} or $M^{-1}s^{-1}$)	E_A (kcal/mol)	Rate Constants
Initiation			
TDB	15.0	68.5	α_f^A
DDC	16.5	79.0	α_f^B
Termination			
	8.5	0	ω_T
β-scission*			
B	14.8	28.3	$k_{\mu_1}^A$
2°	13.0	28.5	$k_{\mu_2}^B$
1°	13.0	26.5	$k_{\mu_3}^A, k_{\mu_3}^B, k_{\mu_3}^B, k_{\mu_3}^B$
Hydrogen Abstraction**			
B + 2° H	8.5	18.5	$k_{21}^{A,B}, k_{11}^{A,A}, k_{13}^{A,A}, k_{21}^{A,A}, k_{23}^{A,A}, k_{23}^{A,B}$ $k_{11}^{A,B}, k_{13}^{A,B}$
B + 3° H	8.5	17.0	$k_{22}^{A,B}, k_{12}^{A,B}$
B + B H	8.5	14.0	$k_{12}^{A,A}$
3° + 2° H	8.5	14.5	$k_{21}^{B,B}, k_{23}^{B,B}, k_{21}^{B,A}, k_{23}^{B,A}$
3° + B H	8.5	10.0	$k_{22}^{B,A}$
2° + 2° H	8.5	12.5	$k_{13}^{A,A}, k_{31}^{A,A}, k_{11}^{B,B}, k_{13}^{B,B}, k_{13}^{B,B}, k_{31}^{B,B}, k_{11}^{A,B}, k_{13}^{A,B}$ $k_{13}^{A,B}, k_{31}^{A,B}, k_{33}^{A,B}, k_{31}^{B,A}, k_{33}^{B,A}, k_{11}^{B,A}, k_{13}^{B,A}$ $k_{11}^{B,A}, k_{13}^{B,A}$
2° + 3° H	8.5	11.0	$k_{12}^{B,B}, k_{12}^{B,B}, k_{32}^{B,B}, k_{12}^{A,B}, k_{32}^{A,B}$
2° + B H	8.5	8.0	$k_{12}^{A,A}, k_{32}^{A,A}, k_{12}^{A,A}, k_{32}^{A,A}, k_{12}^{B,A}$
1° + 2° H	8.5	10.5	$k_{21}^{A,A}, k_{23}^{A,A}, k_{31}^{A,A}, k_{33}^{A,A}, k_{21}^{B,B}, k_{23}^{B,B}, k_{31}^{B,B}$ $k_{21}^{A,B}, k_{23}^{A,B}, k_{33}^{A,B}, k_{31}^{A,B}, k_{21}^{A,B}, k_{23}^{A,B}, k_{31}^{A,B}$ $k_{31}^{B,A}, k_{33}^{B,A}$
1° + 3° H	8.5	9.0	$k_{22}^{B,B}, k_{32}^{B,B}, k_{22}^{A,B}, k_{32}^{A,B}$
1° + B H	8.5	6.0	$k_{22}^{A,A}, k_{32}^{A,A}, k_{22}^{B,A}, k_{32}^{B,A}$

* Reactions indicate type of radical produced (B - Benzyl, 2° - Secondary, 1° - Primary)

** Reactions indicate type of abstracting radical and type of hydrogen abstracted, respectively

FIGURE 1: TDB-DDC PRIMARY COPYROLYSIS MECHANISM

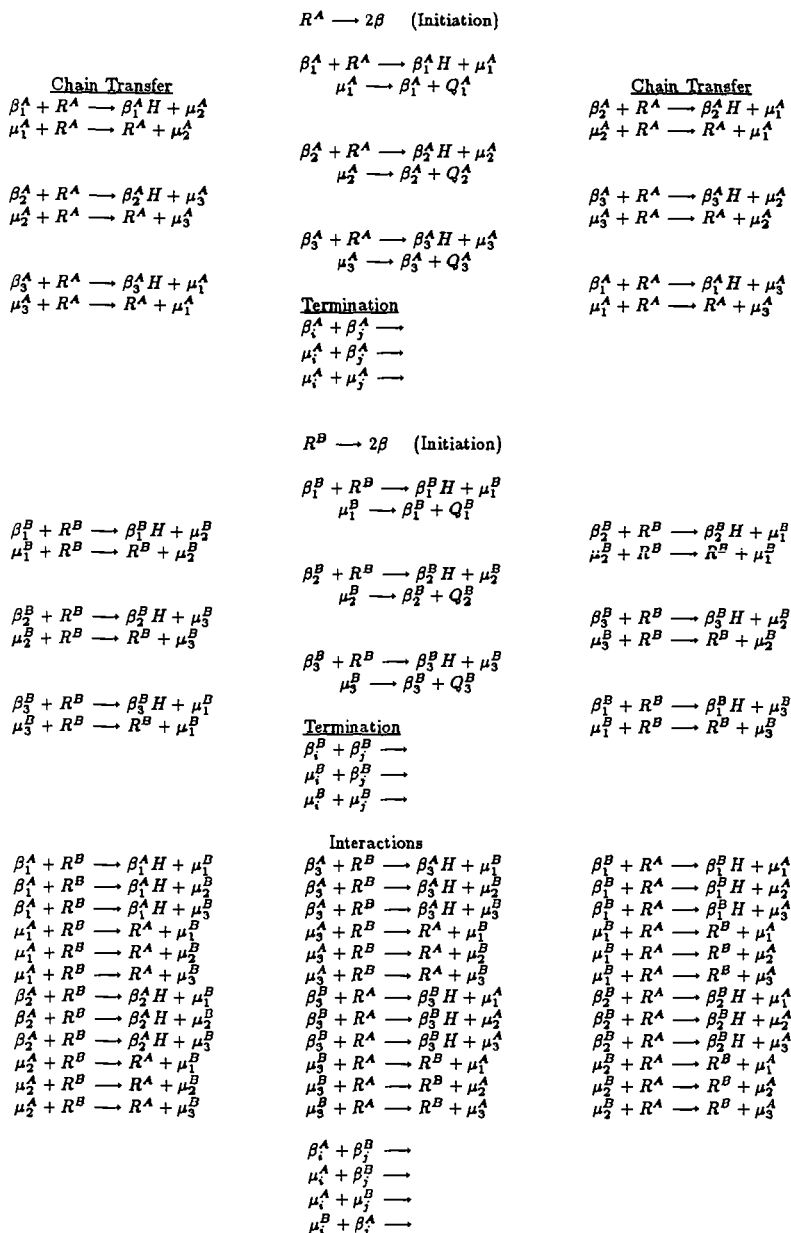
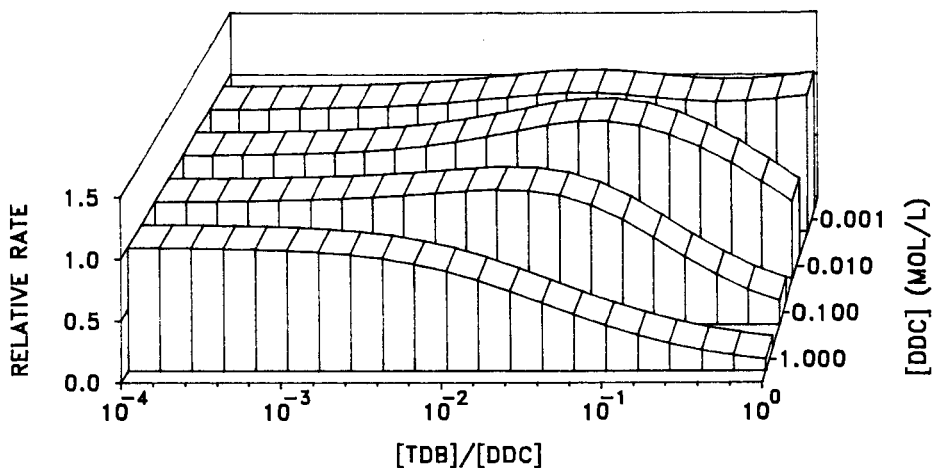
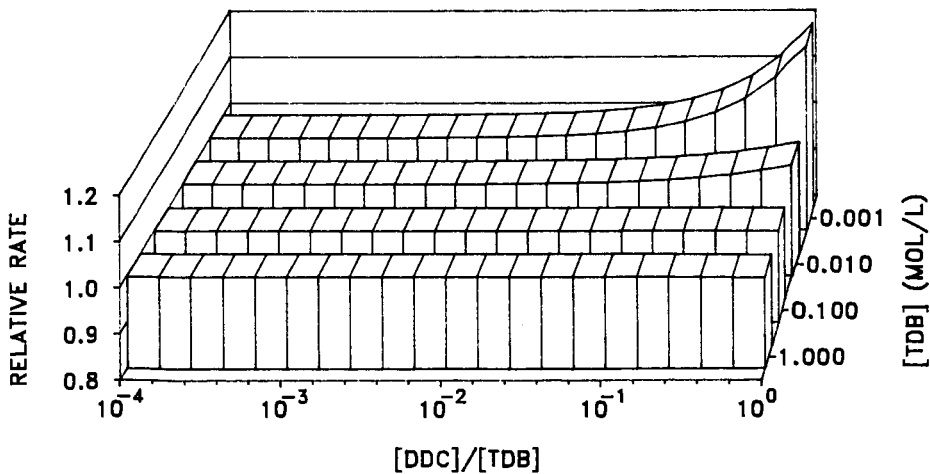


FIGURE 2: DDC-TDB COPYROLYSIS SIMULATION
RELATIVE RATE FOR DDC



RELATIVE RATE FOR TDB



PYROLYSIS OF COALS LOADED WITH POLYCYCLIC AROMATIC HYDROCARBONS

Ripudaman Malhotra, Gilbert St. John,
Doris S. Tse, and Donald F. McMillen

Chemical Kinetics Department, Chemical Physics Laboratory
SRI International, 333 Ravenswood Avenue, Menlo Park, CA 94025

INTRODUCTION

The relative simplicity of pyrolysis offers significant advantages as a coal conversion approach. However, char yields are typically high and volatile products are generally distributed between low value light hydrocarbons and tars that can be very difficult to upgrade. Consequently, the pyrolysis of coals under conditions that would produce larger yields of condensable and readily upgradable hydrocarbons is clearly a desirable goal, and the literature contains many examples of approaches to augmenting pyrolysis yields. For this reason, it is desirable that additional efforts be conducted as much as possible in light of what is known about the mechanism of volatiles production.

A fundamental aspect of the problem that is well recognized is the desirability of carrying out the process under reducing conditions in order to meet the stoichiometric requirements of bond rupture (replacement of C-C bonds with C-H bonds) and the ultimate desire (for fuel purposes) for substantially aliphatic products. This desirability has resulted in various hydrolysis approaches involving heating in the presence of medium- or high-pressure hydrogen. These approaches generally result in improved yields only when the reaction time is long, or when the temperature exceeds roughly 600°C (1112°F). (1,2) At short reaction times and temperatures below 600°C, the principal impact of H₂ pressure is to decrease volatile yields, apparently through the impeding of volatiles transport out of the coal and from the pyrolysis region. The lack of any enhancement in volatiles yield is a result of the fact that below 600°C, H₂, although thermodynamically powerful, is kinetically an ineffective reducing agent owing to the high strength of the H-H bond and the resulting difficulty in thermally achieving significant concentrations of hydrogen atoms. Unfortunately, the 400 to 600°C region is precisely where coals become very reactive, and need effective reducing agents to prevent retrograde processes.

Recent mechanistic work indicates that bond scissions occurring during liquefaction (3) and pyrolysis (4) are not simply spontaneous thermal rupture of inherently weak bonds, but include to a substantial extent hydrogen-transfer-induced scission of strong bonds as well. One potentially effective way of engendering scission of strong bonds is by H-transfer from hydroaromatic (cyclohexadienyl) radicals. This suggestion finds support in the work of Hutter and Sperling who have subjected several coals to rapid pyrolysis after loading with aromatics, hydroaromatics, or alkylaromatics and found increases in the tar yields and decreases in the char yields of 5 to 10 percentage points. (5) In contrast, Solomon and Serio have not observed any increase in the tar yields upon pyrolyzing coals in an atmosphere of aromatic hydrocarbons. (6) Earlier work by Mazumdar and coworkers with reduced coals shows significant enhancement in pyrolysis yields, but does not distinguish between the effect of hydroaromatic hydrogen introduction and bond cleavage that may have occurred during reduction. (7,8)

Other work in this area appears to have focused on the impact of such additives on liquefaction yields, and on meso-phase formation during coke production. Mochida and co-workers have found some hydrogenated petroleum pitches to be effective liquefaction

agents.(2) These same researchers, as well as a number of other workers, have found additives rich in PCAH to markedly extend the range of fluidity in time and temperature and to promote the development of anisotropy during coke formation.

In order that the loading with aromatics be an effective pretreatment, the reaction conditions must allow for an opportunity for the aromatics to react with the coal before they are simply devolatilized. Liquefaction and coking provide ample opportunity for reactions between the added aromatics and the coal while pyrolysis conditions generally do not favor such interactions. In this paper we report our efforts at determining the range of conditions under which loading of coals with PCAH may result in beneficial effects during pyrolysis.

EXPERIMENTAL PROCEDURE

Coals and Coal Loading. Three coals were tested in this study: a Wyodak (WYO-1, courtesy Univ. of Wyoming), an Illinois No. 6 (PSOC 1098), and a Pittsburgh No. 8 (PSOC 1099). The coals were loaded either with a highly aromatic coal tar (Wt. Av. MW 310) or a vacuum residue derived from a hydroprocessed petroleum pitch (Wt. Av. MW 908).

A simple evaporative loading technique has been used for all of the experiments reported here. The additive was dissolved in THF (stabilized) to produce a 10 wt% "solution," which was filtered through a 0.45 μ m millipore filter. The filtrate was added to the ground coal, and then removed, with periodic stirring, using a stream of argon. In order to minimize removal of extractable materials by THF, and to maximize deposition of the additive within the pores of the coal, the solution was added only to the point of incipient wetness. Nevertheless, since it was anticipated that some extraction would inadvertently occur and perhaps have a deleterious effect (10), "blank" coal samples were prepared by carrying out the loading procedure with pure THF. These THF-treated coals were used as the basis for judging the impact of the additives on loaded additive.

Pyrolysis. The TGA pyrolyses under argon were performed using a Dupont 1090 TGA system. The "rapid heating TGA" pyrolyses were performed using a specially constructed TGA consisting of a vertical tube furnace with a Cahn microbalance. The pyrolyses were performed with the maximum heating rate possible in this apparatus by raising the furnace, preheated to 1000°C, around a quartz vacuum envelope containing ~ 60 mg of coal suspended from the microbalance in a -1-inch diameter quartz flask. This procedure provided a heating rate of about 600°C/min as measured by a thermocouple placed near the flask containing the coal sample. The PY-FIMS experiments were carried out in the programmed temperature inlet of a field ionization mass spectrometer (FIMS). This instrument provides molecular ion profiles and organic weight loss as a function of temperature up to 500°C, and has been extensively used for analysis of high boiling, complex mixtures.

RESULTS

Following the rationale cited above, we have begun a series of experiments designed to test the effect on pyrolysis yields of loading coals with PCAH mixtures. We have thus far used three different pyrolysis techniques with slow to moderate heating rates. These are: pyrolysis-FIMS at high vacuum, TGA in one atmosphere of argon, and rapid heating TGA in vacuum, at heating rates of 2.5°C/min, 20°C/min, and 600°C/min respectively. The results from these experiments are shown in Table 1. The yields have been adjusted for tar vaporization, assuming that the volatility of the tar is not changed by being loaded into the coal. This assumption is of course not strictly true;

the temperature profile of the coal tar components in the PY-FIMS experiments show that vaporization is retarded by about 50°C. However, because the total amount of tar used is only about 10% of the weight of the coal, the error in overestimating tar volatility leads to no more than a 2% underestimate of the coal devolatilization.

From the limited data given in Table 1, we note two significant results. First, with none of the three pyrolysis techniques did the addition of 5 to 13 wt% of coal tar, hydrogenated coal tar, or vacuum resid from a hydrotreated petroleum resid, significantly increase the volatiles yield over THF-treated "blank" coals. Second, the THF treatment itself appears to have a deleterious effect on the release of volatiles from Wyodak coal, particularly above 500°C.

Effect of Changing Pyrolysis Conditions. It was anticipated that the impact of PCAH-loading would tend to increase with increasing heating rate and/or ability to retain the additive through the region of maximum tar formation reactivity. Specifically, since the results of Hüttlinger and Sperling (5) were obtained at heating rates of 1000°C/s, we felt that increasing the heating rate from 20°C/min to 600°C/min would increase the chances of seeing substantial beneficial effect. Furthermore, rapid heating is known to increase the impact of coking additives on fluidity.(11) Although the data in Table 1 definitely show higher yields for the 600°C/min heating in vacuum as expected (12), there was no improvement in the response to tar treatment itself even at this higher heating rate.

Pre-Hydrogenation of the Tar. Although FIMS and nmr analyses show the coal tar to have essentially no hydroaromatic character and only a small amount of alkylaromatic of the fluorene type), the known and projected benefits of large PCAH in shuttling indigenous coal hydrogen for use in conversion led us to use the tar as is for one series of experiments. However, because the added benefit of hydroaromatic hydrogen is well known, the tar was also subjected to mild hydrogenation and used for the coal treatment. The FI mass spectrum of the reduced tar showed 10 to 20 percent of the various PCAH were converted to the respective dihydroaromatics; nevertheless, treatment with this tar still showed no impact on pyrolysis yields.

Use of a Higher Boiling Additive. Since the coal tar itself was found to be 70% volatilized by 350°C (i.e., before the region of maximum chemical reactivity of the coal) under the atmospheric pressure TGA conditions and 88% under the PY-FIMS vacuum conditions, a slightly higher boiling additive was judged to be desirable under these slow heating conditions. Accordingly, we tested the use of the vacuum resid portion of a hydrogenated atmospheric resid (72% volatile at 350 under PY-FIMS conditions), but found this switch to a higher boiling (but less aromatic) additive did not result in any benefit to the pyrolyses, under the conditions thus far used.

DISCUSSION

Further efforts to define the extent of improvement in pyrolysis yields to be gained from PCAH additives as a function of coal type and reaction conditions will focus on the use of higher heating rates, higher boiling PCAH mixtures, and variations in the degree of sample confinement. It seems reasonable to assume any benefits to volatiles production will be maximized at high heating rate for the following three reasons.

- Volatiles yields tend to increase with increasing heating rates;(1,12)
- Coals of high fluidity tend to benefit most from this increase in heating rate;(3)
- PCAH additives increase fluidity under coking conditions.(11)

The probable impact of pressure is less clear. On the one hand, volatiles yields are often substantially larger under vacuum, owing to improved volatiles

transport. (1,12) On the other hand, higher pressures (up to 5 - 10 atm) have been reported to accentuate fluidity increases brought about by pitch additives. (11) Thus, it is not clear what trend will be observed with changing pressure. The experiments of Hüttinger and Sperling (5) were performed under nominal vacuum, but with the sample moderately confined in a Curie point pyrolysis capillary. This combination, along with the rapid heating, apparently resulted in enough of the various naphthalene derivatives remaining with the coal till temperatures of high coal reactivity were reached. Thus beneficial effects were observed notwithstanding the low boiling point of the additives. It was for this reason that we originally thought that a higher boiling tar, with PCAH components known to be much better coal conversion agents (albiet liquefaction) than naphthalene derivatives, would likely show significant beneficial effects - even at the lower heating rates used in this study.

The apparent detrimental effect of THF in the treatment of Wyodak coal is potentially informative, since low rank coals are known to be particularly susceptible to retrograde reactions or other factors that can significantly decrease their convertibility. In the present case, comparison of the FI-mass spectra of the raw and THF-treated Wyodak samples reveals the the high mass envelope (which is never large in this coal) is significantly decreased by the THF treatment. Examination of the temperature profiles for the peaks in this range shows that these are evolved at substantially lower temperatures than the dominant peaks in the spectrum, the dihydroxybenzenes and the phenols. The devolatilization of the high mass materials is consistent with these materials being more aliphatic and pre-existing in the coal, whereas the low molecular weight phenols and dihydroxybenes are products of pyrolysis. With this difference in mind, it may be significant that substantial detrimental effect of the THF treatment was not observed until the temperature exceeded 500°C: aliphatics, though they have high hydrogen content and are potential sources of hydrogen for hydrocracking, cannot generally make this hydrogen readily available until the thermal hydrolysis temperature range (i.e., ~ 600°C). The extent and nature of this detrimental effect will be further explored.

Acknowledgement: Financial support for this work by the U.S. Department of Energy, METC, under contract No. DE-AC21-87MC23286 is gratefully acknowledged.

REFERENCES

1. Howard, J. B., "Fundamentals of Coal Pyrolysis and Hyropyrolysis," in Chemistry of coal Utilization, Second Supplementary Volume, M. A. Elliott, Ed., John Wiley and Sons, New York, 1982, p. 665.
2. O'Brien, R. J.; Gibbins-Matham J. R.; Snape, C. E.; Kandiyoti, R. in Proceedings of the 1987 International Conference on Coal Science, J. A. Moulijn, K. A. Nater, and H.A.G. Chermin, Editors, Elsevier Science Publishers B. V., Amsterdam, 1987, p. 695.
3. McMillen, D. F.; Malhotra, R.; Chang, S.-J.; Hum, G. P., *Energy & Fuels*, 1987, 1, 193.
4. McMillen, D. F.; Malhotra, R.; Nigenda, S. E., "The Case for Induced Bond Scission During Coal Pyrolysis," *Am. Chem. Soc.*, Div. Fuel Chem. Preprints, 1987, 32(3), 180.
5. Hüttinger, K. J.; Sperling; R. E.; "Flash Hydrolysis of Coals Doped with Aromatics," in Proceedings of the 1987 International Conference on Coal Science,

J. A. Moulijn, K. A. Nater, and H.A.G. Chermin, Editors, Elsevier Science Publishers B. V., Amsterdam, 1987, p. 699.

6. Solomon, P. S.; Serio; M. A., private communication.
7. Bhattacharyya, A. C.; Mazumdar, B. K.; Lahiri, A., Fuel, 1964, 43, 181.
8. S. Ganguly; Mazumdar, B. K., Fuel, 1964, 43, 281.
9. Mochida, I; Moriguchi; Y.; Korai; Y.; Fujitsu, H.; Takeshita, K., Fuel, 1981, 60, 746.
10. O'Brien, R. J.; Gibbins-Matham J. R.; Kandiyoti, R., Fuel Processing Technology, 1987, 15, 71.
11. Green, P. D.; Patrick, J. W.; Mark Thomas, K; Walker, A., Fuel, 1985, 64, 1431.
12. Gibbins-Matham, J. R.; Kandiyoti, R., "The Effect of Heating Rate and Hold Time on Primary Coal Pyrolysis Product Distribution," Am. Chem. Soc., Div. Fuel Chem. Preprints, 1987, 32(4), 318.
13. Reasoner, J. W.; Hower, J. C.; Yates, L. P.; Lloyd, W. G., Fuel, 1985, 64, 1269.

Table 1

WEIGHT LOSS FOR PYROLYSIS OF COALS AND TAR LOADED COALS

Coal Treatment	2.5°C/min/vac 500°C	% Wt. Loss*			
		20°C/min/Ar		600°C/min/vac	
		500°C	900°C	500°C	900°C
Wyodak					
Raw	30	27.9	63.1	-	-
Blank (THF)	32	22.0	43.8	41.8	61.7
Coal-Tar	34	22.0	44.8	36.6	54.5
H-Coal-Tar	32	-	-	40.4	53.4
Ill. No. 6					
Raw	-	12.0	30.3	-	-
Blank (THF)	32	16.5	31.9	-	-
Coal-Tar	29	8.7	30.3	-	-
H-Coal-Tar	-	-	-	-	-
H-Pet-Res	28	-	-	-	-
Pitts. No. 8					
Raw	-	-	-	-	-
Blank (THF)	-	-	-	30.0	46.8
H-Coal Tar	-	-	-	30.9	45.6
H-Pet-Res	-	-	-	-	-

* The %-volatility of the tars alone in vacuum and in Ar up to 500°C was 95 and 80% respectively. The volatilities shown above are for the whole coals. They are corrected for tar volatilities for the tar-loaded cases.

Chemical Characteristics of Tars Produced in a Novel Low Severity, Entrained Flow Reactor

by
J.D. Freihaut, W.M. Proscia and D.J. Seery
United Technologies Research Center
East Hartford, Ct. 06108

Introduction and Approach

The devolatilization of a high volatile bituminous coal follows the sequence indicated in Figure 1. The formation and evolution of heavy molecular weight hydrocarbons, tars, account for more than half the total mass loss of such coals (1,2,3,4). As observed in a wide range of heating conditions, the tars dominate the initial mass loss of bituminous particles. In addition, gas phase, "secondary" reactions of tars can account for major fractions of the light gas yields, depending on the heating conditions. The distribution of the light gases and chemical characteristics of the collected tars are dependent on the both the transient particle temperature and ambient gas temperature (5,6).

A number of investigators have reported that a range of coal types follows the same phenomenological sequence, although the tar yields vary significantly with coal rank characteristics (4,7,8). Moreover, chemical structural characteristics of "primary" tars are reported "similar" to those present in the parent coal, that is, the tar "monomers" reflect the coal "polymer" (3,9,10). "Primary" tars are those collected in conditions in which "secondary" reactions have been minimized. Some of these investigators have noted that, within the limits of experimental resolution, the chemical kinetic parameters that describe tar evolution from a wide range of coals do not vary with coal type (3,9). From this perspective, the phenomenological sequence, monomer-polymer relationship between tar and parent coal, and chemical kinetic parameters describing tar formation and evolution are all invariants in coal devolatilization.

On the other hand, some investigators note the phenomenological sequence of disperse phase devolatilization is the only commonality among coals of varying rank characteristics. Tar yields and chemical characteristics, relative to other coal tars as well as to the parent coal, vary significantly with coal type. In addition, secondary reaction behavior varies according to chemical characteristics of the primary tars (7,11). Implicit in these structural observations with respect to primary tars is a questioning of the invariance of devolatilization/pyrolysis kinetics with coal type. Since all primary tars are not equally "similar" to the parent coal and the distribution of functional groups varies so extensively with coal type, it becomes difficult to understand the extent to which the same tar evolution and light gas formation chemical kinetic parameters could be used for a wide range of coal types.

Other investigators have noted the appreciable role transport parameters can exert in determining devolatilization phenomena. The formation of a glass-like "melt" as an intermediate phase during devolatilization of a

bituminous coal (12,13,14) and the observed changes in molecular weight characteristics of heavy hydrocarbons with ambient pressure (15,16), have led some investigators into a detailed examination of intraphase and interphase mass transport phenomena contributions in mass loss kinetics. Ignoring the details of product distributions and chemical characteristics of tars with changes in pyrolysis conditions, still other investigators have indicated that weight loss kinetics is determined primarily by heat transfer considerations (17,18).

As apparent from the diverse perspectives, a conceptual understanding of disperse phase coal devolatilization remains elusive and, consequently, comprehensive rate models remain difficult to extrapolate to a wide range of conditions. Among the considerable experimental difficulties are: rapidly quenching a heterogeneous process whose overall mass loss rate appears to adjust itself to heating conditions; isolating char particles, tar aerosols and light gas species that are coupled in product streams; minimizing gas phase reactions of thermally labile heavy molecular weight organic compounds; subsequent analysis of large, fragile organic species which have considerably different functional forms, depending on heating conditions and parent coal characteristics.

Batch reactors and single particle systems are often criticized for generating too small a tar sample in conditions unrepresentative of rapid heating. Continuous reactor systems, such as entrained flow reactors, provide acceptable heating conditions but due to residence time, the hot entrainment gases, and the large entrainment flow/sample mass, make it difficult to either time resolve weight loss kinetics or isolate primary tars for subsequent analyses.

This communication reports the utilization of a novel entrained flow reactor and product isolation system. In contrast to the operation of most entrained flow reactors, no attempt is made to match the entrainment gas and wall temperatures. Entrainment gas temperatures are purposely kept below wall temperatures to minimize extra-particle gas phase reactions of tars. To obtain char-free tar samples, an aerosol phase separation system is employed to isolate a significant fraction of entrained tar species from the char mass. Both the char particle and aerosol arms of the product separation system contain serially staged particulate separation systems followed by porous metal final filters that collect "pure" tar species.

Experimental

Reactor and Product Separation System

Figures 2 - 4 display the essential components of the entrained flow reactor, product separation and gas analysis systems. Figures 5 - 7 display the total power density, radiative power density and gas temperature profiles as a function of reactor position. The flux rate profiles are measured by specially designed, calibrated probes. Incident, center-line radiative flux rates range from several watts/sq. cm. at wall temperatures of 750 C to approximately 25 watts/sq. cm. at wall temperatures of 1270 C. Gas temperature

profiles vary as shown. Gas temperature profiles were obtained by making a series of measurements with a set of decreasing thermocouple bead sizes with the asymptotic temperatures approached defined as the "true" local gas temperature. In general, the gas temperatures measured in this manner are consistent with those estimated from the magnitude of the convective heat transfer determined from the power density measurements.

The reactor creates a heat transfer field in which entrained particles are heated by radiation to the local, axial, entrained gas temperature within the reactor (Figures 8 , 9). The radiation flux induces an inverse diameter dependent heating rate on particles in an attempt to drive the particles to equilibrium with the radiating walls. The carrier gas imposes an inverse diameter squared component on the particle heating rate, which in effect insures small particle temperatures are not very different from the local gas temperature, assuming the devolatilization process is weakly endothermic or thermally neutral. Estimated particle heating rates are of the order of 5000 7000 C/sec in these conditions. Such heating rates are greater than that reproducibly obtainable in a heated grid apparatus operated in the same laboratory, but less than that expected in conventional entrained flow reactors wherein heating rates approaching 100,000 C/sec are indicated with estimated transient flux rates at the particle surface of nearly 100 watts/sq. cm. Operating an entrained flow reactor in this manner minimizes gas phase pyrolysis reactions of the initial tar species and allows collection of large quantities of tar species.

Normally, 60 - 75% of the total reactor flow is drawn through the aerosol separation (impactor train) system, that is F of Figures 3 and 4 is of the order 0.25. The temperature and path length of the cooled aerosol transfer line are varied according to the nature of the tars being collected, which, in turn, varies with the parent coal characteristics and reactor heating conditions. The aerosol phase separator is designed to "pull off" all particles or aerosols that are less than 2 microns. A qualitative check of the performance by scanning electron microscope examination of the deposits indicated that designed behavior is followed, provided proper flow rates are maintained throughout an experiment. Inertia carries larger particles into the char separation (cyclone train) system. Both separation trains contain porous metal filters as final stages. Performance of the system is monitored by measuring the flow through the separation arms, pressure drop across the filter housings and determining the tar mass deposited on each of the filter systems. Tar mass ratios are expected to be of the ratio of the average mass flow ratio through the two separation systems during an experiment. This is observed to be the case.

Sample Selection

The feed system utilized is capable of sustained delivery of optically thin streams of particles at constant mass delivery rate, provided the feeder is loaded with a narrow particle size range initially. Particle sizes as low as 10 microns and as large as 300 micron have been utilized. Since the feeder operates on aerodynamic principles, aerodynamically separated samples were employed (See acknowledgements). The location of the parent coal sample set on

a pseudo-coalification band plot is shown in Figure 10.

Sample Measurements

Mass loss is determined by ash tracer techniques. It is observed that experiment specific determinations of the parent coal ash need to be determined. This is accomplished by operating the system in cold flow conditions before and after a particular hot wall devolatilization test and determining the ash content of the particles collected in the first stage cyclone. This value becomes the initial ash value. It is observed that lower density particles are fed into the reactor initially despite the rather extensive efforts to match the aerodynamic characteristics of the feeder with those of the size separated samples provided. Consequently, sustained operation over a sequence of devolatilization conditions leads to significant variations in the average density, mineral content, of the feed, which, in turn, leads to inconsistent determinations in particle mass loss via ash tracer.

Elemental characteristics of evolved tars and chars are determined by use of a Perkin-Elmer 240 instrument. IR absorbance characteristics are determined by an alkali-halide technique using a Fourier Transform - Infrared Spectrometer (FT-IR). The FT-IR is also used to determine the composition of the pyrolysis gases. The streams from the two separation systems are recombined and continuously passed through a multi-pass cell. The 43.5 meter path length is needed to measure the low levels of IR active light gases generated. Concentrations are low because the initial stages of devolatilization, the focus of this investigation, generate small amounts of such gases which are entrained in a relatively large volume of carrier gas.

Results

HVA Bituminous Coal

For the PSOC 1451D coal, an Appalachian high volatile bituminous coal, the ash tracer volatile yields for two particle sizes is shown in Figure 11. As indicated, despite the factor of three difference in particle size, the reactor temperature sensitivity of the mass loss is very similar between the size cuts. Temperature calculations using the measured reactor characteristics as heat transfer conditions indicate this should indeed be the case (See above). Figure 12 shows the relative gas yields, normalized with respect to maximum yields of each gas and plotted with respect to the peak reactor gas temperature, since gas phase reactions of tars are thought to account for substantial fractions of "coal" pyrolysis gases. It is noted that significant increases in acetylene and hydrogen cyanide gases are not observed until peak gas temperatures of 700 C are achieved. At lower gas temperatures, light gas yields are dominated by CH₄, C₂H₄, CO and H₂O, but these gases account for only 10 - 15% of the total 0.2 - 0.25 particle mass fraction loss observed for these reactor conditions. For this coal, tar yields dominate the mass loss at these and lower gas-particle temperatures. Appreciable tar yields, 0.10 - 0.15 mass fraction, are observed at gas temperatures of 350C (wall temperatures of 790C).

Examination of the elemental composition of the tars indicates that the tar evolution process resembles a distillation process from the point of view of hydrogen concentration versus characteristic temperature, gas or reactor wall (Table I). As implied by the insensitivity of the total mass loss with particle size and as indicated by the temperature calculations, the elemental composition of the tars evolved from the two different particle sizes and for a particular stage of the reaction process should be similar. As indicated in Table I the elemental composition of the the 20 -30 micron tars and the 63 - 75 micron tars are quite similar in elemental composition. A distillation-like tar evolution process would also imply changing functionality and relative molecular weight characteristics of the samples with characteristic temperature. Figure 13 displays the relative -CH₂- concentration of the tars for increasing reactor temperature and Table II indicates relative molecular weight moments as a function of reactor temperature.

In summary, the results indicate the hydrogen level, in particular the polymethylene concentration hydrogen level, of the collected tars systematically decreases with peak reactor temperature as the total tar yield increases. As the hydrogen level gradually decreases the relative molecular weight moments of the evolved tars increase to the point where the tar yield is believed to be maximized. Lower temperature tars contain less total oxygen and sulfur mass fractions than the total tar mass evolved to the point of maximum tar yield. Absolute tar yields are difficult to determine using an entrained flow reactor but investigation of the tar evolution process on a heated grid apparatus indicate total tar yields are 0.30 - 0.35 of the parent coal mass on an ash-free basis for this coal.

Coal Rank Effects

It is desirable to determine the change in the nature of the tars produced with changes in the chemical characteristics of the parent coal, while keeping the heating conditions constant. The heating conditions that maximized the tar yields for the high volatile bituminous coal (930C wall, 500 - 600 C gas temperature) while minimizing gas phase secondary reactions were selected, although it is recognized that each coal type may require a unique set of heating conditions to maximize its tar yield.]

Figures 14 and 15 compare the hydrogen and sulfur + oxygen levels of the tar species to those observed in the parent coals. As the rank characteristics of the parent coal increase the elemental composition of the tars become more like the parent coal. The similarity ratios asymptote toward unity. Conversely, the lower the rank of coal the more unlike in elemental composition are the primary tars. Figure 16 indicates the %H of the low rank coal tars can be as great as 9% in these conditions.

The most striking difference in the IR absorbance spectra of the low rank coal tars relative to the higher ranks resides in the polymethylene absorbance region (2920 cm⁻¹). The low rank coal tars generally display much greater absorbance levels in this region per unit mass of sample than the high rank coal tars. Assuming the absorption coefficients of this band do not vary significantly with coal rank, such behavior implies increasing concentrations of -CH₂- levels with decreasing coal rank. The -CH₂- absorbance band

correlates with the % H level in the tars (Figures 16,17,18).

The difference in structural characteristics of the low temperature tars evolved from the lignite and subbituminous coals, relative to the bituminous coal tars, is again emphasized by comparing the molecular weight moments obtained by gel permeation chromatography. The data in Figure 19 indicates the tars evolved from the low rank coals at a particular temperature have greater molecular weight moments than the corresponding high rank coal tars. In the most elementary sense, the polystyrene calibrated gpc technique indicates only that aliphatic, hydrogen-rich low rank coal tars are structurally "larger" than the more aromatic bituminous coal tars with respect to a length to weight ratio parameter. These results likely reflect variation in conformational aspects of the tars as a function of rank rather than molecular weight or polarity differences. The long chain aliphatic tars characteristic of the low rank coals are not efficiently retained by the gel permeation column and, consequently, elute in the short retention times characteristic of heavy polystyrene standards. The molecular "weight" moments appear to be more characteristic of relative molecular geometry than actual mass size when comparing tars from a range of coal ranks. The general observations with respect to the variations in low temperature coal tars with rank characteristics of the primary coal are indicated in Figure 20, the lower the rank of parent coal the more unlike the parent coal are the low temperature, primary tars. The dissimilarity appears primarily related to the aliphatic to aromatic hydrogen distribution and the oxygen-sulfur heteroatom content of the tars relative to the parent coal. Significant polymethylene concentrations variations are observed with variation in coal type.

Although the nature of tars varies significantly with coal type, the particle devolatilization and gas phase reaction sequence did not. Table III displays the composition of tars from a subbituminous coal (PSOC 1520D) at various reactor temperatures. As in the high volatile bituminous coal, the hydrogen rich, more aliphatic, lighter molecular weight species vaporize before the heavier, more aromatic species during the evolution to the point of maximum tar yield. At gas temperatures of 700 C or above, gas phase reactions of pyrolysis of the polymethylene rich tars quickly leads to ring formation in the tar species. C₂H₄ and CO are major light gas products of these reactions and, at still higher temperatures, C₂H₂, CO and HCN. In short, the same light gas formation temperature pattern as indicated in Figure 12 for a HVA bituminous coal is followed by the lower rank coals. However, the absolute quantities vary significantly with the nature of the low temperature tars.

Summary and Conclusions

The entrained flow reactor investigation indicates that the phenomenology of coal devolatilization and pyrolysis is similar for a wide range of coal ranks. The phenomenology is summarized in Figure 1. Heavy hydrocarbons are "formed" within (ATP = Attached Tar Precursors) the coal particle at relatively low temperatures (300 - 450 C). Further heating results in the extra-particle evolution of these heavy hydrocarbons (tars) and the onset of light gas production (450 - 700 C). The low temperature light gases consist mainly of CH₄ and higher alkanes, CO, CO₂, H₂O and some C₂H₄. The absolute quantities of these species vary with coal type as do the absolute yields of

"primary" tars. Gas and particle temperatures greater than 700 C preferentially produce C₂H₂, HCN, CO and C₂H₄.

Although the sequence of tar evolution is phenomenologically similar, the structural characteristics of tars evolved from a range of coal types indicates quite different processes are occurring chemically. The lower the rank of coal, the more unlike the parent coal are the low temperature tars. Low temperature lignite tars appear to consist mainly of long chain aliphatic species with significant levels of associated carboxylic and carbonyl groups. Low temperature tars from bituminous coals have structural characteristics more reflective of, but never identical to, the parent coal.

Gas phase reactions of low temperature, primary tars are rapid at gas temperatures of 700 C and above, common operating temperatures of conventional entrained flow reactors. Such reactions quickly lead to the ring formation reactions from polymethylene-rich low temperature tars coincidental with the evolution of the heavier tar species from the devolatilizing particle itself. Tars collected in these conditions, particularly tars collected in separation systems without extensive phase separation, will appear to be more like the parent coal than the primary tars originally evolved and collected in the above reactor system or other systems that minimize secondary tar reactions. The phenomenological sequence of heavy hydrocarbon formation, tar evolution and gas phase reactions appear similar for a wide range of coals, but the relationship between the chemical structures of primary tars and parent coal varies widely with coal type.

The question of invariance in kinetic parameters among a range of coal types and whether chemical or transport phenomena dominate the evolution processes requires a multi-reactor approach in which the phases of tar formation and evolution can be deconvoluted. This will be the subject of future communications.

Acknowledgements

The authors are grateful to the Department of Energy, Pittsburgh Energy Technology Center, for coal samples provided in this investigation. In addition some of the results presented were obtained using funding provided by DE-AC22-84PC70768. The technical expertise of Gerald Wagner and Dave Santos are present throughout the work performed in this investigation. Brian Knight was responsible for the implementation and practical design of the phase separation system for this particular reactor.

References

1. Suuberg, E.M., Peters, W.A. and Howard, J.B., *Ind. Eng. Chem. Proc. Design and Dev.*, 17,37 (1978).
2. Arendt, P. and van Heek, K.H., *Fuel*, 60, 779 (1981).
3. Solomon, P.R. and Colket, M.B., *Seventeenth Symposium (Internat.) on Combustion*, 131, The Combustion Institute (1979).
4. Freihaut, J.D., Zabielski, M.F. and Seery, D.J., *Nineteenth Symposium (Internat.) on Combustion*, 1159, The Combustion Institute (1982).
5. Doolan, K.R., Mackie, J.C. and Tyler, R.J., *Fuel*, 66, 572 (1987).
6. Serio, M.A., Peters, W.A. and Howard, J.B., *Ind. Eng. Chem. Res.*, 26, 1831 (1987).
7. Tyler, R.J., *Fuel*, 59, 218 (1980).
8. Teo, K. C. and Watkinson, A.P., *Fuel*, 65, 949 (1986).
9. Solomon, P.R., et. al., *Nineteenth Symposium (Internat.) on Combustion*, 1139, The Combustion Institute (1982).
10. Squire, K.R., et.al., *Fuel*, 65, 833 (1986).
11. Galkins, W.H. and Tyler, R.J., *Fuel*, 63, 1119 (1984).
12. Klose, W. and Lent, M., *Fuel*, 64, 193 (1985).
13. Oh, M.S., Howard, J.B. and Peters, W.A., "Modeling Volatiles Transport in Softening Coal Pyrolysis", presented at AIChE National Meeting, San Francisco, November 1984.
14. Suuberg, E.M., "Mass Transfer Effects in Coal Pyrolysis", in *Chemistry of Coal Conversion*, ed. by R.H. Schlosberg, 67, Plenum Press (1985).
15. Oh, M.S., "Softening Coal Pyrolysis", Sc.D. Thesis, Department of Chemical Engineering, MIT, Cambridge, Mass. (1985).
16. Unger, P.E. and Suuberg, E.M., *Fuel*, 63, 606 (1984).
17. Zielinski, E., *Fuel*, 46, 329 (1967).
18. Hertzberg, M. and Ng, Daniel, "A Microscopic and Kinetic Study of Coal Particle Devolatilization in a Laser Beam", in *Fundamentals of the Physical-Chemistry of Pulverized Coal Combustion*, ed. by J. Lahaye and G. Prado, NATO ASI Series, Series E, No. 137,104 (1987).

TABLE I
 ELEMENTAL COMPOSITION OF TARS - TEMPERATURE EFFECTS
 HVA BITUMINOUS COAL(PSOC 1451D)

REACTOR WALL(C)	MAX. GAS(C)	-----20 - 30 MICRONS-----				
		%C	%H	%N	%(S+O)	H/C
790	350	84.05	6.07	1.64	8.24	0.87
840	400	84.07	5.94	1.67	8.32	0.85
930	510	84.37 84.46	5.86 5.93	1.68 1.76	8.09 7.83	0.83 0.84
1020	665	84.62	5.55	1.69	8.14	0.78
1100	790	85.22	5.40	1.73	7.65	0.76
1190	890	85.55	5.27	1.74	7.44	0.74
1270	1000	86.00	5.08	1.73	7.19	0.71
PARENT COAL.....		82.42 81.07	5.35 5.24	1.57 1.62	10.65 12.04	0.79 0.78
		-----63 - 75 MICRONS-----				
790	350	83.97	6.22	1.64	8.14	0.89
930	510	84.47 84.16	5.83 5.79	1.72 1.74	7.98 8.29	0.83 0.83
1270	1000	85.50	5.29	1.76	7.43	0.74
PARENT COAL.....		82.55 81.86	5.53 5.43	1.59 1.66	10.32 11.02	0.80 0.80

TABLE II
 Relative Molecular Weight of Characteristic of Tars
 Reactor Temperature Effects *
 PSOC 1451D, 20-30 Microns

Reactor Wall Temperature (C)	Position (cm)	Residence Time (msec)	Mn	Mw
750	36	620	438	641
840	36	580	452	665
930	36	520	481	719
1020	36	470	491	743
1100	36	420	518	801
1190	36	385	509	803
1270	36	360	506	807

* Argon Carrier Gas

TABLE III
 ELEMENTAL COMPOSITION OF TARS - TEMPERATURE EFFECTS
 SUBBITUMINOUS COAL (PSOC 1520D)

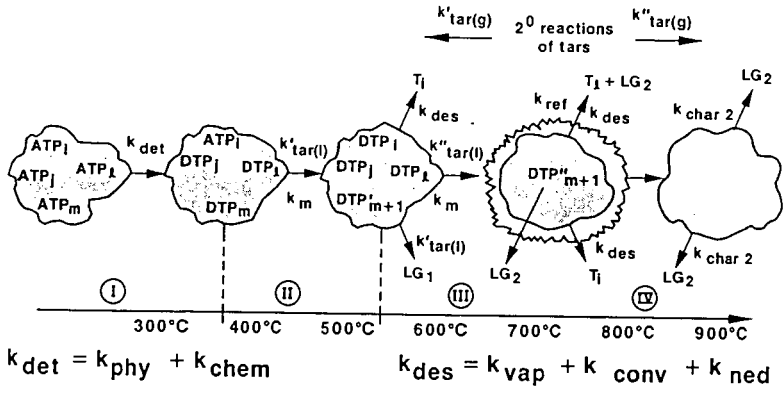
790	350	78.21	8.43	0.63	12.73	1.29
930	510	78.15	7.83	0.79	13.23	1.20
		77.78	7.63	0.81	13.77	1.17
1270	1000	78.97	6.72	0.98	13.32	1.02
PARENT COAL.....		63.77	4.54	0.83	30.84	0.86

* TARS - SPECIES COLLECTED ON FINAL FILTER OF IMPACTOR TRAIN

ARGON CARRIER GAS
 PARTICLE RESIDENCE TIME: 600 msec

Fig. 1

COAL DEVOLATILIZATION / PYROLYSIS



RA24197X.026

Fig. 2

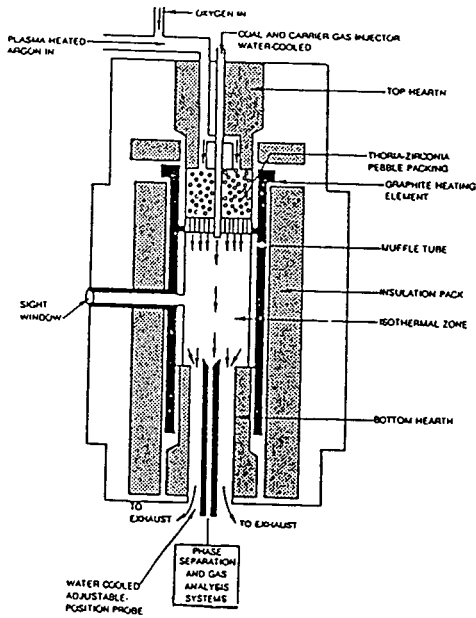
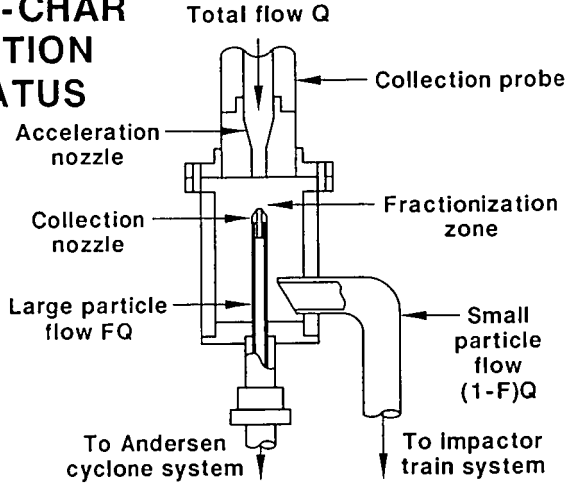


Fig. 3

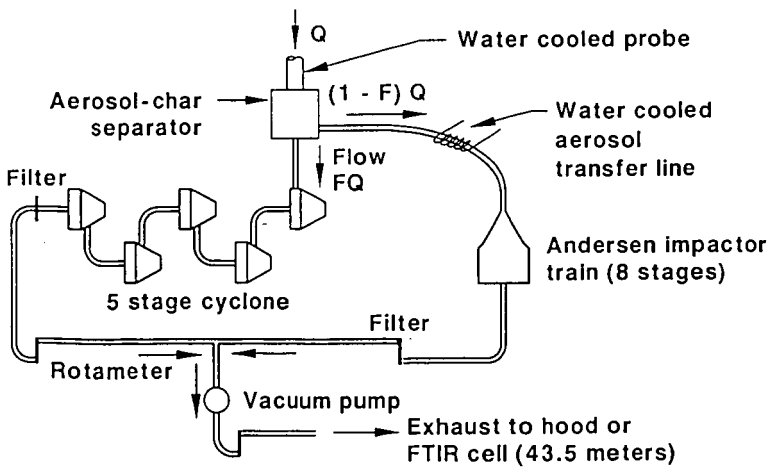
AEROSOL-CHAR SEPARATION APPARATUS



RA21912.M1

Fig. 4

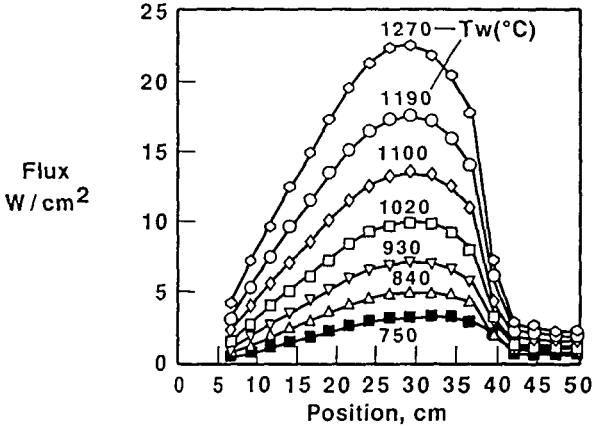
UTRC-EFR SAMPLE COLLECTION SYSTEM



RA21912.002

Fig. 5

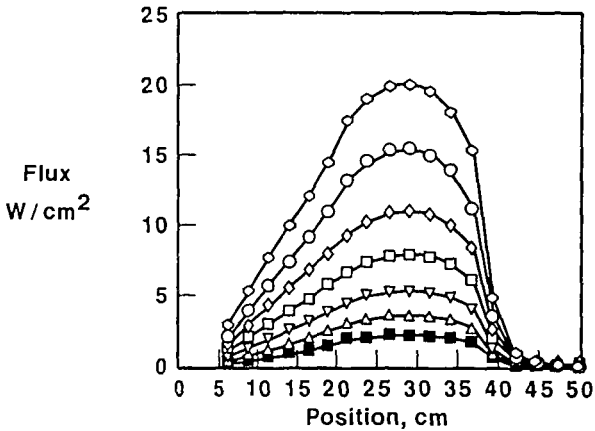
UTRC-EFR REACTOR TOTAL FLUX PROFILES



RA2416TX.001

Fig. 6

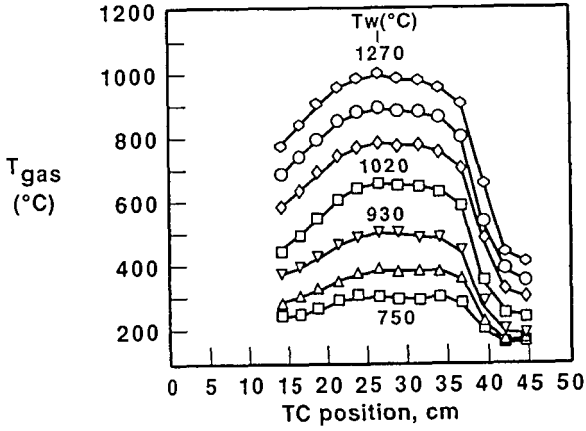
UTRC-EFR REACTOR RADIATIVE FLUX PROFILES



RA2416TX.002

Fig. 7

UTRC-EFR COOLED PROBE 0.1016 CM BEAD DIA



RA2415TX.003

Fig. 8

UTRC ENTRAINED FLOW REACTOR - PARTICLE TEMPERATURE 840 C WALL TEMPERATURE

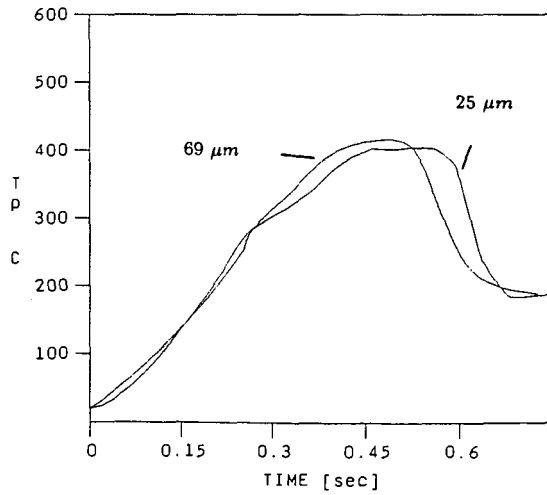


Fig. 9

UTRC ENTRAINED FLOW REACTOR - PARTICLE TEMPERATURE
930 C WALL TEMPERATURE

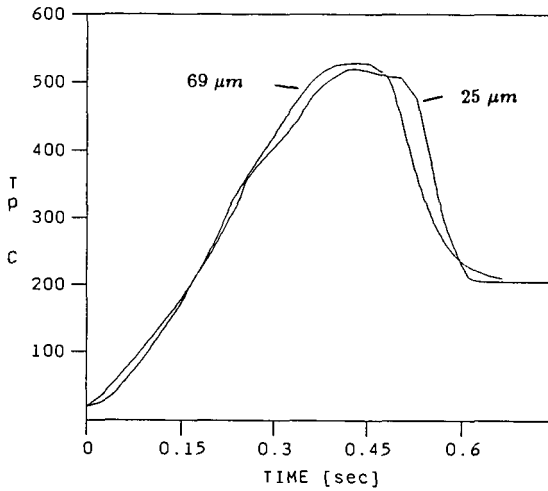


Fig. 10

**H/C vs. (S+O)/C OF
PSOC XXXXD COALS**
20-30 microns, coals fed to UTRC
EFR-cold flow, C₀ capture

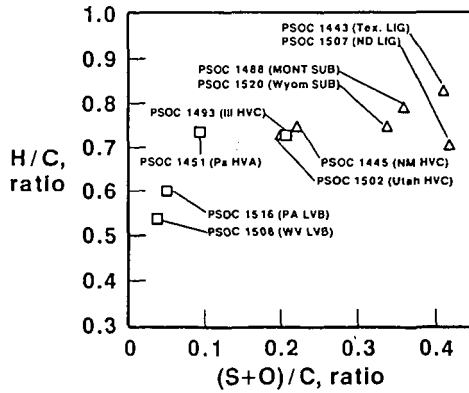
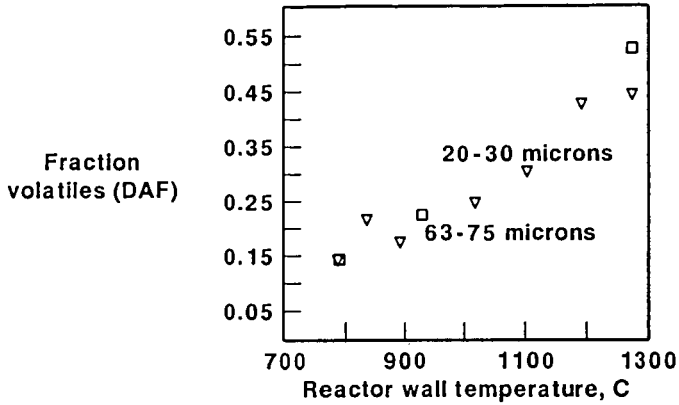


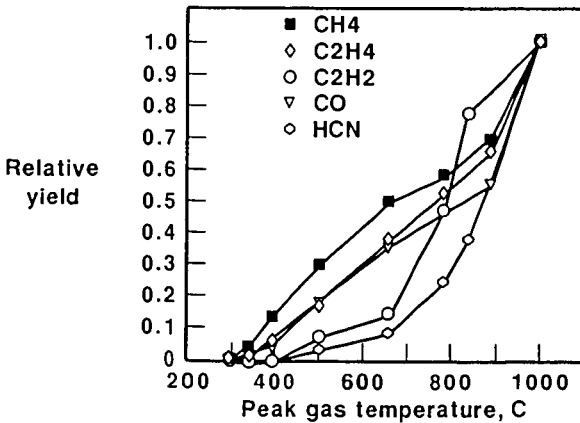
Fig. 11



RA2416TX.010

Fig. 12

LIGHT GAS YIELDS vs. PEAK GAS TEMP. (C) PSOC 145 1D, 20-30 MICRONS, 600 MSEC

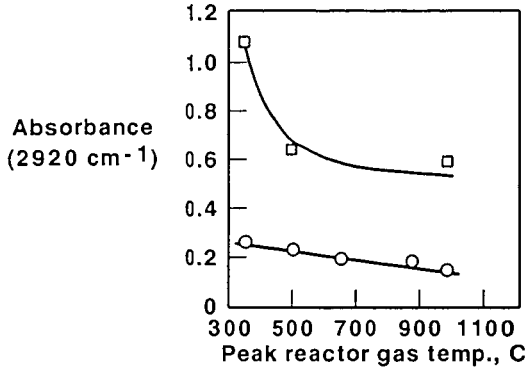


RA2416TX.008

Fig. 13

-CH₂- STRETCH ABSORBANCE (2920 CM⁻¹) vs. GAS TEMPERATURE

Triangle = PSOC 1451D, square = PSOC 1520D, 20-30 microns

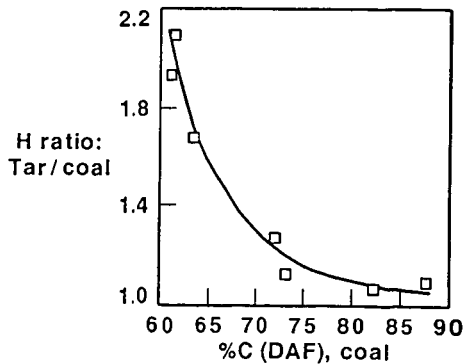


RA2418TX.009

Fig. 14

%H(TAR) / %H(COAL) vs. COAL RANK

(PSOC XXXXD coals) 20-30 micron, particles,
peak reactor gas temperature = 510C

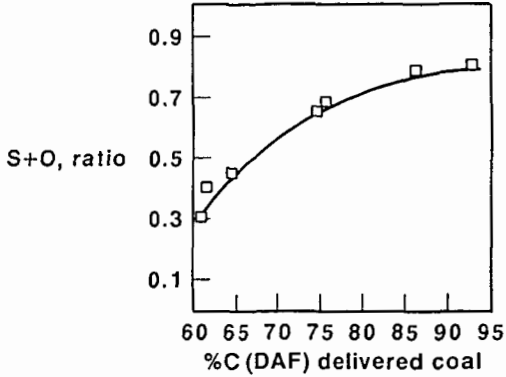


RA2418TX.012

Fig. 15

% (S+O) - TAR / % (S+O) - COAL vs. COAL RANK

(PSOC XXXXD coals) 20-30 micron particles,
reactor peak gas temperature = 510C



RA2415TK.012

Fig. 16

% HYDROGEN IN TAR vs. COAL RANK

(PSOC XXXXD coals) 20-30 micron, particles,
peak gas temperature = 510C

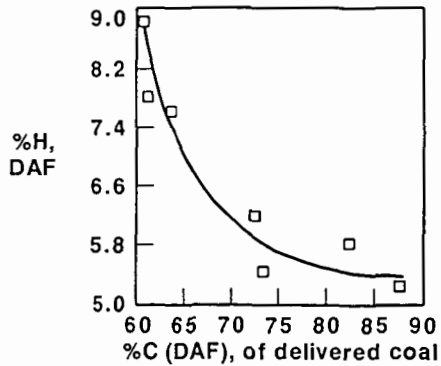
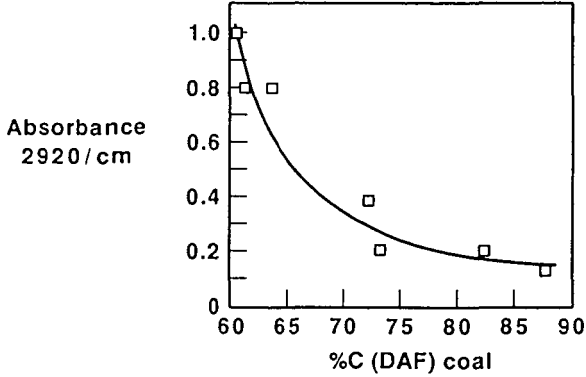


Fig. 17

2920 CM-1 ABSORBANCE OF TARS vs. COAL RANK

(PSOC XXXXD coals) 20-30 micron particles,
peak gas temperature = 510C

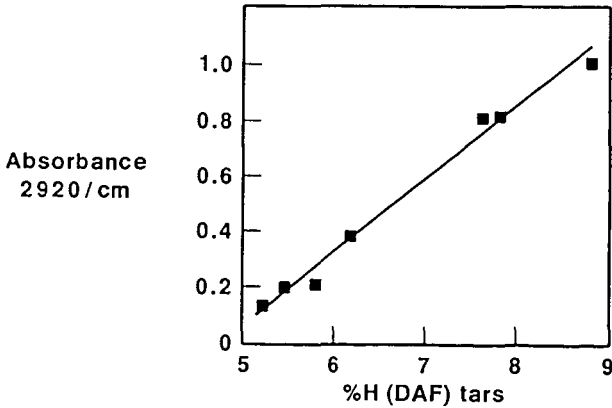


RA2415TX.016

Fig. 18

ABSORBANCE (2920 / CM) vs. % H (DAF) IN TARS

(PSOC XXXXD coals) 20-30 micron particles, peak gas temp. = 510C

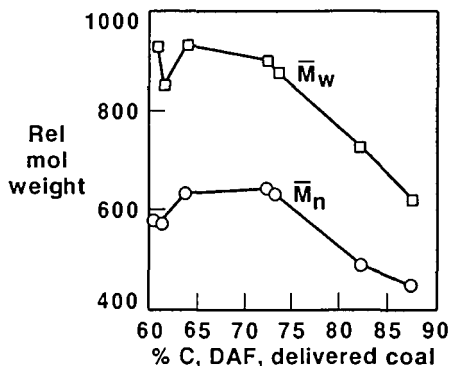


RA2415TX.016

Fig. 19

RELATIVE NUMBER AND MASS AVERAGE MW OF TARS AND COAL TYPE

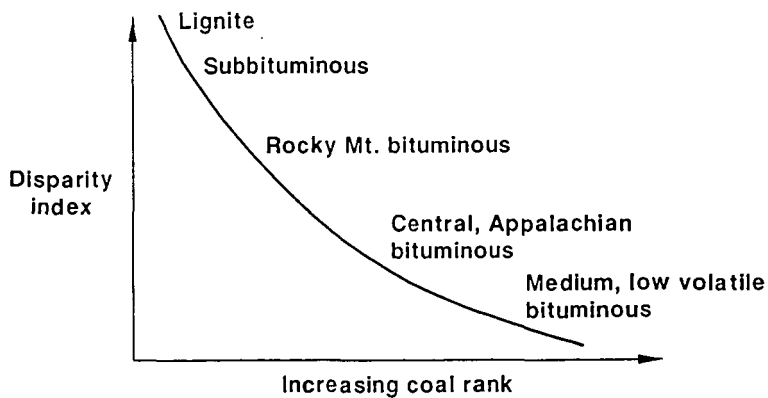
PSOC XXXX D coals, 20-30 microns, 510C peak gas temp.



RA2415TX.008

Fig. 20

PRIMARY TAR ← PARENT COAL: STRUCTURAL COMPARISONS



RA2415TX.011

THERMAL AND KINETIC STUDY OF THE MILD PYROLYSIS OF SINGLE SUBBITUMINOUS COAL PARTICLES

Guangwei Huang, Francis J. Vastola and Alan W. Scaroni

The Pennsylvania State University
The Combustion Laboratory
404 Academic Activities Building
University Park, PA 16802

INTRODUCTION

A detailed knowledge of coal pyrolysis is fundamental to the understanding of the early stages of many coal conversion processes. Pyrolysis studies have been conducted using a variety of techniques including the use of electric grids (1-3), thermogravimetric analyzers (4-6), entrained flow reactors (7-9), and fluidized beds (10,22). In order to eliminate the complexity introduced by particle interactions, some research has been directed towards the behavior of single coal particles (12-16). For example, Huang et al. (12) measured the transient temperature gradients in the gas surrounding a captive 1 mm diameter coal particle with a fast response thermocouple array (12) and found steep gradients up to 4 mm from the surface. Saito et al. (16) reported on differences between high temperature devolatilization in air and N₂ for 2-4 mm-sized particles, and conducted an isothermal kinetic analysis of the data. Hertzberg (17) analyzed experimental data from laser-heated coal pyrolysis experiments and concluded that the pyrolysis rate was controlled by the heat flux to the particle surface and by thermodynamic transport constraints within the particle. He proposed a "rate coefficient", which is the reciprocal of the overall enthalpy required for heating and devolatilization. The significance of heat transfer effects on coal pyrolysis were recently reviewed by Suuberg (18) and Gavalas (19), and it is clear that heat transfer plays an important role. Nevertheless, few references can be found in the literature on the instantaneous rate of heat transfer to pyrolyzing coal particles. Most measurements in this area have been made using Differential Scanning Calorimetry (DSC) which is limited to low heat fluxes during the heatup to pyrolysis temperature. The current work is an attempt to relate experimentally measured particle temperature and mild pyrolysis rates in order to determine meaningful kinetic parameters.

EXPERIMENTAL

Temperature Measurements

Pyrolysis experiments on 1 mm diameter coal particles were performed in a captive reactor, details of which have been provided elsewhere (12,13). It consists essentially of two enclosing horizontal tube furnaces which are heated electrically to preheat the incoming gas and maintain the reactor at a predetermined temperature. A subbituminous coal (volatile matter 50.5%, fixed carbon 36.0%, ash 13.5%) was used in this study. Prepurified nitrogen was used to purge air from the reactor but prior to the start of a run, the gas flow was stopped so that the experiments were essentially in a static system. For each run a 1 mm diameter coal particle was injected into a minicrucible inside the 873 K reactor. Temperature gradients in gas surrounding the reacting particle were measured by a thermocouple array (TCA) composed of four extra-fine thermocouples spaced 1.0 mm apart. The distance from the coal particle surface to the closest thermocouple was approximately 1 mm. A microcomputer collected the responses of the thermocouples at millisecond time intervals.

All experiments were conducted on dry coal particles, the coal being dried overnight at 383°K in a vacuum oven prior to use. A char particle was prepared by injecting a coal particle into the reactor in flowing nitrogen at 873 K for 5 minutes.

Measurements of Weight Loss

Weight loss data for pyrolysis were obtained in a Dupont 951 Thermogravimetric Analyzer (TGA). To simulate the process of dropping a cold coal particle into a hot reactor, the TGA quartz tube was kept in the furnace during heatup in a 75 cc/min flow of prepurified nitrogen. The sample housing was then rapidly introduced into the hot quartz tube in the furnace after the furnace temperature had

stabilized (20,21). The same experimental conditions were used in the TCA and TGA experiments (temperature, particle size, etc.).

RESULTS AND DISCUSSION

Heat Transfer

The temperature histories measured by the TCA in the surrounding gas at different distances from the coal particle surface during pyrolysis are shown in Figure 1. Curves 1 to 4 express instantaneous temperatures at 1, 2, 3, and 4 mm from the particle surface, respectively. Because of thermal continuity in the gas surrounding the pyrolyzing coal particle, the measured data were extrapolated to the particle surface by a three order polynomial correlation in order to obtain the instantaneous particle surface temperature (Figure 2). The extrapolated surface temperature (T_s) is plotted as curve 0 in Figure 1. The temperature of the gas phase 5 mm from the particle was taken to be the furnace temperature (T_f) in the extrapolation. The validity of this assumption is based on solid evidence. Firstly, as heat was transferred to the vicinity of a cold coal particle, the temperature of the surrounding gas recovered to, but did not exceed, the furnace temperature (12). Secondly, the temperature perturbation decreased with distance from the particle surface. Figure 2 provides information on spatial temperature gradients, from which heat transfer boundary conditions were determined. Under the experimental conditions, the boundary was a spherical region with a radius of approximately 5 mm.

The three order polynomial used in the extrapolation is expressed as:

$$T = A_0 + A_1X + A_2X^2 + A_3X^3 \quad 1)$$

where A_i ($i = 0, 1, 2, 3$) is constant at a given time t , X is the dimensionless distance expressed by:

$$X = \frac{x}{x_b} \quad 0 \leq X \leq 1 \quad 2)$$

in which x is the distance from the particle surface and x_b is the distance from the particle surface to the heat transfer boundary. From Equation (1) T_s can be determined by:

$$T_s = T|_{x=0} = A_0 \quad 3)$$

and bulk gas temperature can be expressed as:

$$T_f = T|_{X=1} = \sum_{i=0}^3 A_i \quad 4)$$

Figure 3 shows temperature histories for char particles under the same experimental conditions as for the coal particles in Figure 1. The char particles were recovered from the preceding coal run. Since the coal used in this study is non-swelling (free swelling index = 0) the particle size and external surface areas of the coal and char particles were considered to be the same.

Particle surface temperatures for the coal and char are plotted in Figure 4. During the early stage of heatup to 700 K (up to ~2s) T_s for the coal was about 80 K lower than T_s for the char. This is due to the initial mass difference between the coal and char particles. At the onset of pyrolysis for the coal, there was an inflection in the T_s curve. Endothermic pyrolysis reactions kept the coal particles at a lower temperature than the char which was undergoing a rapid heatup to the furnace temperature. The unambiguous surface temperature histories in Figure 4 indicate that there will be a gross error if the particle surface temperature is assumed to be the furnace temperature.

Heat flux by radiation from the furnace wall to the coal and char particles can be calculated from the following equation:

$$q'_R = \epsilon \sigma (T_f^4 - T_s^4) \quad 5)$$

To estimate maximum radiation, the emissivity ϵ of coal and char is assumed to be unity. The rate of heat transfer by conduction from the hot surrounding gas can be expressed as:

$$q_c = K \bar{A} \frac{\Delta T}{\Delta x} = K \bar{A} \frac{(T_f - T_s)}{(d_b - d_s)} \quad 6)$$

where

$$\bar{A} = \frac{A_b - A_s}{\ln \left(\frac{A_b}{A_s} \right)} = \frac{\pi (d_b^2 - d_s^2)}{2 \ln \left(\frac{d_b}{d_s} \right)} \quad 7)$$

Assuming the coal and char are surrounded by nitrogen, the thermal conductivity of nitrogen can be used in the calculation. The heat flux due to conduction to the coal and char particles can be estimated by:

$$q'_c = q_c / A_s \quad 8)$$

The heat transfer coefficient for convection is determined from the Nusselt number (taken as two) (22) and the diameter of the particle, d_s , by:

$$h = Nu K d_s \quad 9)$$

where K is the thermal conductivity of the surrounding gas. The heat flux to the particle by convection can be determined by:

$$q'_v = h(T_f - T_s) \quad 10)$$

The heat fluxes due to radiation, conduction, and convection as function of the time are shown in Figures 5 and 6 for coal and char particles, respectively. The instantaneous heat fluxes are a strong function of the residence time. The total heat fluxes varied from 27 w/cm² at the beginning to zero at the end of a run corresponding to a 9 s time interval. The dominant mode of heat transfer was conduction. Radiation contributed less than convection in the early heat up stage. However, after 2 s the same amount of heat was supplied by radiation as supplied by convection.

A comparison of the total heat flux to the coal and char particles is shown in Figure 7. The smooth decay in heat flux for both the char and coal in the early stage (< 2s) characterizes the heatup processes. An obvious inflection occurs in the heat flux curve for the coal, which implies the initiation of pyrolysis. More heat is received by the coal than the char to meet the needs of endothermic pyrolysis until the coal is converted into char. The total heat required to heat and pyrolyze the coal particles can be calculated by integrating the heat flux:

$$Q = \frac{A_s}{W_d} \int_0^{\infty} q'_t dt = \frac{A_s}{W_d} [\Sigma (q'_c + q'_v + q'_R) \Delta t] \quad 11)$$

where W_d is the sample weight on a dry basis. The calculated heats required by the coal and char are shown in Figures 8 and 9, respectively. The figures show clearly that the heat transferred through the

surrounding gas by conduction and convection amounts to 80% of the total. Only 20% of the heat is contributed by radiation. This is not surprising since heat transfer by conduction and convection is proportional to the temperature difference, $\Delta T = T_f - T_s$, whereas the driving force for radiation is proportional to the difference between the fourth powers of the temperatures, $T_f^4 - T_s^4$, a much stronger function of the absolute furnace temperature. Therefore, at higher T_f , radiation plays a more important role. From Eq. (11) the total heat needed to heat the char to 873 K is 1917 J/g. The heat required to heat coal and pyrolyze it is 2219 J/g (dry basis). Assuming that the original coal, char and volatiles have the same specific heats, about 300 J/g is needed for the decomposition. This is less than 15% of the total heat required by the coal. Therefore, the heat capacity is the major term in the heat transfer calculation.

Kinetics

Devolatilization results from the TGA experiments are presented in Figure 10. The data are expressed as the percentage weight loss of the coal (daf) versus residence time. The particle surface temperature for the same size coal particles at the same furnace temperature as for the TGA method is also plotted in Figure 10. The inflection point A on the T_s curve is the pyrolysis initiation point, as discussed before, and the completion point B is defined as the time when T_s equals T_f . The weight loss data are consistent with these temporal characteristics. Before the initiation point, only about 2% weight loss is observed, but up to the completion point more than 95% of the total weight loss is reached. The total weight loss is about 37% (daf) which is less than the ASTM proximate volatile matter (~ 50%). This is because the experiments were performed at a temperature of more than 300 K less than the ASTM test.

The fact that negligible weight loss was observed before point A proves that two distinct processes occur during pyrolysis, namely heatup and reaction. Badzioch and Hawksley (23) reported negligible weight loss until the coal particles reached about 673 K, before the pyrolysis reaction became significant. They expressed the total pyrolysis time as:

$$t_T = t_H + t_R \quad (12)$$

where the subscripts T, H, and R represent the total, heatup, and reaction times, respectively. For millimeter-sized coal particles, the heatup stage is more significant. Under the conditions in this study, for 1 mm particles, it took 2 s to initiate the pyrolysis reaction.

As a first attempt to determine pyrolysis rates for the millimeter-sized single coal particles in the TGA, a simple first order model was used:

$$\frac{dV}{dt} = kV \quad (13)$$

where
$$V = 1 - \frac{W}{W_\infty} \quad (14)$$

and
$$k = k_0 \exp(-E/RT_p) \quad (15)$$

Because of the difficulty of measuring the particle temperature, T_p , most kinetic studies use Eq. (13) with the assumption that the coal particle is instantaneously heated to the furnace temperature. This may be allowable for smaller pulverized coal but is not acceptable for millimeter-sized, or larger particles, although it has still been used by others (16). In this study an attempt was made to reduce the error caused by the improper assumption of isothermality. The particle surface temperature, T_s , is substituted into Eq. (15) for T_p . This is based on the assumption that the thermal conductivity of the coal is infinite. This is not correct but is an improvement over use of the heat source temperature. Therefore, Eqs. (13) and (15) can be expressed as:

$$\frac{dV}{dt} = k_0 \exp(-E/RT_s) V \quad (16)$$

or:

$$\ln \left(\frac{1}{\bar{V}} \cdot \frac{dV}{dt} \right) = \ln k_0 - \frac{E}{R} \cdot \frac{1}{T_s} \quad (17)$$

The logarithm term on the left hand side of Eq. (17) is plotted against the reciprocal of T_s in Figure 11. The activation energy and pre-exponential factor were derived from the slope and the intercept of the straight line in Figure 11. The activation energy estimated from Eq. (17) is 34.0 kcal/mole and the pre-exponential factor is $4.8 \times 10^8 \text{ s}^{-1}$. The activation energy is more than four times that reported by Saito et al. (16) for pyrolysis of millimeter-sized subbituminous coal particles.

CONCLUSIONS

A thermocouple array was used to measure temperature gradients in the gas phase around captive coal and char particles during heatup and pyrolysis in preheated nitrogen. Instantaneous particle surface temperatures were extrapolated from the measured gas temperatures at different distances from the particles. Based on basic heat transfer principles, heat fluxes of conduction, convection, and radiation were calculated. Heat fluxes to the particles were strongly dependent on residence time, varying from 27 W/cm^2 to 0 at the completion of pyrolysis. The total heat required for heatup and pyrolysis was determined by integration. The results indicated that 80% of the total heat was transferred through the gas phase by conduction and convection. Radiation at the low operating temperature made a minor contribution to the total heat transfer.

The temperature history of the 1 mm diameter coal particles indicated that pyrolysis did not occur isothermally. Two seconds elapsed prior to the onset of pyrolysis. Particle surface temperatures were substantially lower than the furnace temperature until pyrolysis was completed.

An attempt was made to use instantaneous particle temperatures in a kinetic analysis. Weight loss data were obtained using a modified TGA method which simulated the TCA conditions. An activation energy and pre-exponential factor were estimated from a first order rate expression the values being 34 kcal/mole and $4.8 \times 10^8 \text{ s}^{-1}$, respectively.

ACKNOWLEDGEMENTS

Financial support for this work was provided by the Penn State Cooperative Program in Coal Research. The coal was supplied by the Penn State/DOE Sample Bank and Data Base.

NOMENCLATURE

\bar{A}	Logarithm average area, cm^2	q_V	Heat flux of convection, W/cm^2
A_b	Area of heat transfer boundary, cm^2	R	Universal gas constant
A_s	Area of particle surface, cm^2	T_f	Furnace temperature, K
d_b	Heat transfer boundary diameter, cm	T_p	Particle temperature, K
d_s	Particle diameter, cm	T_s	Particle surface temperature, K
E	Activation energy, kcal/mole	t	Time, s
h	Coefficient of convective heat transfer, $\text{W}/\text{cm}^2 \text{ K}$	t_H	Heatup time, s
K	Thermoconductivity, $\text{W}/\text{cm K}$	t_R	Reaction time, s
k	Rate constant, s^{-1}	t_T	Total time, s
k_0	Pre-exponential factor, s^{-1}	V	Fraction of remaining volatiles
Nu	Nusselt number	W	Weight loss at time t
Q	Total heat, J	W_d	Sample weight on dry basis, g
q_c	Heat transfer rate by conduction, W	W_∞	Maximum weight loss, g
q_c	Heat flux by conduction, W/cm^2	X	Dimensionless distance
q_R	Heat flux by radiation, W/cm^2	x	Distance, cm
q_T	Total heat flux, W/cm^2	x_b	Distance from particle surface to heat transfer boundary, cm
		ϵ	Emissivity
		σ	Stefan-Boltzmann Constant

REFERENCES

- 1) Anthony, D. B., Howard, J. B., Hottel, H. C. and Meissner, H. P. *15th Symp (Int.) on Combustion*, The Combustion Institute, 1974, p. 1303.
- (2) Suuberg, E. M., Peters, W. A., and Howard, J. B. *17th Symp. (Int.) on Combustion*, The Combustion Institute, 1978, p. 117.
- (3) Niksa, S., Russel, W. B., and Saville, D. A. *Fuel*, 1982, 61, 1207.
- (4) Geng, L. and Guo, S. *Journal of Fuel Chemistry and Technology*, 1986, 11(3), 211.
- (5) Vernekav, V.R.P., Rao, J. R.M., Rao, B.K.S. and Tiruhavayanan, M. A. *Fuel*, 1982, 61, 634.
- (6) Smith, S. E., Neavel, R. C., Hippo, E. J. and Miller, R. N. *Fuel*, 1981, 60, 458.
- (7) Tsai, C. Y. and Scaroni, A. W. *Energy & Fuels*, 1987, 1, 263.
- (8) Maloney, D. and Jenkins, R. G. *20th Symp (Int.) on Combustion*, The Combustion Institute, 1984, 1435.
- (9) Samuelson, G. S., Trolinger, J. D., Heap, M. P. and Seeker, W. R. *Combust. and Flame*, 1981, 40, 7.
- (10) Desypris, J., Murdoch, P. and Williams, A. *Fuel*, 1982, 61, 807.
- (11) Barooah, J. N. and Long, V. D. *Fuel*, 1976, 55, 116.
- (12) Huang, G., Vastola, F. J. and Scaroni, A. W. *Prepr.-Amer. Chem. Soc., Div. Fuel Chem.*, 1987, 32(3), 1.
- (13) Gomez, C. O. and Vastola, F. J. *Fuel*, 1985, 64, 558.
- (14) Ragland, K. W. and Yang, J. T. *Combust. and Flame*, 1985, 60, 285.
- (15) Zghoul, A.M. and Essenhigh, R. H. *Second Annual Pittsburgh Coal Conference Proceedings*, 1985, pp. 658-665.
- (16) Saito, M., Sadakata, M., Sato, M. and Sakai, T. *Fuel*, 1987, 66, 717.
- (17) Hertberg, M., Zlochower, I. A., Conti, R. S. and Cashdollar, K. L. *Prepr.-Am. Chem. Soc., Div. Fuel Chem.*, 1987, 32(3), 24.
- (18) Suuberg, E. M. *Prepr.-Am. Chem. Soc., Div. Fuel Chem.*, 1987, 32(3), 51.
- (19) Gavalas, G. R. *Coal Pyrolysis*, Elsevier, New York, 1982.
- (20) Huang, Y. H. and Serageldin, M. A. *Thermochimica Acta*, 1987, 112, 161.
- (21) Serageldin, M. A., and Wang, H. National Conference of Standards Laboratories, 1986 Workshop and Symposium Proceedings, 1986. 1, 8-1.
- (22) Mitchell, R. E. and McLean, W. J. *19th Symp. (Int.) on Combustion*, The Combustion Institute, 1982, 1113.
- (23) Badzioch, S., Hawksley, G. M. *Ind. Eng. Chem. Process Des. Dev.*, 1970, 2, 421.

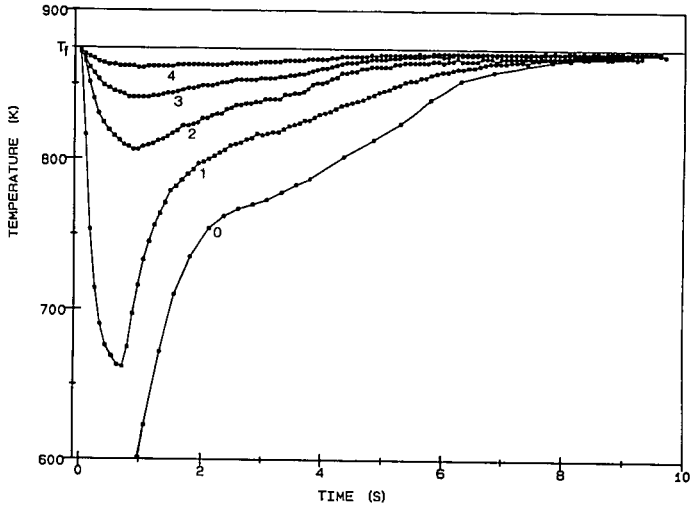


Figure 1. Gas Phase Temperature (0-4 mm From Particle Surface) During Pyrolysis of a 1 mm Diameter Coal Particle at 873 K

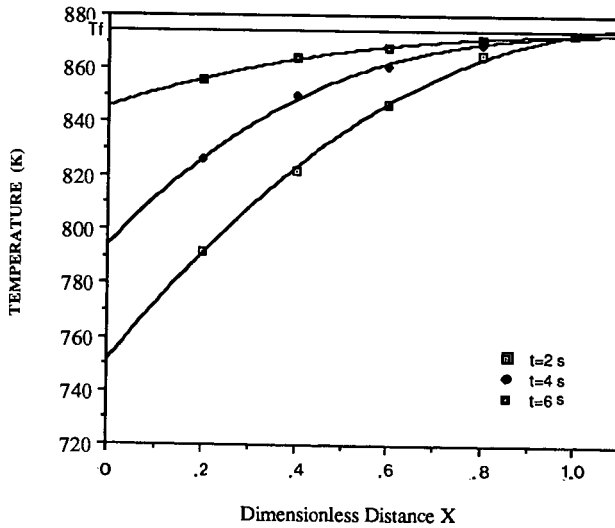


Figure 2. Extrapolation of Data from Figure 1 to Predict Surface Temperature

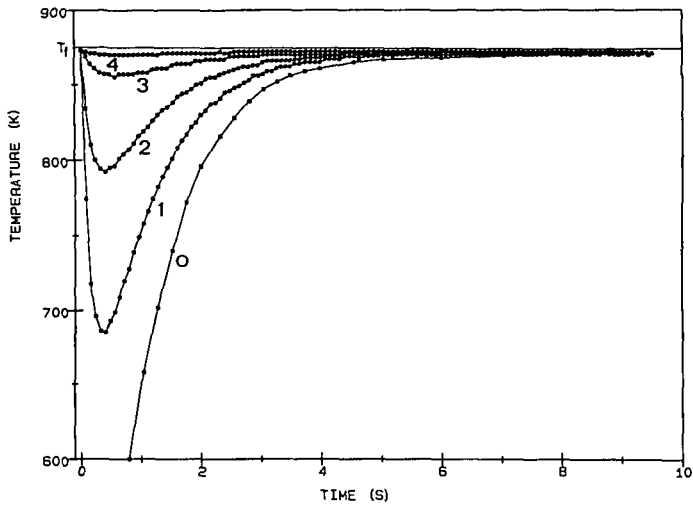


Figure 3. Gas Phase Temperature (0-4 mm From Particle Surface) During Heatup of a 1 mm Diameter Char Particle at 873 K

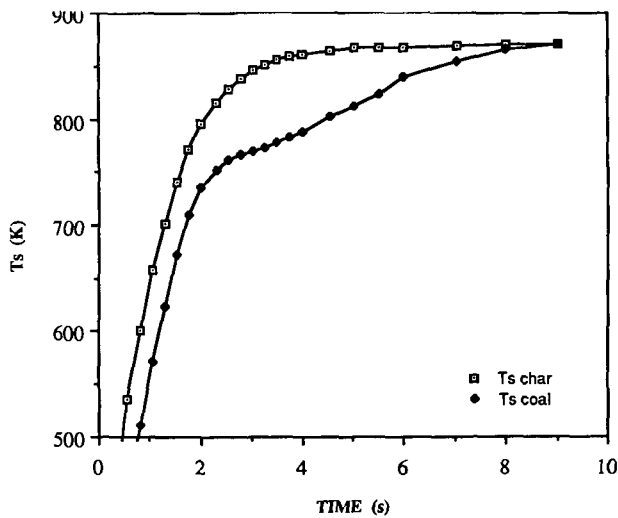


Figure 4. A Comparison Between Coal And Char Surface Temperatures as a Function of Time During Heating in Nitrogen at a Furnace Temperature of 873 K

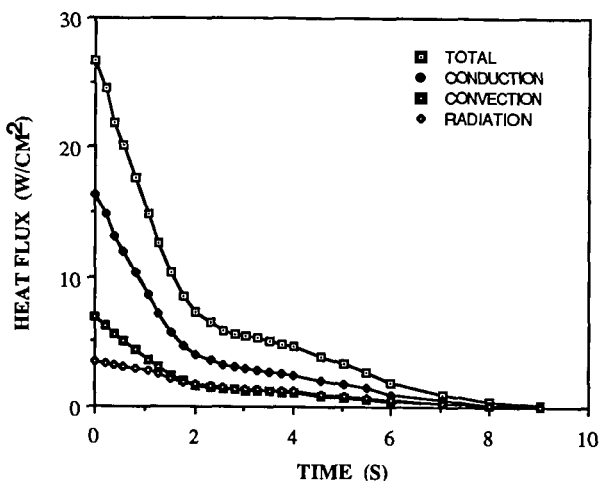


Figure 5. Time Dependency of the Contribution of Conductive, Convective and Radiative Heat Fluxes to the Total Heat Flux to a 1 mm Diameter Coal Particle Heated in Nitrogen at a Furnace Temperature of 873 K

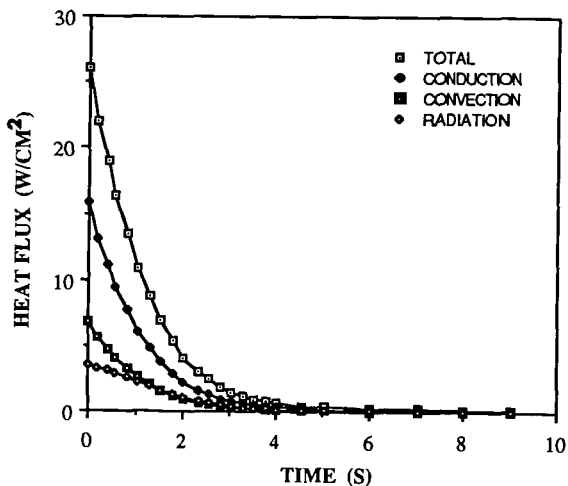


Figure 6. Time Dependency of the Contribution of Conductive, Convective and Radiative Heat Fluxes to the Total Heat Flux to a 1 mm Diameter Char Particle Heated in Nitrogen at a Furnace Temperature of 873 K

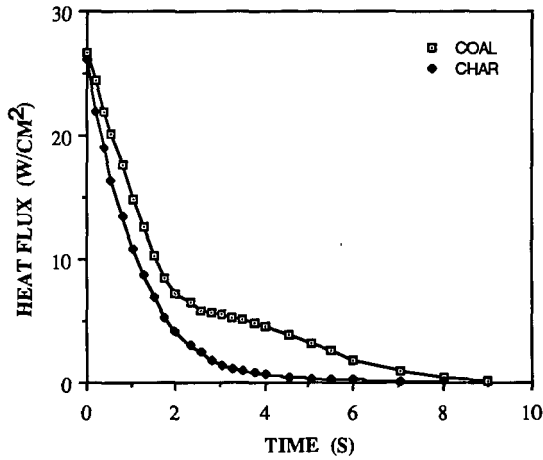


Figure 7. Comparison Between Total Heat Flux to 1 mm Diameter Coal and Char Particles Heated in Nitrogen at 873 K as a Function of Time

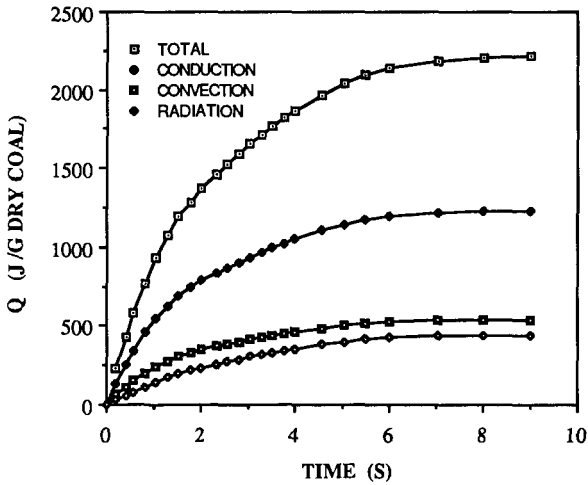


Figure 8. Heat Absorbed by a 1 mm Diameter Coal Particle Heated in Nitrogen at 873 K as a Function of Time

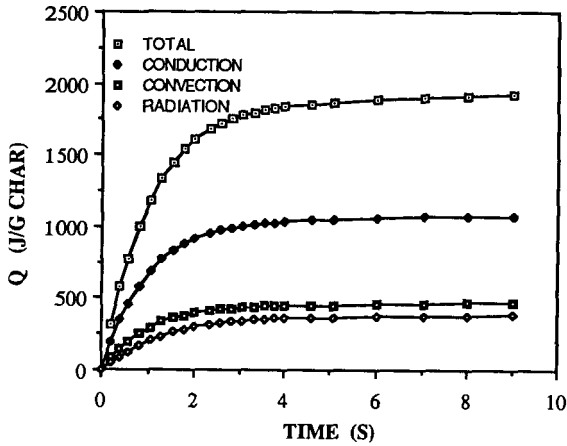


Figure 9. Heat Absorbed by 1 mm Diameter Char Particles Heated in Nitrogen at 873 K as a Function of Time

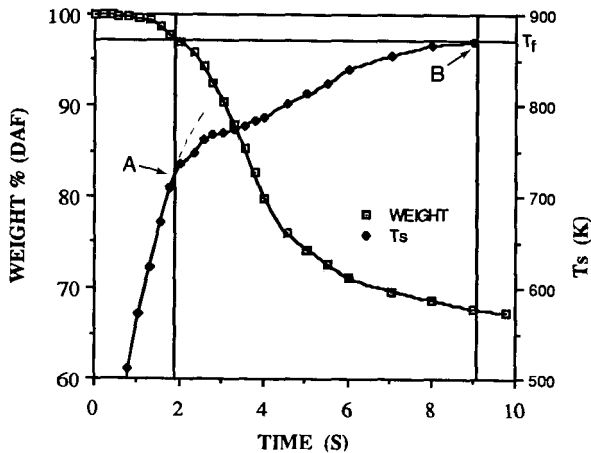


Figure 10. Weight Loss and Surface Temperature as a Function of Time for 1 mm Diameter Coal Particles Heated in Nitrogen at a Furnace Temperature of 873 K

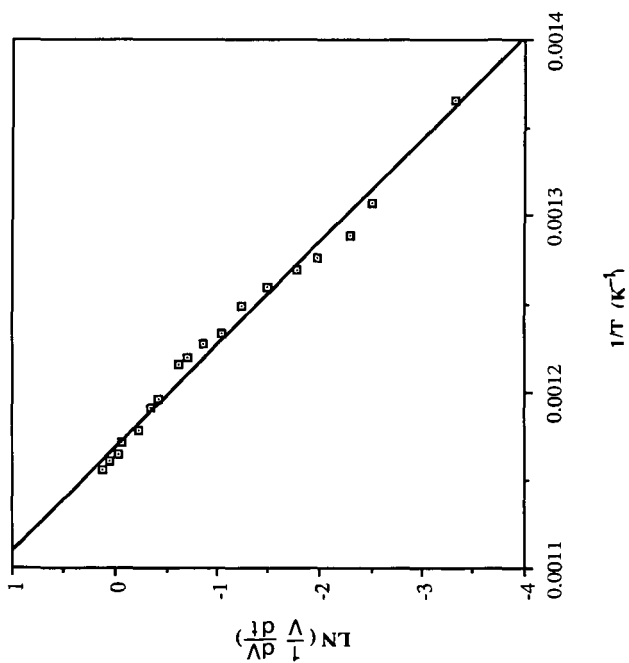


Figure 11. Arrhenius Plot for the Pyrolysis of 1 mm Diameter Coal Particles in N_2 at a Furnace Temperature of 873K

PYROLYSIS OF THE ARGONNE PREMIUM COALS UNDER SLOW HEATING CONDITIONS

M.A. Serio, P.R. Solomon, and R.M. Carangelo

Advanced Fuel Research, Inc., 87 Church St., East Hartford, CT 06108 USA

INTRODUCTION

The establishment of the Argonne Premium Sample Bank (1) will allow more meaningful comparisons to be made between pyrolysis studies from different laboratories. This sample bank also provides a good suite of coals for examining rank dependent phenomena, such as the kinetics of primary gas evolution. A recent "general" model of coal pyrolysis proposed by our research group (2-4) has as one of its assumptions that the kinetics of primary product evolution are rank-insensitive. This assumption was tested by a thorough examination of our data from experiments where only coal type was varied as well as data from similar experiments in the literature (5). The conclusion was that, with few exceptions, the kinetic rate constants for individual species evolved from coals pyrolyzed under the same conditions show little variation with rank. However, this conclusion remains controversial. The Argonne premium samples provide an opportunity to further test this assumption with a set of coals that was designed to cover a wide range of coal types. A slow, constant heating rate experiment was used, which is the most sensitive to rate variations.

A second controversial area is the importance of heating rate on the volatile product yield and distribution. Evidence has been presented which suggests no intrinsic effect of heating rate on pyrolysis yields (6) and other studies have indicated the converse to be true (7,8). However, often these studies have been done under sufficiently different experimental conditions that direct comparisons are difficult. Our own work has indicated a role for heating rate on tar yields for bituminous coals and on tar molecular weight distributions for lignites (3,9). We plan to extend this work to the Argonne coals in order to better establish these trends. The current paper is concerned primarily with pyrolysis of the Argonne coals under slow heating conditions in a unique TG-FTIR instrument developed in our laboratory. Results from slow heating rate pyrolysis into a FIMS apparatus are also presented. Experiments have also been done under rapid heating conditions. These will be the subject of another paper.

EXPERIMENTAL

Coal Properties - Elemental data are given for the Argonne coals in Table I. This information was obtained from Ref. 1.

TABLE 1 - ELEMENTAL ANALYSES OF ARGONNE PREMIUM COAL SAMPLES (1)

	%daf basis			% dry basis	
	C	H	O	S	Ash
1. Pocahontas	91	4.7	3	0.9	5
2. Upper Freeport	87	5.5	4	2.8	13
3. Pittsburgh #8	83	5.8	8	1.6	9
4. Upper Kanawha	81	5.5	11	0.6	20
5. Utah Blind Canyon	79	6.0	13	0.5	5
6. Illinois No. 6	77	5.7	10	5.4	16
7. Wyodak	74	5.1	19	0.5	8
8. Beulah-Zap	73	5.3	21	0.8	6

TG-FTIR - The apparatus is the TG/PLUS offered by Bomem, Inc.. It consists of a sample suspended from a balance in a gas stream within a furnace. As the sample is heated, the evolving tars and gases are carried out of the furnace directly into a 5 cm diameter gas cell (heated to 150°C) for analysis by FT-IR. The TG/PLUS couples a Dupont 951 TGA with a Bomem Michelson 100 FT-IR spectrometer.

The apparatus is designed to carry evolved products from the furnace to the gas cell over a short path to minimize secondary reactions or condensation on cell walls. In addition, the furnace geometry, the sample size, the sweep gas and flow rate have been chosen to ensure that the condensable products form a submicron aerosol mist. This size aerosol has two advantages: 1) the particles follow the gas stream lines, thus minimizing condensation; and 2) the particles produce little scattering in the mid I.R., so the condensable products can be analyzed directly in the FT-IR cell.

The FT-IR can obtain spectra every 30 seconds to determine quantitatively the evolution rate and composition of most pyrolysis products. The system allows the sample to be heated in a gas flow of selected composition on a pre-programmed temperature profile at rates between 1°C min⁻¹ and 100°C min⁻¹ up to a temperature between 20 and 1000°C and held for a specified time. The system continuously monitors: 1) the time-dependent evolution of the gases (including specific identification of the individual species such as CO, CO₂, H₂O, CH₄, C₂H₄, C₂H₂, benzene, heavy paraffins, heavy olefins, HCN, HCl, NH₃, NO, NO₂, SO₂, CS₂, COS, CH₃OH, CH₃CHO and CH₃COCH₃); 2) the tar evolution rate and its infrared spectrum with identifiable bands from the functional groups; and 3) weight of the non-volatile material (char plus mineral components). An analysis of C, H, N and S in the residue at the end of the pyrolysis experiment can be obtained by introducing oxygen to burn the residue and analyzing the combustion products.

For the experiments reported here, approximately 35mg of each coal sample was heated at 30°C/min, first to 150°C for drying and then to 900°C for pyrolysis. Additional details on the TG-FTIR apparatus can be found in Refs. 10 and 11.

FIMS - Molecular weight distributions of the primary pyrolysis tars were determined at SRI, International using the Field Ionization Mass Spectrometry (FIMS) apparatus described by St. John et al. (12). The samples were heated at 0.05°C/sec in a vacuum chamber.

RESULTS AND DISCUSSION

The quantitative gas evolution plots from all eight coals are presented in

Figs. 1-6 for tars plus aliphatics, CH₄, CO₂, CO, SO₂ and H₂O respectively. The coals are arranged on each plot according to the rank order given in Table 1. The actual temperature-time profiles are given on the first plot in each figure.

The results show how the structure of the product gas evolution curves varies from simple in the case of hydrocarbons to complex in the case of oxygenated species. One reason is that the latter are likely to be influenced by mineral decomposition peaks. Of course this can be assessed to a large extent by running demineralized samples, which we are in the process of doing.

In order to determine how well pyrolysis of the Argonne coals agreed with the assumption of rank-insensitive kinetics, a compilation was made of the temperatures for maximum evolution rate for the evolution of the most consistently prominent peaks for each gaseous product. This was difficult in some cases because of the fact that numerous "subpeaks", shoulders and minor peaks were often present. However, it was the usual case that an identifiable peak appeared in the same temperature vicinity for each coal. The results of this analysis are tabulated in Table 2.

In general, the standard deviations are greatest for oxygenated gases (CO₂, CO, SO₂, H₂O) compared to hydrocarbon gases (CH₄, tar/aliphatics). This phenomena was also observed previously (5). If one assumes a 50 Kcal/mole activation energy, a range in the peak temperature of 40°C corresponds to a factor of 5 in the rate while a range in the peak temperature of 65°C corresponds to a factor of 10 (5). It appears that about one-half of the 10 products show a variation of x5 or less, while one-half show a variation of x10 or less.

An interesting feature of the tar evolution curves in Fig. 1 is a low temperature evolution peak which is probably due to unattached guest molecules in the coal. These are most apparent in the Pittsburgh and Upper Freeport evolution curves. A comparison of the infrared spectra obtained at the low and high temperature peaks is presented in Fig. 7. The spectrum taken at the early peak (Fig. 7b) has been scaled up to compare to the spectrum from the later peak (Fig. 7c). The earlier peak appears to have a slightly higher aliphatic to aromatic content compared to the later peak. This would be consistent with the concept of some guest polymethylene in the coal, perhaps mixed with small molecules more representative of the coal's average organic structure.

FIMS Analysis

Molecular weight distributions of coals were obtained at SRI International using the Field Ionization Mass Spectrometry (FIMS) apparatus described by St. John et al. (11). The coal samples were pyrolyzed directly in the FIMS apparatus. The FIMS technique produces little fragmentation of the evolved tars and so provides a good determination of the tar molecular weight distribution. Figures 8 and 9 present the weight loss of six of the eight Argonne coals heated in the FIMS apparatus at 0.05°C/sec.

The spectra show a distinct progression from low to high rank. The highest rank coals, Pocahontas (Fig. 8a) and Upper Freeport (Fig. 8b) both show low intensities at low molecular weights (100 - 200 amu). This suggests few one and two ring clusters. The intensity in the 200 - 600 amu range, however, suggests the presence of three, four and higher ring cluster sizes and dimers and trimers of these. The low yield for the Pocahontas is due to its higher bond energies (525°C tar peak in Fig. 1) and lower number of small ring clusters capable of being volatilized.

The intermediate rank coals, Pittsburgh (Fig. 9a), Utah (Fig. 9b) and Upper Knawha (Fig. 8c) all have similar molecular weight distributions showing substantial intensities in the 100 to 200 amu region indicative of one and two ring clusters as well as in the 200 to 600 amu range.

The low rank coal, Myodak (Fig. 9c) shows high intensity between 100 and 200 amu, but substantially lower intensity above 200 amu. This is typical of the Zap lignite also, and has been explained by extensive cross linking related to carboxyl groups in low rank coals (4).

CONCLUSIONS

1. For most species there is a trend of increasing evolution temperature with increasing rank. However, the variations are small enough that the assumption of rank-insensitive kinetics is a good first approximation for nearly all of the major volatile products.
2. There is a systematic variation in the tar molecular weight distribution with rank. Higher rank coals show greater intensity in the high molecular weight range (200-600 amu), while lower rank coals show greater intensity in the lower molecular weight range (100-200 amu).

ACKNOWLEDGMENTS

This work was supported under DOE Contract DE-AC21086MC23075. Justin L. Beeson is the Project Manager.

REFERENCES

1. Vorres, K.S., ACS Fuel Chem Div. Preprints, **32**(4), 221 (1987).
2. Solomon, P.S., Hamblen, D.G., Deshpande, G.V. and Serio, M.A., 1987 Int. Conf. on Coal Science, p. 601, Maastricht, The Netherlands, (Oct. 26-30, 1987).
3. Solomon, P.R., Hamblen, D.G., Carangelo, R.M., Serio, M.A. and Deshpande, G.V., ACS Fuel Div. Preprint, **32**(3), 83 (1987).
4. Solomon, P.R., Hamblen, D.G., Carangelo, R.M., Serio, M.A. and Deshpande, G.V., Combustion and Flame, **71**, 137 (1988).
5. Solomon, P.R. and Hamblen, D.G., Prog. Energy Combust. Sci., **9**, 323 (1983).
6. Howard, J.B., Chemistry of Coal Utilization, (M.A. Elliott, Ed.), John Wiley, NY, Chapter 12, p. 665 (1981).
7. Niksa, S., Heyd, L.E., Russel, W.B. and Saville, D.A., 20th Symp. (Int) on Combustion, The Combustion Institute, University of Michigan, Ann Arbor, MI, pp. 1445-1453 (August 12-17, 1984).
8. Gribbins-Matham, J. and Kandigoti, R., ACS Fuel Div. Preprints, **32**(4), 318 (1987).

9. Solomon, P.R., Hamblen, D.G., Carangelo, R.M., Serio, M.A. and Deshpande, G.V., "A General Model of Coal Devolatilization", submitted to Energy and Fuel (1987).
10. Carangelo, R.M., Solomon, P.R. and Gerson, D.J., Fuel, 66, 960 (1987).
11. Whelan, J.K., Solomon, P.R., Deshpande, G.V., and Carangelo, R.M., Energy and Fuels, 2, 65, (1988).
12. St. John, G.A., Buttrill, Jr., S.E. and Anbar, M., ACS Symposium Series, 71, 223 (1978).

TABLE 2
 Comparison of Temperatures for Maximum Evolution Rate for Volatile
 Products from Pyrolysis of the Argonne Premium Coals

SPECIES	PEAK #	POCAHONTAS	UPPER FREEPORT	PITTSBURGH	UPPER KNAWAH	UTAH	ILLINOIS	WYODAK	ZAP	AVERAGE
SO ₂	1	-	-	375	375	375	360	360	330	363 ± 20
CO ₂	1	-	435	420	465	465	435	435	420	439 ± 19
CO	1	495	525	-	465	465	450	435	465	470 ± 30
Tar/ Aliphatics	1	525	510	485	485	485	470	465	465	485 ± 22
H ₂ O	1	585	555	510	525	495	525	495	495	525 ± 32
CH ₄	1	570	555	555	555	555	555	555	570	560 ± 7
SO ₂	2	600	615	615	600	615	585	570	600	600 ± 16
CO ₂	2	705	750	705	660	735	735	690	615	700 ± 45
CO	2	780	795	795	765	705	780	795	765	773 ± 30
H ₂ O	2	815	840	795	795	825	765	-	-	807 ± 28

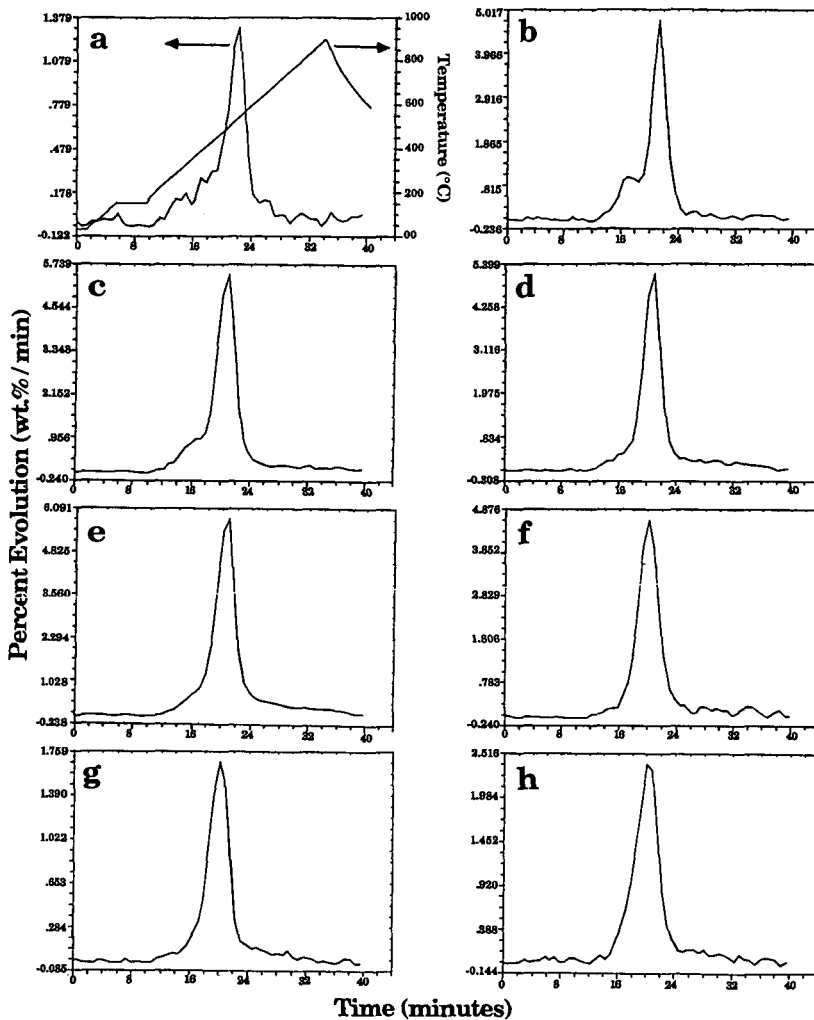


Figure 1. Evolution Rate for Tars/Aliphatic from the Eight Argonne Coals in a TG-FTIR at 0.5°C/s. a) Pocahontas; b) Upper Freeport; c) Pittsburgh; d) Upper Knawha; e) Utah Blind Canyon; f) Illinois No. 6; g) Wyodak; h) Zap.

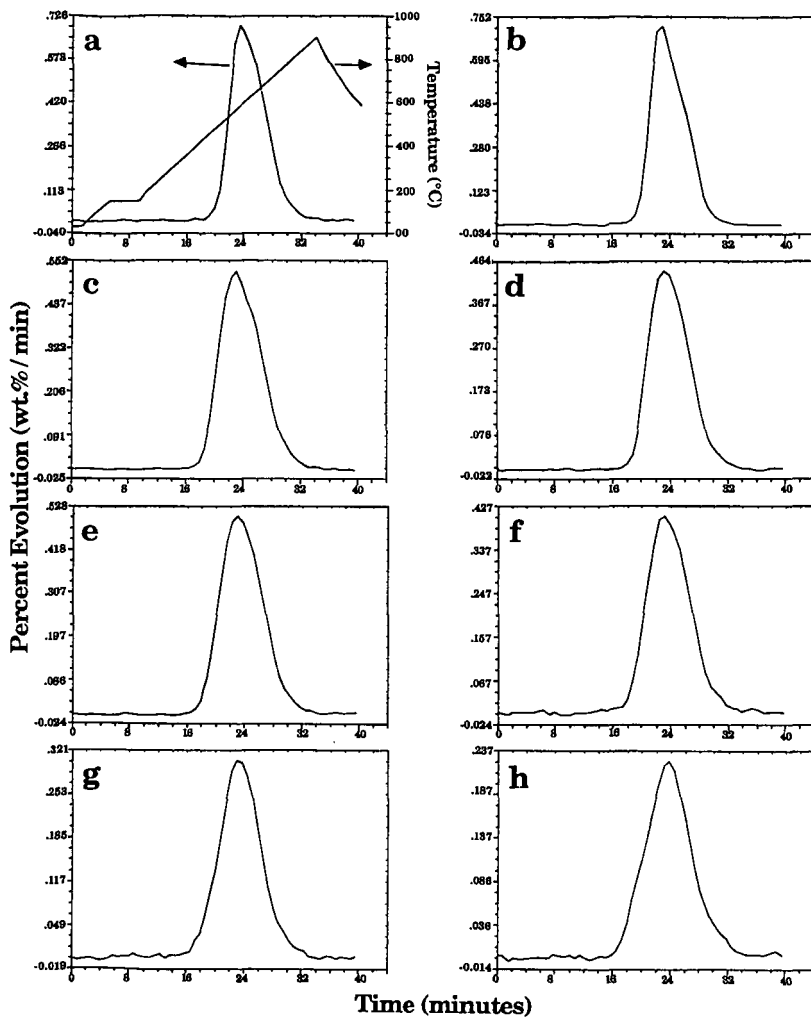


Figure 2. Evolution Rate for CH_4 from the Eight Argonne Coals in a TG-FTIR at 0.5°C/s . a) Pocahontas; b) Upper Freeport; c) Pittsburgh; d) Upper Knawha; e) Utah Blind Canyon; f) Illinois No. 6; g) Wyodak; h) Zap.

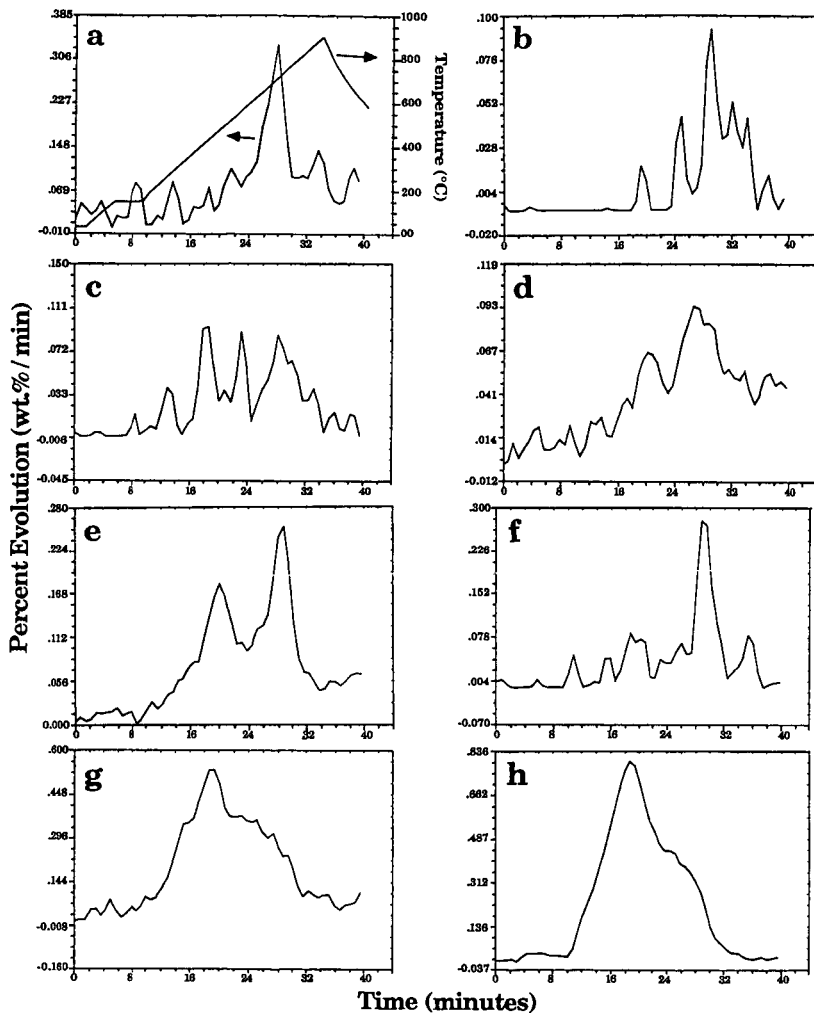


Figure 3. Evolution Rate for CO_2 from the Eight Argonne Coals in a TG-FTIR at 0.5°C/s . a) Pocahontas; b) Upper Freeport; c) Pittsburgh; d) Upper Knawha; e) Utah Blind Canyon; f) Illinois No. 6; g) Wyodak; h) Zap.

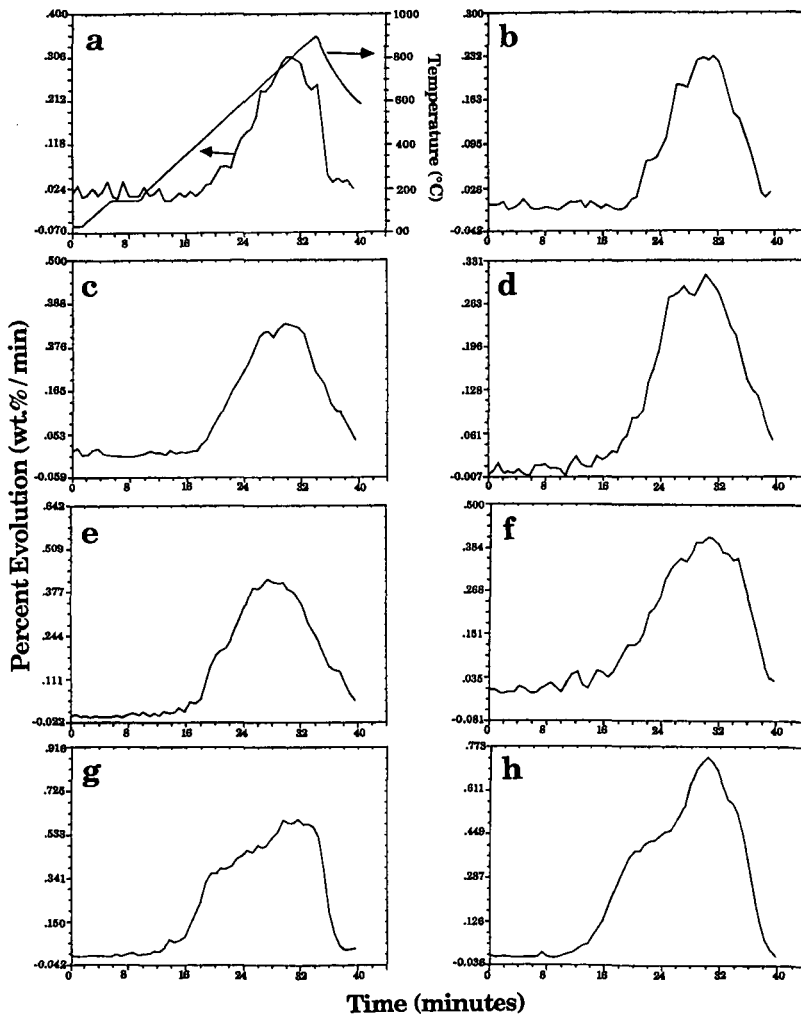


Figure 4. Evolution Rate for CO from the Eight Argonne Coals in a TG-FTIR at 0.5°C/s. a) Pocahontas; b) Upper Freeport; c) Pittsburgh; d) Upper Knawha; e) Utah Blind Canyon; f) Illinois No. 6; g) Wyodak; h) Zap.

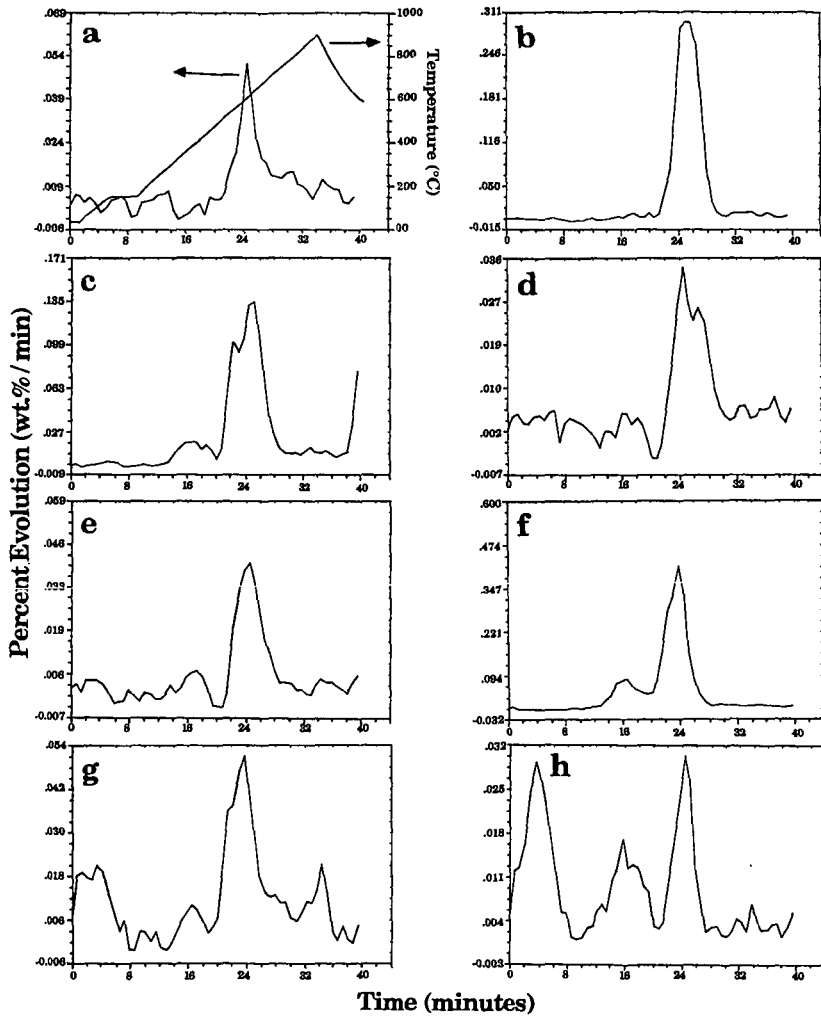


Figure 5. Evolution Rate for SO_2 from the Eight Argonne Coals in a TG-FTIR at 0.5°C/s . a) Pocahontas; b) Upper Freeport; c) Pittsburgh; d) Upper Knawha; e) Utah Blind Canyon; f) Illinois No. 6; g) Wyodak; h) Zap.

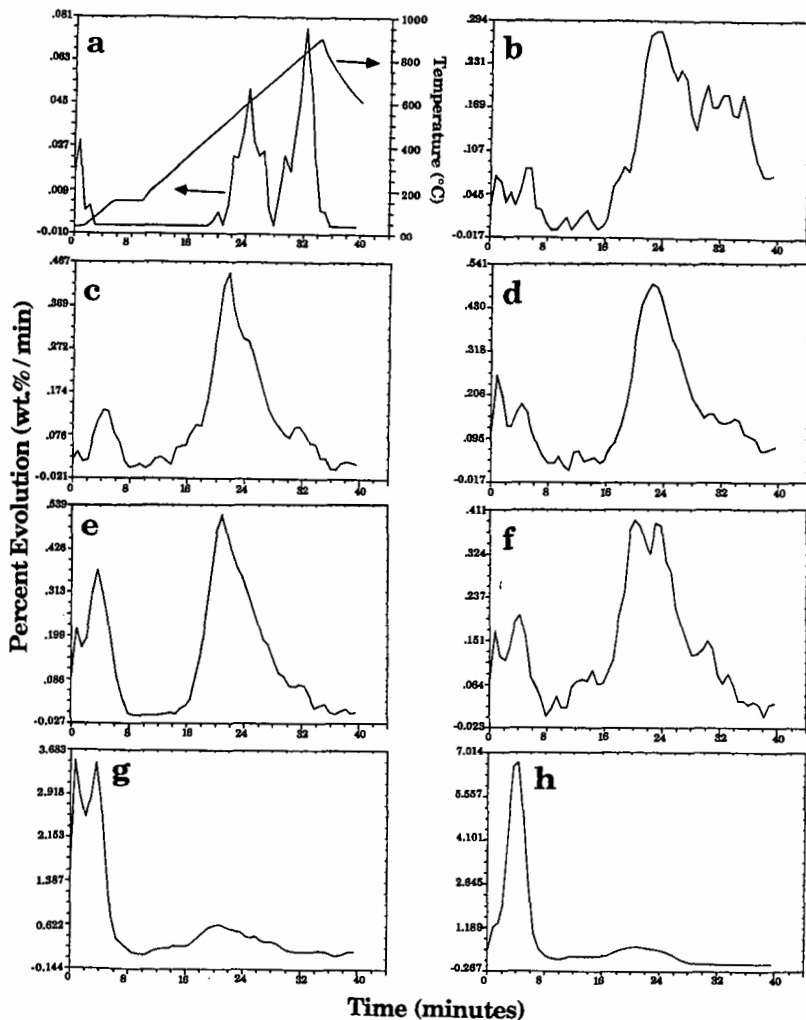


Figure 6. Evolution Rate for H_2O from the Eight Argonne Coals in a TG-FTIR at $0.5^\circ C/s$. a) Pocahontas; b) Upper Freeport; c) Pittsburgh; d) Upper Knawha; e) Utah Blind Canyon; f) Illinois No. 6; g) Wyodak; h) Zap.

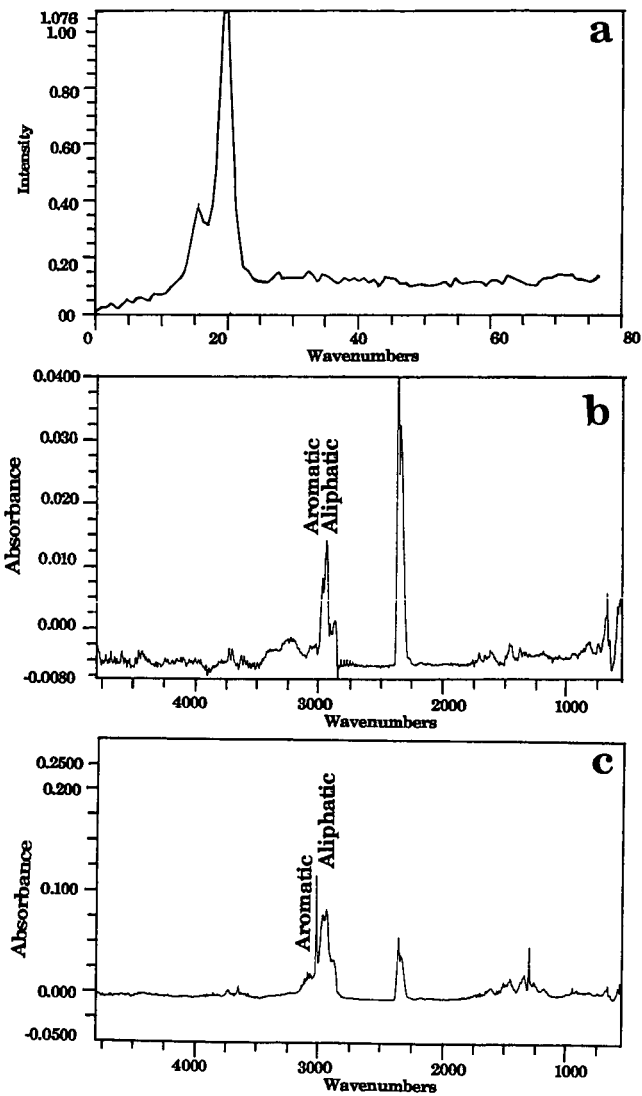


Figure 7. Spectrum of Products Evolved in Pyrolysis. a) Rate for Tar Evolution showing two Peaks, b) Spectrum at First Peak and c) Spectrum at Second Peak.

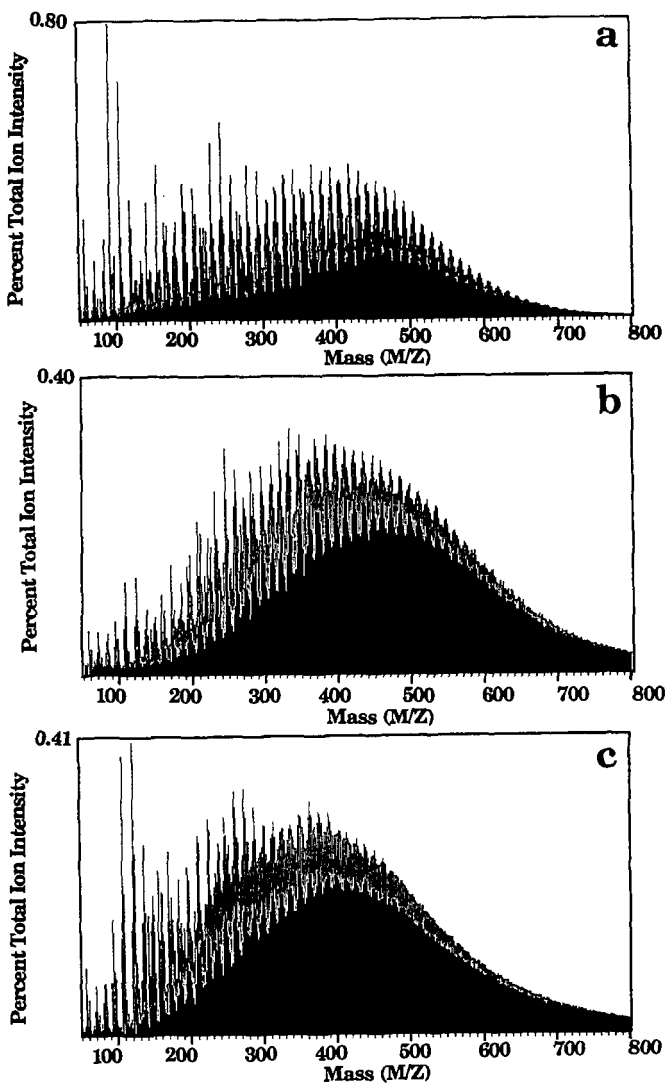


Figure 8. Tar Molecular Weight Distributions for Three Argonne Coals Pyrolyzed in the SRI FIMS Apparatus at 0.05°C/s. a) Pocahontas; b) Upper Freeport; c) Pittsburgh.

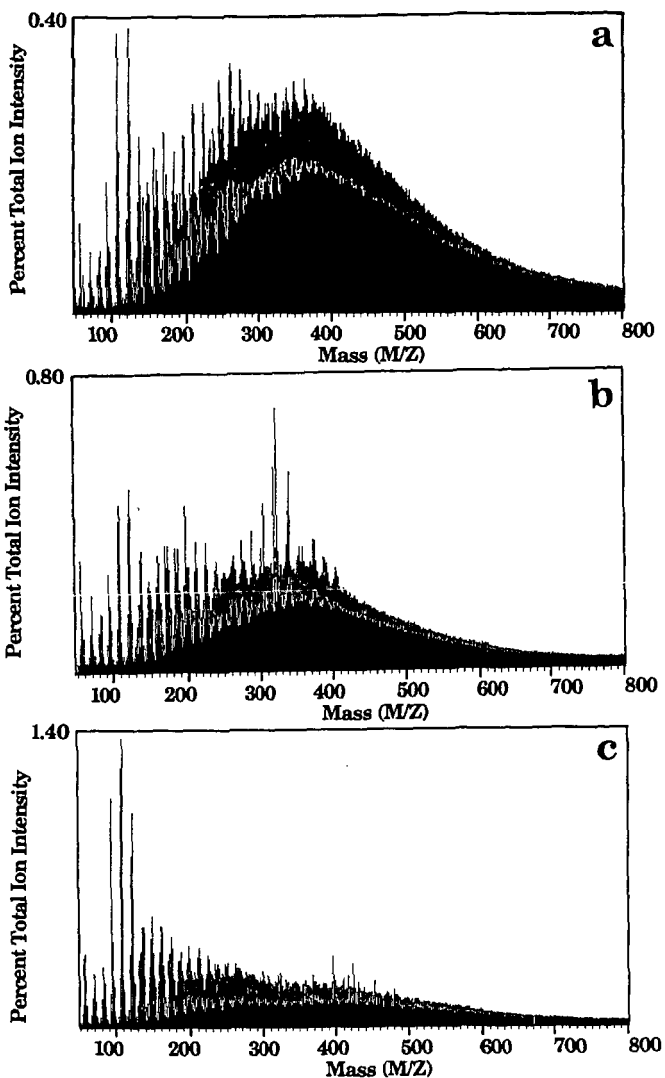


Figure 9. Tar Molecular Weight Distributions for Three Argonne Coals Pyrolyzed in the SRI FIMS Apparatus at 0.05°C/s. a) Upper Knawha; b) Utah Blind Canyon; c) Wyodak.

CROSSLINKING REACTIONS IN COAL PYROLYSIS

G.V. Deshpande, P.R. Solomon, and M.A. Serio

Advanced Fuel Research, Inc., 87 Church Street, East Hartford, CT 06108

INTRODUCTION

During coal pyrolysis, the break up of the coal macromolecular network is controlled by the relative rates of bond breaking, crosslinking and mass transport. Crosslinking reactions are important because the ultimate tar yield and tar molecular weight distribution are dependent on the extent of these reactions. Crosslinking, as measured by solvent swelling experiments, is observed to be rank dependent, with lignites crosslinking at lower temperatures than bituminous coals.

In a recent study of crosslinking, Suuberg et al. (1) observed that the crosslinking rate appeared to correlate with the evolution of CO₂. This correlation was confirmed by Solomon et al. (2,3). It appears that crosslinking may be related to the decomposition of carboxyl groups (whose concentration is rank dependent) to form CO₂. Recent research (4) has also demonstrated that substantial reductions in the crosslinking reactions can be achieved by ultra rapid heating. The high heating rate conditions for lignites produce melting and swelling of char, higher yields of soluble products, and product molecular weight distributions previously seen only for melting, easily soluble coals.

This paper describes a study of crosslinking behavior in which chars of a number of coals have been pyrolyzed under a variety of temperature histories and analyzed at intermediate extents of pyrolysis for solvent swelling behavior, functional group compositions and gas evolution. The behavior is consistent with the hypothesis that low temperature crosslinking is related to the decomposition of carboxyl groups to form CO₂.

EXPERIMENTAL

Coals Examined

Experiments were done with North Dakota (Zap), Big Brown Texas, and perdeutero-methylated Big Brown Texas lignites, Wellmore Kentucky #9, Pittsburgh Seam (high ash), Pittsburgh Seam (Argonne sample) bituminous coals and oxidized Pittsburgh Seam (high ash) bituminous coal. The ultimate analysis of each coal is given in Table I.

Char Preparation

The experiments described here were carried out on chars formed from the coals given in Table I. The chars were formed by heating in an inert gas within an entrained flow reactor (EFR) and a heated tube reactor (HTR) for a variety of residence times and maximum temperatures, or by heating in a Thermogravimetric Analyzer (TGA) at 30°C/min to 900°C where the volatiles are analyzed on-line by Fourier Transform Infrared (FT-IR) spectroscopy (TG-FTIR). A more detailed description can be found in Ref. 5.

Char Characterization

The chars were analyzed by quantitative FT-IR spectroscopy using the KBr pellet method (6,7). The chars were also analyzed using the solvent swelling techniques developed by J.W. Larsen and coworkers (8,9) to quantify and monitor the densities of covalent crosslinks inside the macromolecular framework of coal chars.

RESULTS AND DISCUSSION

Rank Dependence of Crosslinking Reactions

Measurements of the appearance of crosslinks during coal pyrolysis were recently reported by Suuberg et al. (1). Their results showed that lignites crosslink at temperatures (650 K) far below those where bituminous coals crosslink (800 K). This motivated the present study of systematically measuring the extent of crosslinking in coal pyrolysis.

Figure 1 shows the volumetric swelling ratio for Zap and Big Brown Texas lignites and Wellmore Kentucky #9, Pittsburgh Seam (Argonne sample) and Oxidized Pittsburgh Seam (high ash) bituminous coals measured as a function of temperature. The swelling ratio profiles are presented as $(1-X)$ where X is the change in the solvent swelling ratio between the coal and char, normalized by the maximum change. The curves are quite different among the five samples. The lignites crosslink at much lower temperatures than the bituminous coals, while the oxidized bituminous coal is an intermediate case.

The extent of low temperature crosslinking correlates with the carbonyl concentration of the coal as measured by FT-IR. The carbonyl concentration is directly related to the concentration of carboxyl groups. The high rank coals have a very low concentration of carboxyl groups, as seen by a low intensity carbonyl band at 1700 wavenumbers, in Fig. 2. The oxidized Pittsburgh Seam coal and the low rank coals have much higher carbonyl peaks.

Big Brown Texas lignite shows a slightly slower rate of crosslinking than Zap lignite. Schobert et al. (10) compared the ESCA spectra of Big Brown Texas and Beulah Zap lignites and found that the carboxylic peak to be less pronounced in the Big Brown spectrum. Spackman (11) has also reported that Big Brown Texas lignite had a lower carboxylic content than the North Dakota Zap lignite. When both lignites are heated at 30°C/min to 600°C, Big Brown Texas lignite evolves less CO₂ (8%) than Zap lignite (11.3%). The area corresponding to the carbonyl peak in the FT-IR spectrum of Big Brown Texas lignite is also less (1.29) than for the Zap lignite (1.69). These observations are consistent with the hypothesis that early crosslinking reactions in lignites occur with loss of carboxyl groups and evolution of carbon dioxide and the extent of crosslinking is directly related to the amount of these labile carboxyl groups present in coal. Bituminous coals which do not have a large concentration of these groups do not undergo early crosslinking reactions. A major contribution of hydroxyl groups in early crosslinking reactions is not likely because bituminous coals have a larger concentration of hydroxyl groups than the carboxyl groups and do not crosslink at low temperatures.

Heating Rate Dependence of Crosslinking Reactions

An important observation was made that crosslinking reactions could be minimized by carrying out the pyrolysis at a very high heating rate. In Fig. 3, the effect of heating rate on tar yield and volumetric swelling ratio in pyridine for North Dakota (Zap) lignite is compared for rapid pyrolysis (20,000°C/s) and slow pyrolysis (0.5°C/s). It can be clearly seen that the lignite starts to crosslink prior to the tar evolution in slow pyrolysis, whereas crosslinking occurs simultaneously with tar evolution in rapid pyrolysis. The tar yield obtained during rapid pyrolysis is higher than that obtained at low heating rate by more than a factor of two. Figure 4 compares scanning electron micrographs of lignite chars produced at 800°C with heating rates of 600°C/s and 20,000°C/s. The 600°C/s char shows little evidence of fluidity while the 20,000°C/s char shows fluidity, bubbling, and swelling. This is believed to be due to reduced crosslinking reactions.

Chemical Modification of Crosslinking Reactions

In order to test the hypothesis of low temperature crosslinking in lignites due to carboxyl groups, slow pyrolysis (heating rate, 0.5 K/s) of Big Brown Texas and perdeutero-methylated Big Brown Texas lignites were carried out in the TG-FTIR. The sample of perdeutero-methylated Big Brown Texas lignite was provided for this study by Dr. Ron Liotta. The gas evolution rate profiles (in arbitrary units) for gas species CO, CO₂, paraffins, CH₄, and H₂O are shown in Figs. 5a-5e, respectively, for Big Brown Texas and perdeutero-methylated Big Brown Texas lignites. The amount of gas species evolved is proportional to the area under the curve. It can be seen that during the pyrolysis stage (Time < 2000 s) the amount of CO₂, CO, and H₂O evolved is less for the perdeutero-methylated coal while the amount of CH₄ evolved is slightly more.

The amount of paraffin evolved (which is related to the amount of tar evolved) is also higher for the perdeutero-methylated coal. The weight loss profile for these two coals is shown in Fig. 5f. The initial weight loss profile (Time < 800 s, T < 300°C) is different while the rest of the weight loss profile during the pyrolysis stage (800 < Time < 2000 s; 300 < T < 900°C) seems to be very similar. The increase in weight at 2040 sec is due to noise in the balance and is not a real effect. CO, CO₂, and H₂O evolution is lower and CH₄ and paraffin (300 < T < 900°C) is higher for the perdeutero-methylated coal. Hence the difference in the weight loss profiles of the two lignites.

The effect of reduction in crosslinking reactions observed in pyrolysis of perdeutero-methylated coal is not only on the total amount of tar evolved but also on the molecular weight distribution of the tar. Figure 6 compares the FIMS spectra for raw and perdeutero-methylated Big Brown Texas lignites. The average molecular weight is substantially increased from that of the unmethylated coal and now resembles that of a bituminous coal.

Effects of Minerals on Crosslinking Reactions

Several investigators (12-15) have studied the role of exchangeable cations in gasification and pyrolysis of low rank coals. The ion-exchange technique as outlined by Schafer (16,17) is used to exchange cations with ammonium ions or load the coal with a certain cation (e.g. calcium) in different amounts.

Tyler and Schafer (13) found that the removal of cations from Gelliondale coals increased the yields of both tar and total volatile matter. The converse was also observed in that the addition of Ca²⁺ ions to an acid-form coal reduced the yields. The reversibility of the phenomena shows that the increase in yields on cation removal is not the result of any permanent chemical modification or degradation of the organic structure of the coal during the acid treatment (2N HCl at room temperature).

This motivated the study of effect of minerals on crosslinking reactions. As calcium has been the cation most extensively studied and low rank coals have a large amount of calcium cations attached to the carboxylate anions, Indian Head Zap lignite was used in this study. Two techniques were used to remove the calcium cations, the details of which can be found elsewhere (18,19). In the first technique, calcium ions were ion exchanged with 1N ammonium acetate for three 24 hour periods. The calcium content after ion exchange was reduced from 1.66 to 0.2%. In the second technique, demineralization with HCl and HF was used. The calcium content after demineralization decreased to 0.01%.

The swelling ratio profiles presented as (1-X) where X is the change in the solvent swelling ratio between the coal and char normalized by the maximum change

for ion exchanged Zap lignite, demineralized Zap lignite and Zap lignite are compared in Fig. 7. The crosslinking behavior for ion-exchanged Zap lignite is similar to raw lignite and shows early crosslinking. It should be noted here that the calcium has not totally been removed by the ion-exchange technique in this study.

The crosslinking behavior of demineralized Zap lignite is strikingly different from that of Zap lignite. It shows a shift to a higher temperature for the same loss in swelling due to crosslinking reactions. Both the raw and demineralized Zap lignites were pyrolyzed in the TG-FTIR apparatus. The tar evolved was higher (daf basis) and the CO and CO₂ evolutions were lower for the demineralized case. An increase in tar evolution is expected due to reduced crosslinking reactions. When pyrolysis of two lignites were carried out at high heating rate (5000 K/s) in the entrained flow reactor, the tar yield was increased from 14% (for raw lignite) to 22% due to demineralization. Similar increase in tar yield has been found for increase in heating rate during pyrolysis which has been discussed in the section entitled "Heating Rate Dependence of Crosslinking Reactions". This further supports the idea of reduced crosslinking due to demineralization.

It should be noted that the increase in tar yield due to the removal of calcium found by Tyler and Schafer (13) was for coals whose cations were removed by acid treatment. Both the lignite and the demineralized lignites were exhaustively extracted by pyridine in a soxhlet apparatus to determine whether any depolymerization of lignite had occurred. The amount of pyridine extractable material was 0% for the raw lignite and 2.6% for the demineralized lignite. The volumetric swelling ratio in pyridine was 2.4 for the raw lignite and 2.5 for the demineralized lignite. Both results show that a very small degree of depolymerization had occurred, if any, due to the demineralization procedure employed to remove the cations. Hence the increase in tar amount and shift of the crosslinking curve to a higher temperature for the same amount of loss in swelling due to crosslinking for demineralized Zap lignite appears to be due to the reduced mineral content.

Effect of Oxidation on Crosslinking Reactions

To further study the role of carboxyl groups in crosslinking, Pittsburgh Seam bituminous coal was oxidized in an oven in air to add carboxyl groups to the coal and see whether the oxidized coal behaved like a lignite in slow heating rate pyrolysis. After 239 hours of oxidation, a large increase in the absorption of IR due to carbonyl band at 1700 wavenumbers is observed which is shown in Fig. 2. There is a slight change in the OH band at 3300 wavenumbers, a large decrease in the aliphatic C-H at 2900 wavenumbers. This was consistent with the findings of other (20-22) investigators.

The chars of the oxidized coal formed at intermediate temperatures were swelled in pyridine to determine the crosslink densities. These results are shown in Fig. 1. The oxidized coal shows earlier crosslinking, as seen by the decrease in swelling ratio (decrease in value of $(1-X)$) at temperatures above 300°C. The decrease is not as large as that for the lignites because the concentration of carboxyl groups formed during oxidation is not as large as that found in the lignites. The height of the shoulder peak at 1700 wavenumbers corresponding to carbonyl band for oxidized coal is smaller than both the Zap lignite and the Big Brown Texas lignite.

The on-line FT-IR spectra of the gas evolution products from the raw coal and the oxidized coal were taken during pyrolysis and are shown for different temperatures during pyrolysis in Fig. 8. There is a larger amount of CO evolution at low temperatures for the oxidized coal than for the raw coal. This was also

found by Ignasiak et al. (21) in their study of pyrolysis of oxidized bituminous coals. The amount of CO₂ and CO evolved were higher for the oxidized bituminous coal. This is consistent with the larger carbonyl peak in the FT-IR spectrum of the oxidized coal. The amount of tar evolution (as seen from absorption of C-H band at 2900 wavenumbers) at temperatures between 400°C and 550°C is greater for the raw coal than the oxidized coal. This is consistent with the findings of Furimsky et al. (20). The tar, as it flows out of the pyrolysis chamber of the TG-FTIR into the FT-IR cell, forms an aerosol which causes scattering and results in increased absorption at high wavenumbers. The scattering is maximum at temperatures between 450 and 500°C and is also found to be greater for the raw coal than the oxidized coal.

CONCLUSIONS

1. For the low rank coals, the amount of tar obtained in a pyrolysis process increases with the increase in the heating rate.
2. The initial crosslinking reactions in low rank coals appear to be due to the presence of carboxyl groups. High rank coals which do not have these groups in large concentration do not show this kind of behavior in pyrolysis.
3. Chemical modification of carboxyl groups in lignites by methylating results in increased tar yield and molecular weight distribution of tar looks like that of a bituminous coal.
4. Demineralization of the lignite results in decrease in the rate of crosslinking reaction and increase in tar yield and the increase is higher when pyrolysis is carried out at a higher heating rate. The amount of CO and CO₂ evolution is also decreased due to demineralization. These results are consistent with ion exchanged minerals playing an important role in the crosslinking reactions.
5. Oxidation of bituminous coal results in early crosslinking during pyrolysis due to the presence of carboxyl groups introduced during the oxidation process.

ACKNOWLEDGEMENT

The authors wish to thank the Pittsburgh Energy Technology Center of the Department of Energy for the support of this work under Contract No. DE-FG22-85PC80910. The authors would also like to thank Dr. Ron Liotta for samples of perdeuteromethylated Big Brown Texas lignite.

REFERENCES

1. Suuberg, E.M., Lee, D., and Larsen, J.W., *Fuel*, **64**, 1668, (1985).
2. Solomon, P.R., Hamblen, D.G., Carangelo, R.M., Serio, M.A., and Deshpande, G.V., *Combustion and Flame*, **71**, 137, (1988).
3. Solomon, P.R., Hamblen, D.G., Deshpande, G.V., and Serio, M.A., *Coal Science and Technology II*, (J.A. Moulijn, et al., Ed.) Elsevier Science Publishers, Amsterdam, p. 601, The Netherlands, (1987).
4. Solomon, P.R., Serio, M.A., Carangelo, R.M., and Markham, J.R., *Fuel*, **65**, 182, (1986).

5. Carangelo, R.M., Solomon, P.R., and Gerson, D.J., *Fuel*, **66**, 960, (1987).
6. Solomon, P.R. and Carangelo, R.M., *Fuel*, **61**, 663, (1982).
7. Solomon, P.R. and Carangelo, R.M., "FT-IR Analysis of Coal 2. Aliphatic and Aromatic Hydrogen Concentration", Accepted for publication, *Fuel*, (1988).
8. Green, T.K., Kovac, J., and Larsen, J.W., *Fuel*, **63**, 925, (1984).
9. Green, R.K., Kovac, J., and Larsen, J.W., in *Coal Structure*, (R.A. Meyers, Ed.) Academic Press, NY (1982).
10. Schobert, H.H., Montgomery, G.G., Mitchell, M.J., and Benson, S.A., "Characterization of the Organic Structure of U.S. Lignites by Electron Spectroscopy and Thermal Analysis", presented at the 1983 Int. Conf. on Coal Science, Pittsburgh, PA, pp. 350-353, (1983).
11. Spackman, W.A., et al., US DOE Report FE-2030-16, (1980).
12. Morgan, M.E. and Jenkins, R.G., *ACS Div. of Fuel Chem. Preprints*, **29**, (2), 141, (1984).
13. Tyler, R.J. and Schafer, H.N.S., *Fuel*, **59**, 487, (1983).
14. Jenkins, R.G. and Morgan, M.E., *Fuel*, **65**, 769, (1986).
15. Stournas, S., Papachristos, M., and Kyriakopoulos, G.B., *ACS Div. of Fuel Chem. Preprints*, **32**, (3), 227, (1987).
16. Schafer, H.N.S., *Fuel*, **49**, 197, (1970).
17. Schafer, H.N.S., *Fuel*, **51**, 4, (1972).
18. Solomon, P.R., Hamblen, D.G., Serio, M.A., Smoot, L.D., and Brewster, S., "Measurement and Modeling of Advanced Coal Conversion", First Annual Report, U.S. DOE/METC Contract No. DE-AC21-86MC23075, (1987).
19. Solomon, P.R., Serio, M.A., Hamblen, D.G., Markham, J.R., Bassilakis, R., and Best, P.E., "Chemical and Physical Development of Char Particles during Devolatilization", Seventh Quarterly Report, U.S. DOE/METC Contract No. DE-AC21-85MC22050, (1987).
20. Furimsky, E., MacPhee, J.A., Vancea, L., Ciavaglia, L.A., and Nandi, B.N., *Fuel*, **62**, 395, (1983).
21. Ignasiak, B.S., Clugston, D.M., and Montgomery, D.S., *Fuel*, **51**, 76, (1976).
22. Ignasiak, B.S., Nandi, B.N., and Montgomery, D.S., *Fuel*, **49**, 214, (1970).

TABLE I
 ULTIMATE ANALYSES OF COALS USED (%DAF)

	C	H	N	S	O (diff)
Zap N. Dakota Lignite	66.5	4.8	1.1	1.1	26.5
Big Brown Texas Lignite	72.4	5.5	1.4	1.2	19.5
Wellmore Kentucky #9 Bituminous	86.0	5.4	1.5	1.2	5.9
Pittsburgh Seam #8 Bituminous	82.1	5.6	1.7	2.4	8.2
Pittsburgh Seam #8 (Argonne sample) Bituminous	83.3	5.9	1.6	2.3	6.9

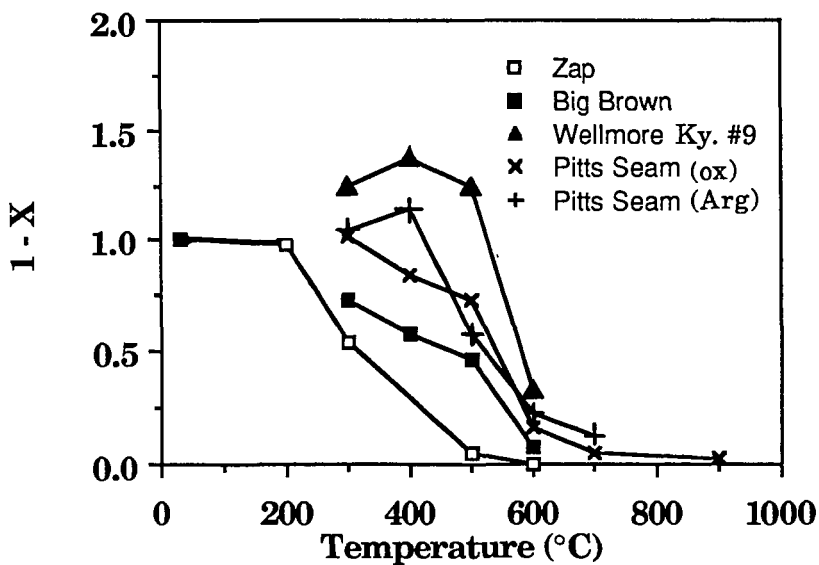


Figure 1. Comparison of Swelling Data of Zap Lignite, Big Brown Texas Lignite, Wellmore Bituminous Coal, Pittsburgh Seam Bituminous (high ash) Oxidized Coal and Pittsburgh Seam (Argonne sample) Bituminous Coal in a TG-FTIR at Various Final Temperatures (Heating Rate = 0.5 K/s).

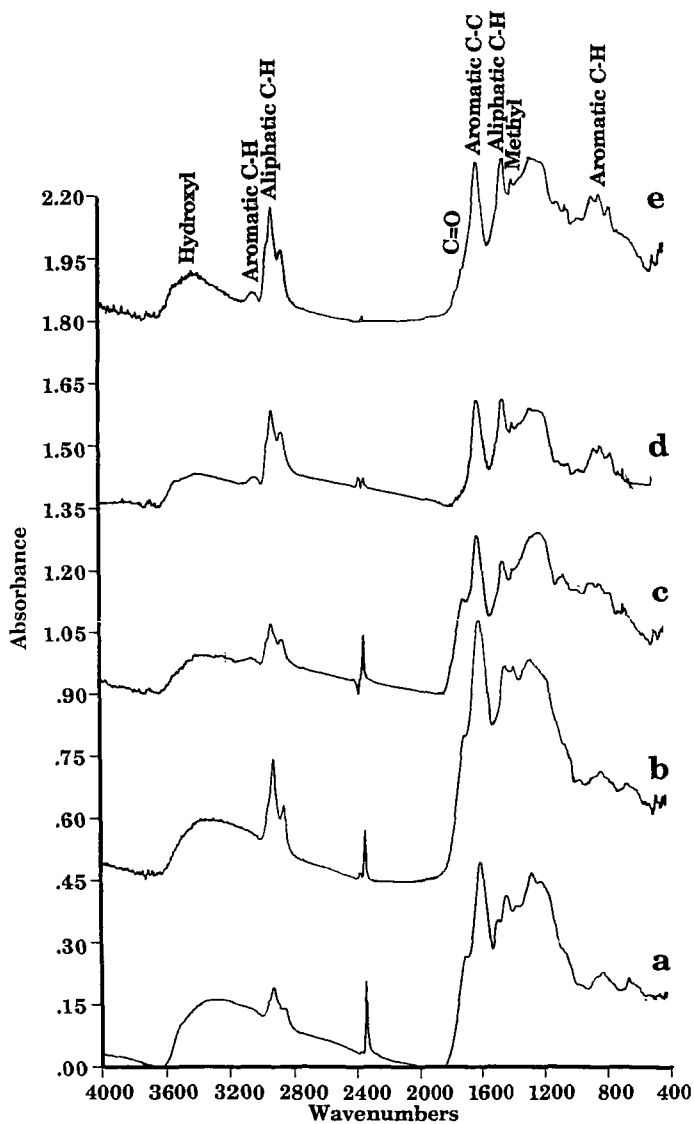


Figure 2. Comparison of the FT-IR Spectra of a) Zap Lignite, b) Big Brown Texas Lignite, c) Pittsburgh Seam Bituminous (high ash) Oxidized Coal, d) Pittsburgh Seam (Argonne) Bituminous, and e) Wellmore Coals Dry, Mineral Matter Corrected.

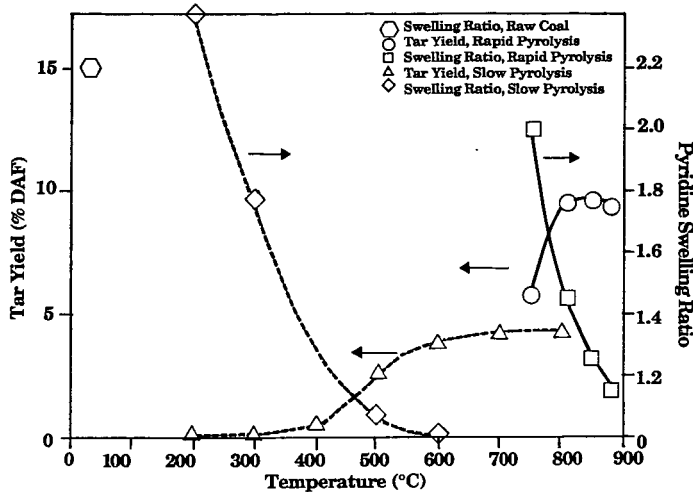


Figure 3. Effect of Temperature on Tar Yield and Pyridine Swelling Ratio of Char for Rapid Pyrolysis of Zap Lignite in Carbon Dioxide (solid line) and Slow Pyrolysis of Zap Lignite in Helium (dashed line).

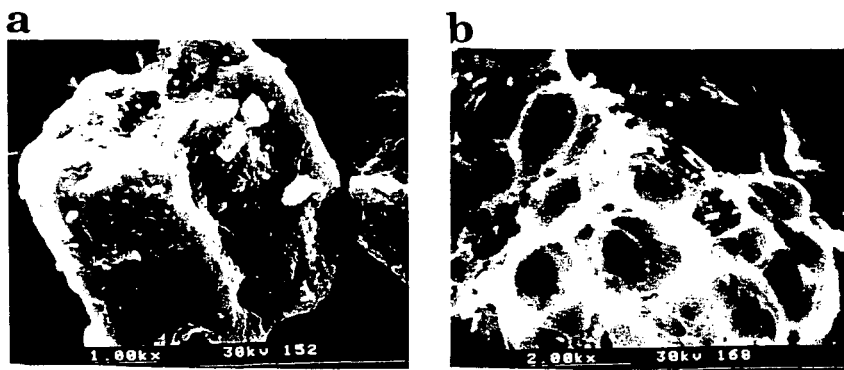


Figure 4. Scanning Electron Micrographs of North Dakota Lignite Chars. a) 600°C/sec Heating Rate and b) 20,000°C/sec Heating Rate.

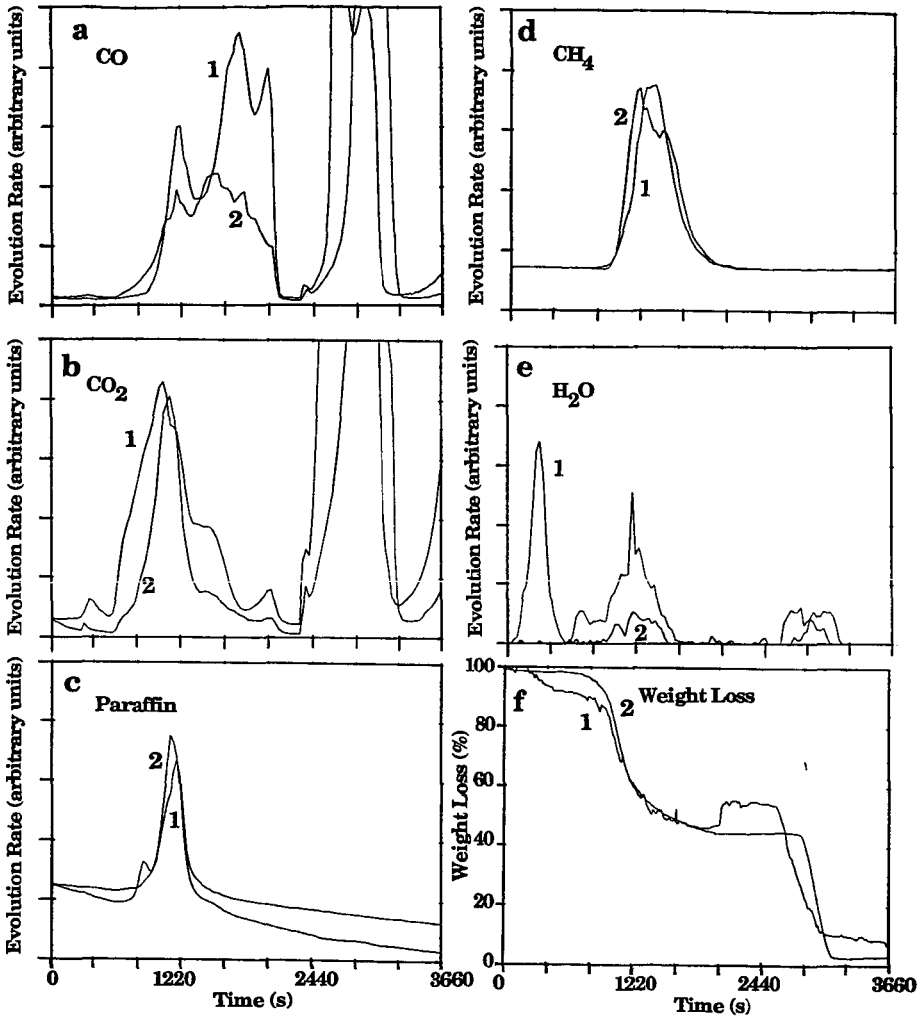


Figure 5. Thermogravimetric/Evolved Gas Analysis of Big Brown Texas and Perdeutero Methylated Big Brown Texas Lignites. a-e) Evolution Rate in Arbitrary Units for Individual Gas Species, and f) Measured Weight Loss. (Heating Rate = 0.5 K/s). 1 = Big Brown Texas Lignite and 2 = Perdeutero Methylated Big Brown Texas Lignite.

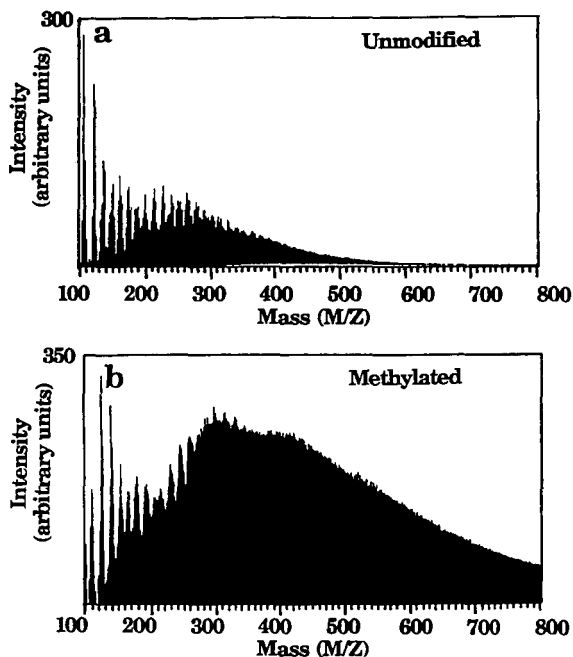


Figure 6. Comparison of FIMS Spectra for Raw and Perdeutero-methylated Big Brown Texas Lignite.

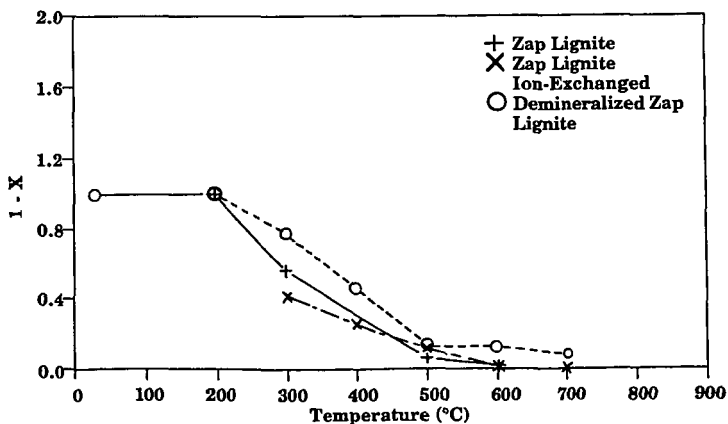


Figure 7. Effect of Removal of Ca by Ion Exchange or Demineralization on Crosslinking Behavior of Zap Lignite.

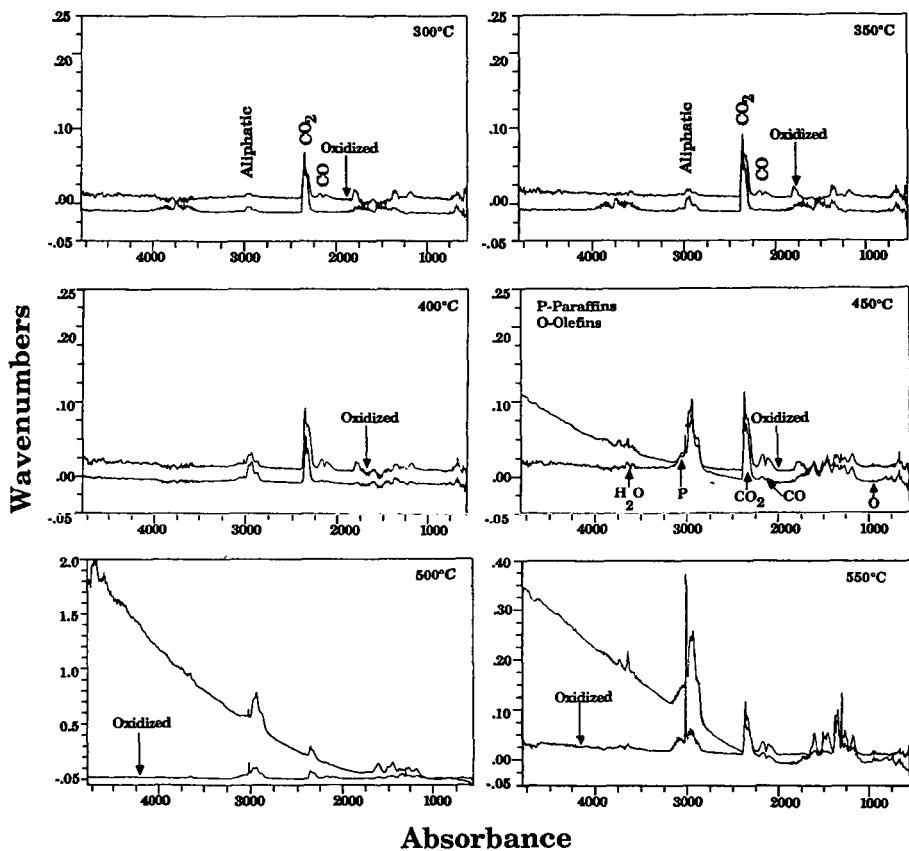


Figure 8. FT-IR Spectra of Evolved Products from Pyrolysis of Pittsburgh Seam Bituminous (high ash) Coal and Pittsburgh Seam Bituminous (high ash) Oxidized Coal.

A CHEMICAL MODEL OF COAL DEVOLATILIZATION USING
PERCOLATION LATTICE STATISTICS

D.M. Grant and R.J. Pugmire, University of Utah
Salt Lake City, UT 84112.
T.H. Fletcher and A.R. Kerstein, Sandia National Laboratories
Livermore, CA

ABSTRACT

We have developed a model for coal devolatilization that incorporates the diversity of coal structure in such a way that the analytical data obtained from solid state NMR provides the initial input data. Using an experimentally determined kinetic rate parameters, it is possible to fit the gas, tar and char production of a lignite and high volatile bituminous coal. We have employed percolation theory to provide analytical expressions for the lattice statistics required in devolatilization modeling. The percolation theory allows one to avoid the more time consuming Monte Carlo technique with no loss of generality or important statistical features. Percolation theory analytically describes the size distribution of finite clusters of sites joined by intact bridges but isolated from all remaining sites by broken bridges. The theory specifies a critical bridge population, depending only on the site coordination number, above which infinite arrays will coexist with clusters of finite size. It is a simple matter to adapt the structural features of percolation theory to both the tar and gas obtained in coal pyrolysis. The infinite arrays of percolation theory are interpreted as the macroscopic lattice of unreacted coal and/or char while the relatively small tar molecules may be identified with the fine clusters of percolation theory. The details of the model will be discussed together with the results obtained in modeling devolatilization behavior of coals of various ranks.

INTRODUCTION

A model for coal devolatilization, the chemical percolation devolatilization (CPD) model, has been developed¹ that incorporates the diversity of coal structure in such a way that the analytical data obtained from solid state NMR provides some of the initial input data. Using kinetic rate parameters reported by others², it is possible to fit the gas, tar, and char production of a lignite (Zap), and a high volatile bituminous coal (Illinois No. 6). Percolation theory is employed to provide analytical expressions for the lattice statistics required in the devolatilization modeling. Percolation theory allows one to avoid the time consuming Monte Carlo techniques with apparently no loss of generality or important statistical features. The straight forward computational technique is very efficient even on a small VAX computer as opposed to the more time consuming Monte Carlo methods which have shown that appropriate lattice statistics are important in coal devolatilization³.

The CPD theory analytically describes the size distribution of finite clusters of sites joined by intact bridges but isolated from all remaining sites by broken bridges. In percolation statistics a critical bridge population exists which depends only on the site coordination number, σ , above which infinite arrays will coexist with clusters of finite size. It is a simple matter to adapt the structural features of percolation theory to both the tar and gas obtained in coal pyrolysis. The infinite arrays of

percolation theory are interpreted as the macroscopic lattice of unreacted coal and/or char while the relatively small tar molecules may be identified with the finite clusters of percolation theory.

EXPERIMENTAL

The devolatilization data is that reported by Serio, et. al.², for a heated tube reactor of advanced Fuel Research. The raw kinetic data was kindly supplied by Serio and Solomon. The kinetic parameters used in the model are those obtained by Serio, et. al.², and are given in Table I. The NMR data for the coals are from Solum, et. al.⁴. The initial and final coal specific parameters are given in Table II.

RESULTS AND DISCUSSIONS

The details of the Chemical Percolation Model have been described by Grant, et. al.¹, and the details of the model will not be repeated. The comparison of the theoretical simulations of the experimental data are given in Figures 1 and 2 for the Illinois No. 6 and ZAP coals. The yields of gas, tar and char/unreacted-coal are given as a function of reaction time along with the corresponding predicted dynamical variables required for the simulations. The success of the simulations is thought to be good considering the number of parameters which were constrained from other work. We are engaged in an assessment of the sensitivity of the simula-

tions upon the several parameters and eventually hope with more experimental data to employ multiregression analysis of devolatilization data as a way to determine an optimal set of parameters. The correlation matrix between the several parameters is expected to enhance our understanding of the manner in which these parameters interact to influence the model.

Several of the features observed for these diverse coals are noteworthy and warrant comment in terms of the dynamical variables required in the simulations shown in Figures 1 and 2. The contrast in the material yields in both coals is quite apparent with the light gas exhibiting the typical exponential character, while the tar release exhibits a precipitous release or "flooding" because of the non-linear percolation statistics superimposed upon the multiexponential kinetic parameters which characterize the bridge-breaking processes. Even though the activation energy used for tar formation is lower than that for light gas release, considerable light gas is produced before any appreciable amount of tar is released. The "flood" of tar observed as the lattice begins to break down dramatizes the importance of lattice statistics in the tar release process. While the qualitative features are somewhat similar in both coals, significant quantitative differences may be observed in both material yields and the dynamical variables plotted for the two coals. The relative release with time of gas and tar have similar characteristics in both coals.

The model accurately predicts the modest but measurable loss of tar weight observed in the experimental data² after the initial "flooding" of tar. The maximum tar weight corresponds closely in time with the complete loss of labile bridges (see Figures 1 and 2). From this point on the decrease in tar weight arises from the release of light gases through continued cracking of the side chains as the material proceeds along the heated tube reactor. The rate of gas release slows with time as the more reactive bridge material is consumed in accordance with the distributed activation energy submodel. It is worth noting that this model predicts for both coals that a reasonably large side chain population will persist in both the tar and char throughout the whole process, and as a result light gases are released until the devolatilization is terminated at the end of the reactor tube. The gas release during the latter part of the process is not due to breaking of labile bonds with the accompanying release of bridge material, as the labile bridge population is zero during most of this latter period for the cases used in these simulations. Thus, the tar cluster size is not changing during this period of the reaction, but instead, the side chains are cracking to reduce the weight fraction of both the tar and the char.

For reaction conditions under 800°C, which obtain in the heated tube reactor experiments (Serio, et. al.²), the model predicts that a significant fraction of side chains persist throughout the whole reaction and

still exist even at the termination of the devolatilization process. Inspection of the plots of dynamical variables indicate that it is the δ variable (side chains) which exhibits the most interesting excursions with time rising and falling in concentration in the dynamical competition for bridge material. It is interesting to note that even when all of the labile bridges have been consumed and the number of char bridges have reached their final population, the reactive side chain population is still both appreciable and changing due to cracking of the side chain material. The amount of side chain material produced in the disappearance of the labile bonds is governed in part by the amount of transferable hydrogen. Thus, the rate constant of the side chain bond breaking would include explicitly the concentration of transferable hydrogen and a good test of the model would be its ability to simulated hydroliquifaction data obtained for various partial pressures of hydrogen.

The well known gas release occurring at early times is provided by low activation energies due to the distributed activation features incorporated in the model. The model also indicates a "tar" mass fraction of a few percent present at time zero in the unheated coals suggesting the presence of extractables in coals at ambient temperatures.

Future work will focus on model refinements to include a transport model. The molecular weight distribution of the tar is provided by the model and we will compare experimental molecular weight distribution data of Suuberg⁵ with the theoretical predictions of the CPD model.

ACKNOWLEDGEMENTS

This work was supported by the Advanced Combustion Engineering Research Center (ACERC) under grant no. CDR-8522618 from the National Science Foundation and by the U. S. Department of Energy. Two authors (DMG and RJP) express appreciation for support from the Associated Western Universities (AWU) to allow them to work for a period of time as guests at the Combustion Research Facility, Sandia National Laboratories. Helpful suggestions and assistance in computing by ACERC personnel (P.J. Smith, L.D. Smoot, L.L. Baxter, and J.D. Smith) are also acknowledged.

REFERENCES

1. D.M. Grant, R.J. Pugmire, T.H. Fletcher, and A.R. Kerstein, submitted for publication, 1988.
2. M.A. Serio, D.G. Hamblen, J.R. Markham, and P.R. Solomon, *Energy & Fuels*, 1987, 1, 178.
3. P.R. Solomon, D.G. Hamblen, G.V. Desphande, and M.A. Serio, 1987. *International Conference on Coal Science*, J.A. Monlijn, K.A. Nater, H.A.G. Chermin (Eds., Elsevier, Amsterdam, 1987, p. 601.
4. M.S. Solum, R.J. Pugmire, W.R. Woolfenden, and D.M. Grant, submitted for publication, 1988.
5. E.M. Suuberg, P.E. Unger, and J.W. Larsen, *Energy & Fuels*, 1987, 1, 305.

Table I
Kinetic Parameters for Coal Devolatilization

<u>Parameter</u>	<u>Value</u>	
	<u>Fitting Parameters</u>	<u>Literature Derived Values</u>
E_b		55.4 Kcal/mole
A_b	$4 \times 10^{15} \text{ sec}^{-1}$	
V_b	2 Kcal/mole	
E_g		69 Kcal/mole (69, 66, 71 Kcal/mole) ^a
A_g		$3 \times 10^{15} \text{ sec}^{-1}$ (3.5, 2.9, 2.6 $\times 10^{15} \text{ sec}^{-1}$) ^a
V_g	7 Kcal/mole	
ρ	0.89 sec^{-1} ^b	

a. Weighted average values for the Illinois #6 bituminous, Rosebud subbituminous, and Zap lignite coals, respectively.

b. As E_p and A_p can not be determined for the relatively small devolatilization temperature range affecting these data only a single effective rate parameter for ρ may be used in this fitting.

Table II
Coal Specific Parameters

Parameter	Zap Lignite	Rosebud Sub-Bit	III #6 High Vol. Bit.
<u>Adjustable Fitting Parameter</u>			
$\sigma + 1$	8.8 (>4.4) ^a	8.8 (>4.1) ^a	
<u>Parameters Set from NMR and Ultimate Gas Yield Data</u>			
$\sigma + 1$			4.3 (4.3) ^a
$p_o (=f_o)^b$	0.44	0.45	0.73
$f_{gas(\infty)}^c$	0.55	0.46	0.41
<u>Calculated Parameters from Fitted and Set Parameters</u>			
$1/\sigma$	0.13	0.13	0.30
$(\sigma + 1) \cdot p_o^d$	3.9	4.0	3.1
$r = m_b/m_a^e$	0.28	0.19	0.32

a. NMR estimates for σ given in parentheses.

b. The simulation value for f_o , which becomes p_o under the assumption of $c_o = \text{zero}$, are estimated reasonably reliably from NMR data on the number of methyls and of side chains attached to an aromatic cluster.

c. Solomon's ultimate light gas yields may be obtained by summing the y_i from $i = 1$ to 17.

d. This quantity measures the number of intact bridges per cluster and is calculated from the above values of p_o and σ .

e. Calculated from σ and $f_{gas(\infty)}$.

f. The NMR estimates for r given in parentheses.

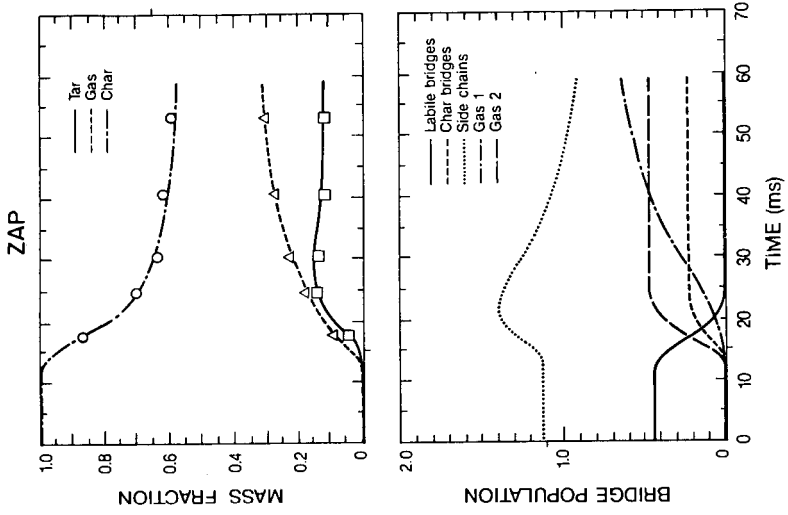


FIGURE 1. Simulation of devolatilization yields of char, tar, and light gases vs. time for Illinois No. 6 P-9h volatile bituminous coal are given in the upper plot. Experimental data are from Serio, et. al.² Bridge dynamical variables are given as a function of time in the lower plot.

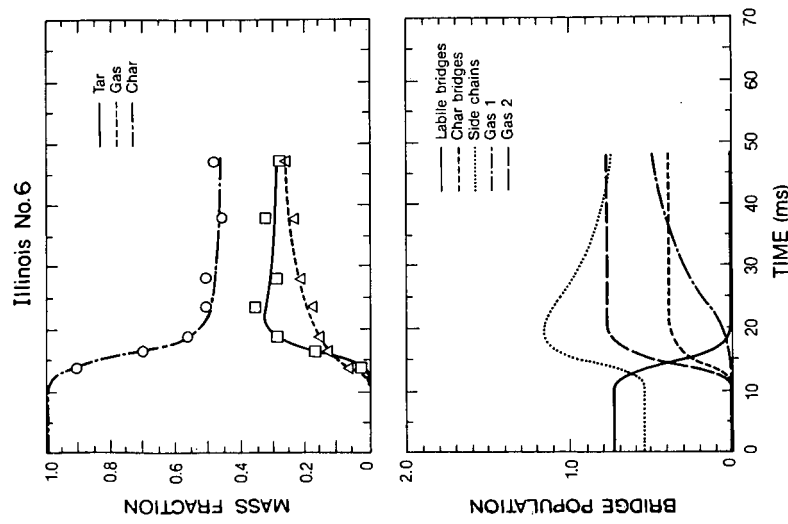


FIGURE 2. Simulations of devolatilization yields of char, tar, and light gases vs. time for North Dakota lignite coal are given in the upper plot. Experimental data are from Serio, et. al.² Bridge dynamical variables are given as a function of time in the lower plot.